Accelerated MRI using Parallel Imaging: A Signal Processing Perspective Grounded in Contemporary Literature

ꝆꝆ

May 2026

This document is a personal technical summary and interpretation of published work. All figures and graphical illustrations in this document were generated using AI-based image-generation tools for the purpose of technical explanation. They do not reproduce or knowingly imitate copyrighted figures from published literature, commercial documentation, or other protected sources. No third-party copyrighted images are used or claimed.

Contents

1 Core Idea of Parallel Imaging

Magnetic resonance imaging (MRI) is intrinsically slower than most other tomographic imaging modalities because spatial encoding is performed through repeated radiofrequency excitation, gradient encoding, and sequential sampling of k-space. In conventional Fourier imaging, acquisition time is closely linked to the number of phase-encoding steps required for adequate spatial sampling. Although the development of fast imaging methods such as turbo spin-echo (TSE), gradient-echo techniques, and echo-planar imaging (EPI) dramatically reduced scan times during the 1980s and 1990s, further acceleration by gradient performance alone gradually encountered technical and physiological limits. Rapid gradient switching places increasing demands on hardware and is constrained by effects such as peripheral nerve stimulation; in fast readout schemes, particularly EPI, eddy-current-related phase errors and other gradient-induced artifacts also become important practical limitations. Physiologic motion imposes an additional constraint on acquisition duration [1–4].

Parallel imaging emerged as a fundamentally different strategy for accelerating MRI. Rather than relying exclusively on gradient encoding for spatial localization, it exploits the intrinsic spatial sensitivity variations of phased-array radiofrequency (RF) receiver coils. In this approach, part of the spatial encoding normally performed by gradients is replaced by spatial information provided by multiple receiver coils with distinct sensitivity profiles. As a consequence, fewer phase-encoding lines need to be acquired, enabling substantial reductions in acquisition time without requiring higher gradient switching rates [1, 2, 5].

The key concept underlying parallel MRI is undersampling of k-space. If only every R-th phase-encoding line is acquired, the scan time can ideally be reduced by approximately the same factor:

$$T_{\text{scan,acc}} \approx \frac{T_{\text{scan,full}}}{R}. \tag{1}$$

The parameter R is commonly referred to as the acceleration factor, or reduction factor, and is defined as the ratio of the amount of k-space data required for a fully sampled acquisition to the amount collected in the accelerated acquisition. Vendor-specific terminology also exists; for example, Siemens has used the designation IPAT for integrated parallel acquisition techniques. In routine clinical practice, parallel imaging is generally applied with modest acceleration factors, commonly in the low single-digit range, whereas substantially higher accelerations may be achieved in specialized research settings using high-density coil arrays. Clinical reviews have suggested that acceleration factors in two-dimensional imaging are typically limited to approximately $R = 4$–5, while much higher values have been demonstrated experimentally, including 16-fold acceleration with a 32-channel coil array [2, 5, 6].

The development of parallel imaging represents one of the most important advances in MRI since the introduction of fast imaging sequences. Early theoretical concepts of massively parallel imaging appeared in the late 1980s, followed by practical implementations that exploited phased-array receiver technology for accelerated acquisition. Important milestones included SMASH (Simultaneous Acquisition of Spatial Harmonics), SENSE (Sensitivity Encoding), and GRAPPA (Generalized Autocalibrating Partially Parallel Acquisitions), which established the foundations of modern parallel MRI [1, 7–9].

Parallel imaging rapidly became integrated into a wide range of MRI applications. In echo-planar imaging and diffusion-weighted imaging, it shortens echo-train lengths and can thereby reduce susceptibility-related geometric distortions, blurring, and signal loss. In cardiovascular MRI, accelerated acquisition enables shorter breath-hold cine studies, improved myocardial perfusion imaging, and more

efficient coronary MR angiography [2, 10]. Parallel imaging has also become important in time-resolved MR angiography, functional MRI, dynamic contrast-enhanced imaging, and applications at higher field strengths such as 3 T and above [2, 5, 10].

More recently, parallel imaging has increasingly been combined with other accelerated imaging strategies, including compressed sensing, low-rank reconstruction methods, simultaneous multislice imaging, CAIPIRINHA-type controlled aliasing techniques, and deep-learning-based reconstruction approaches. These developments reflect a broader shift in MRI acceleration toward combinations of complementary encoding and reconstruction strategies rather than reliance on a single reconstruction paradigm [11–17].

Despite its many advantages, parallel imaging is associated with important limitations. Because fewer k-space data are acquired, the signal-to-noise ratio (SNR) decreases approximately as $1/\sqrt{R}$, with additional spatially varying noise amplification described by the geometry factor (g-factor), such that $SNR_{\text{accel}} \approx SNR_{\text{full}}/(g\sqrt{R})$. Reconstruction artifacts may arise from calibration inaccuracies, imperfect sensitivity estimation, excessive acceleration, patient or coil motion, and suboptimal coil geometry. Consequently, successful application of parallel imaging requires careful optimization of coil-array design, acquisition parameters, calibration strategy, and reconstruction method [2, 5, 8, 10].

In this chapter, the physical principles, mathematical foundations, reconstruction methods, and clinical applications of parallel MRI are reviewed. Emphasis is placed on modern reconstruction approaches, including SENSE- and GRAPPA-type methods, advanced iterative techniques, compressed-sensing hybrids, and contemporary accelerated imaging strategies. In addition, the chapter discusses simulation approaches for modeling parallel MRI acquisitions and reconstructions within computational MRI frameworks.

2 Foundations of Parallel MRI

2.1 Conventional Fourier MRI

To understand the principles of parallel imaging, it is useful to first review the fundamentals of conventional Fourier MRI. In standard MRI, spatial localization is achieved by the combined action of radiofrequency excitation and magnetic field gradients. Frequency encoding and phase encoding generate position-dependent phase shifts in the measured MR signal, allowing reconstruction of the spatial spin density distribution by Fourier transformation.

For a two-dimensional acquisition, the received MR signal may be written as

$$s(k_x, k_y) = \int\int \rho(x, y)\, e^{-i2\pi(k_x x + k_y y)}\, dx\, dy, \tag{2}$$

where $\rho(x, y)$ denotes the transverse magnetization or spin density distribution and (k_x, k_y) are the spatial frequency coordinates in k-space. The k-space coordinates are determined by the applied magnetic field gradients according to

$$k_x(t) = \frac{\gamma}{2\pi} \int_0^t G_x(\tau)\, d\tau, \tag{3}$$

and

$$k_y(t) = \frac{\gamma}{2\pi} \int_0^t G_y(\tau)\, d\tau, \tag{4}$$

where γ is the gyromagnetic ratio and $G_x(t)$ and $G_y(t)$ are the applied gradient fields.

In conventional Cartesian MRI, k-space is sampled line by line. In basic two-dimensional Fourier imaging, one phase-encoding step is acquired during each repetition time (TR). Consequently, the total acquisition time is approximately proportional to the number of phase-encoding lines:

$$T_{\text{scan}} \approx N_{\text{PE}} \cdot TR, \tag{5}$$

where N_{PE} denotes the number of phase-encoding steps. This relationship represents one of the principal limitations of conventional MRI. High spatial resolution requires many phase-encoding lines, which directly increases acquisition time.

Figure 1 shows Cartesian k-space filling.

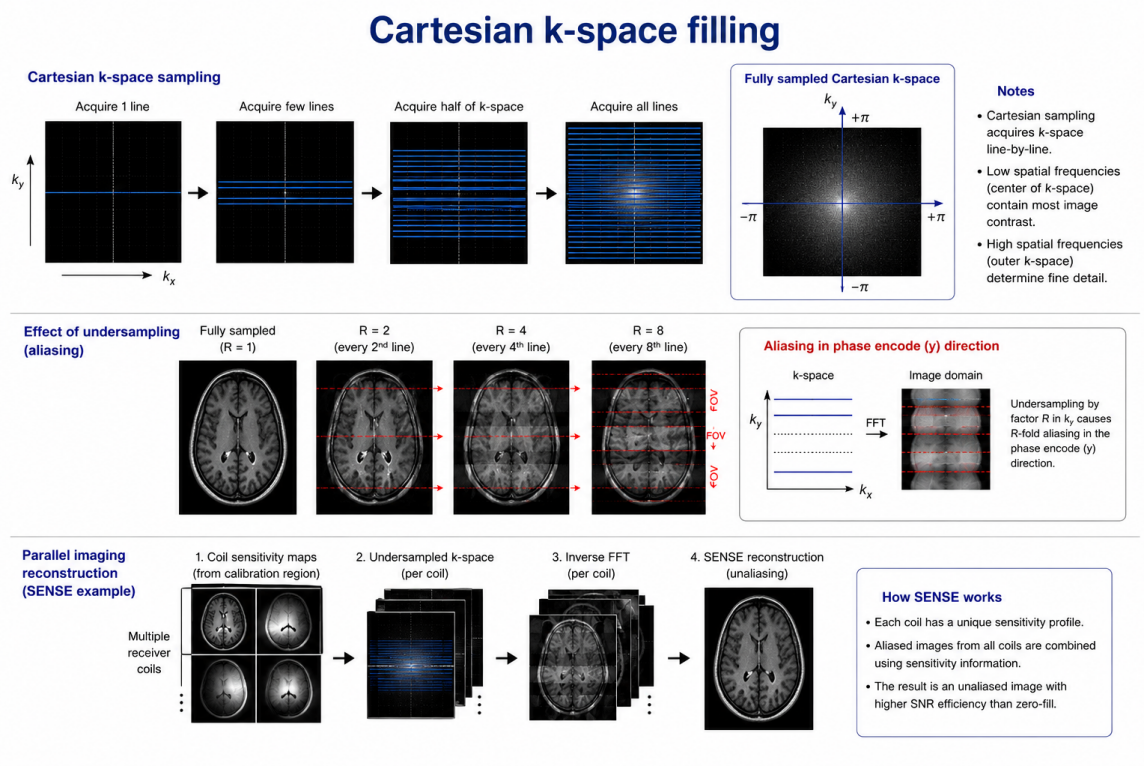

Figure 1: Cartesian k-space filling.

The relationship between the number of phase-encoding lines and total scan duration is described directly by Eq. (5).

The field of view (FOV) in the phase-encoding direction is determined by the spacing of sampled k-space lines:

$$\text{FOV} = \frac{1}{\Delta k_y}, \tag{6}$$

where Δk_y is the distance between adjacent phase-encoding samples. Likewise, spatial resolution depends on the maximum extent of sampled k-space:

$$\Delta y \approx \frac{1}{2k_{y,\max}}. \tag{7}$$

If k-space is undersampled below the Nyquist criterion, aliasing artifacts occur. In Cartesian imaging, undersampling in the phase-encoding direction produces folding of the image along the corresponding

spatial direction. Figure 2 shows Aliasing from k-space undersampling.

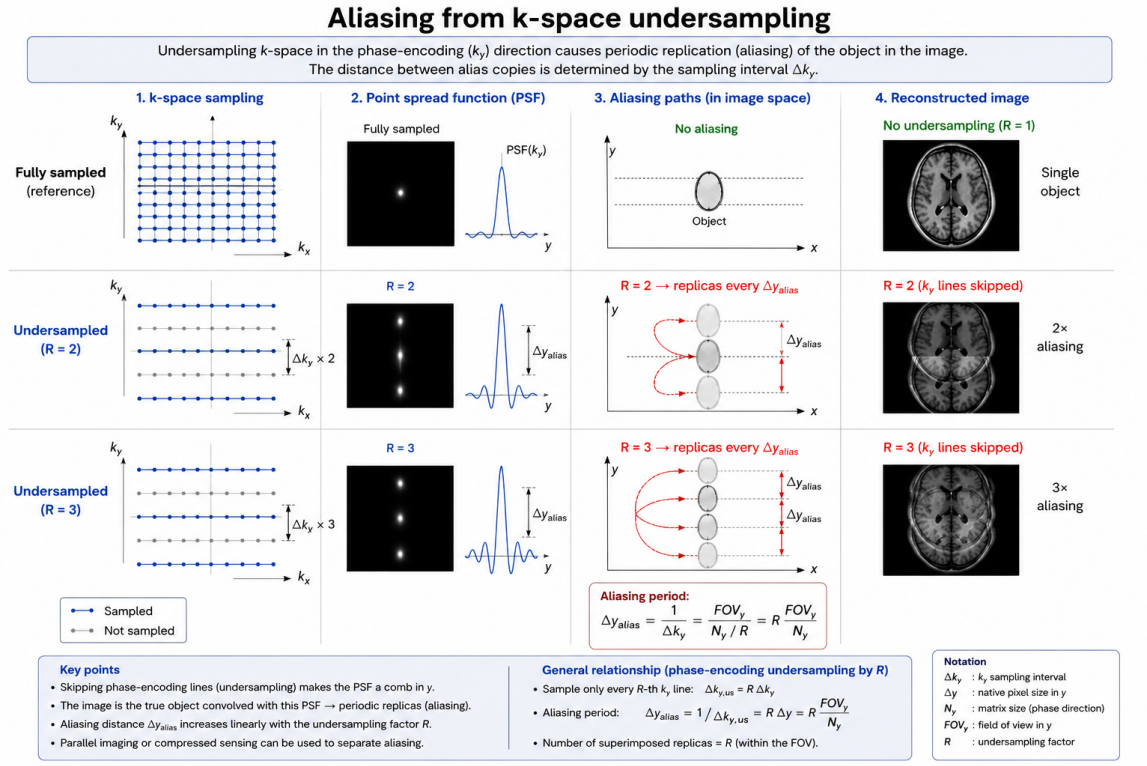

Figure 2: Aliasing from k-space undersampling.

The need to reduce acquisition time motivated the development of increasingly rapid imaging techniques such as turbo spin-echo (TSE), echo-planar imaging (EPI), and fast gradient-echo methods. However, these approaches ultimately remain constrained by gradient performance and physiological limitations. Parallel imaging addresses this limitation by introducing an additional source of spatial encoding information: the spatial sensitivity variations of phased-array receiver coils [1, 5].

2.2 Phased-Array Receiver Coils

The fundamental prerequisite for parallel MRI is the use of phased-array receiver coils. Unlike conventional volume coils, phased-array systems consist of multiple individual coil elements with spatially distinct sensitivity profiles. Each coil element is most sensitive to magnetization in its immediate vicinity and less sensitive to signals arising farther away, thereby providing additional spatial encoding information beyond that generated by the gradient system [1, 2, 5].

The signal measured by the c-th receiver coil may be expressed as

$$s_c(k_x, k_y) = \int\int S_c(x, y)\, \rho(x, y)\, e^{-i2\pi(k_x x + k_y y)}\, dx\, dy, \tag{8}$$

where $S_c(x, y)$ denotes the spatial sensitivity profile of the c-th coil element. The measured signal is therefore modulated by both the underlying object magnetization and the coil sensitivity distribution.

Figure 3 shows Coil sensitivity profiles.

Each coil exhibits high sensitivity near its physical location and progressively reduced sensitivity at larger distances. The spatial variation of these sensitivities constitutes the essential encoding mechanism

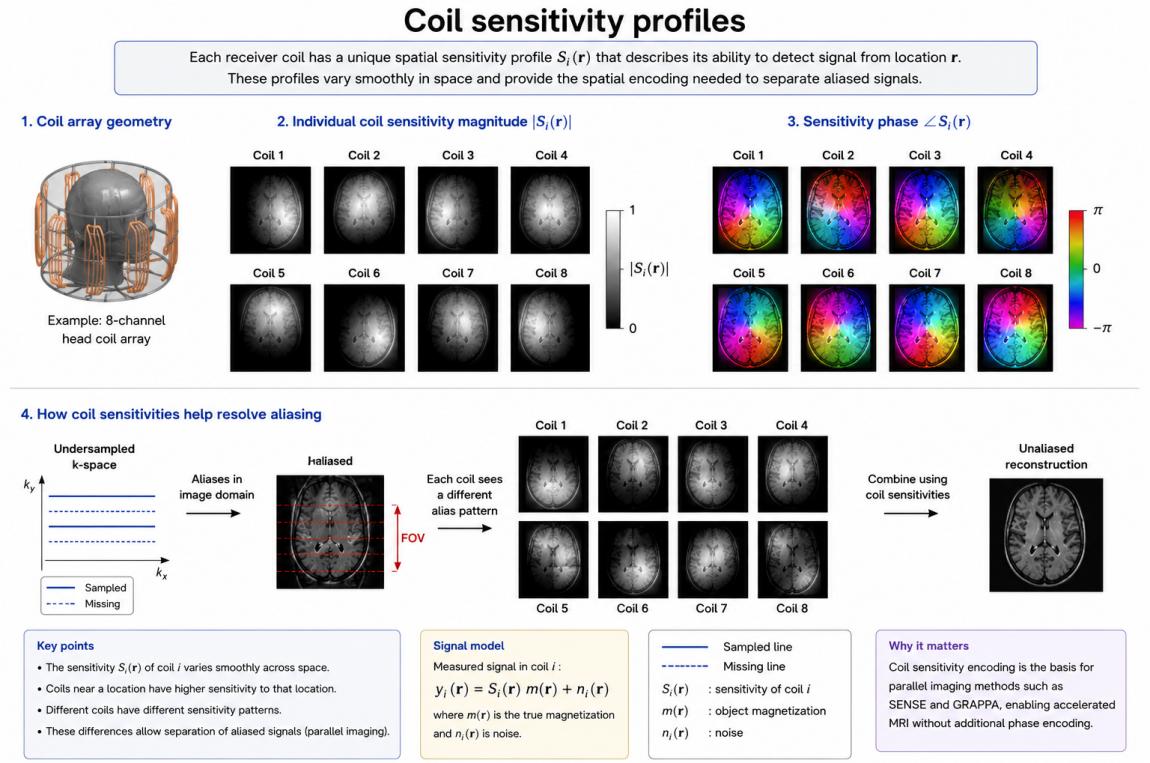

Figure 3: Coil sensitivity profiles.

exploited in parallel imaging.

Historically, phased-array coils were introduced primarily to improve signal-to-noise ratio (SNR) over extended anatomical regions. Small surface coils provide high local sensitivity but only limited spatial coverage. By combining multiple partially overlapping coil elements into an array, it became possible to preserve high local SNR while achieving broader field-of-view coverage than would be feasible with a single surface coil [1, 2].

In conventional phased-array imaging, the individual coil images are typically reconstructed separately and then combined into a single composite image. A common reconstruction approach is the root-sum-of-squares (RSS) combination:

$$I_{\mathrm{RSS}}(x, y) = \sqrt{\sum_{c=1}^{N_c} |I_c(x, y)|^2}, \tag{9}$$

where $I_c(x, y)$ denotes the reconstructed image from coil element c, and N_c is the total number of receiver coils.

The performance of a phased-array system strongly depends on coil geometry, coil sensitivity variation, and the noise correlation structure of the receiver array. Neighboring coil elements must be designed to limit mutual inductive coupling, since coil coupling and overlapping sensitivity regions contribute to correlated receiver noise and may compromise SNR efficiency. Clinical and research MRI systems therefore employ carefully optimized multi-element arrays, commonly with 8, 16, or 32 receiver channels, while still higher channel counts have been developed in specialized settings. High-channel-count arrays are particularly important for highly accelerated parallel imaging because they provide greater spatial encoding diversity and can reduce geometry-dependent noise amplification [10, 18, 19].

An important characteristic of phased-array systems is the spatial overlap of coil sensitivities. If two

spatially distant voxels exhibit sufficiently different sensitivity combinations across the receiver array, their signals can be distinguished even if they become superimposed due to undersampling. Parallel imaging exploits precisely this property to reconstruct images from incompletely sampled k-space data.

The spatial encoding capability of a coil array may be understood intuitively by considering the sensitivity profiles as additional encoding functions superimposed onto conventional Fourier encoding. In this sense, parallel imaging partially replaces gradient encoding by coil sensitivity encoding. Figure 4 shows Gradient encoding versus coil encoding.

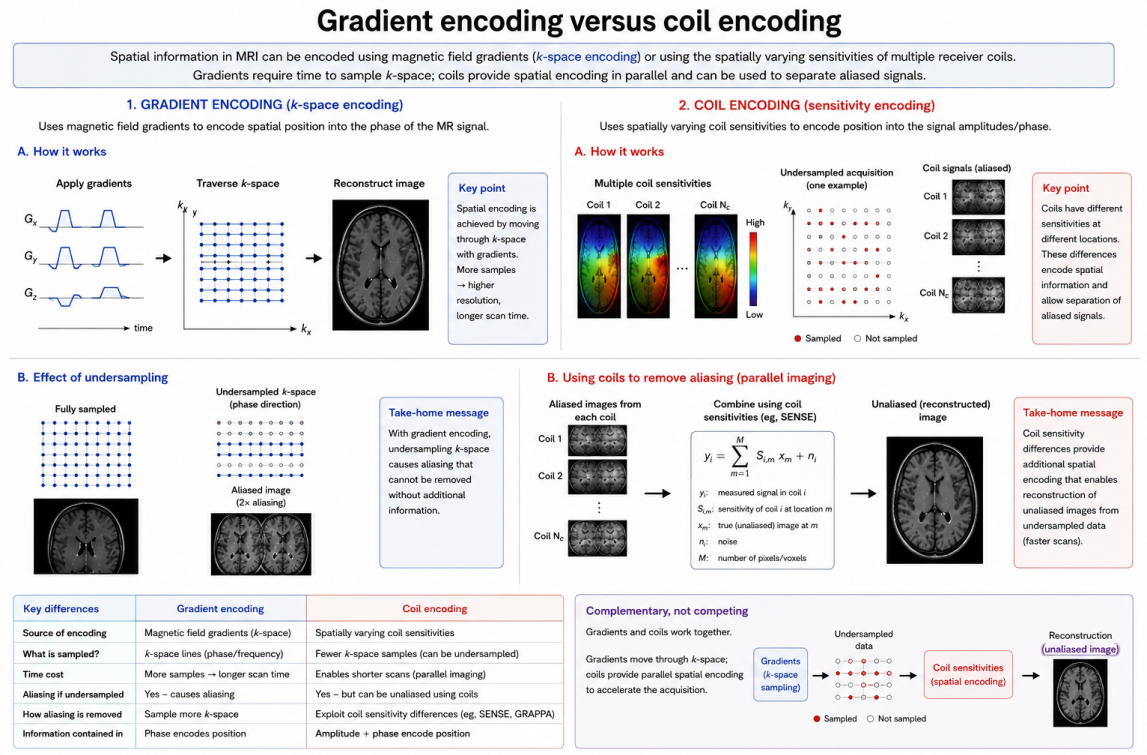

Figure 4: Gradient encoding versus coil encoding.

The quality of parallel imaging reconstruction therefore depends critically on the geometry of the receiver array. Ideally, the coil sensitivities should exhibit distinct and sufficiently nonredundant spatial variation across the imaging volume, particularly along the accelerated encoding direction. Poor coil geometry leads to ill-conditioned reconstructions, increased spatially varying noise amplification, and elevated geometry factors (g-factors), which ultimately limit the achievable acceleration [2, 8, 10].

Modern parallel imaging methods can broadly be divided into two major categories. Image-domain techniques such as SENSE reconstruct unfolded images directly using explicit coil sensitivity maps, whereas k-space methods such as GRAPPA synthesize missing k-space lines from neighboring acquired data without requiring direct inversion in image space. Both approaches rely fundamentally on the spatial encoding information provided by phased-array receiver coils.

2.3 Principle of Parallel Imaging

In a fully sampled conventional Cartesian MRI acquisition, k-space must be sampled sufficiently densely in the phase-encoding direction to satisfy the Nyquist criterion and avoid spatial aliasing. For basic two-dimensional Fourier imaging, the total scan time increases approximately linearly with the number

of phase-encoding steps, as summarized in Eq. (5); although fast spin-echo and related techniques may acquire multiple k-space lines within a single repetition period, the number of required phase encodes remains a central determinant of acquisition time. Parallel imaging accelerates MRI by intentionally undersampling k-space and subsequently recovering the missing spatial information from the spatial sensitivity variations of phased-array receiver coils [2, 5].

The simplest form of acceleration consists of skipping phase-encoding lines during acquisition. For an acceleration factor R, only every R-th k-space line is acquired:

$$N_{\mathrm{PE,acc}} = \frac{N_{\mathrm{PE}}}{R}, \tag{10}$$

where N_{PE} denotes the number of phase-encoding lines in the fully sampled acquisition and $N_{\mathrm{PE,acc}}$ is the number of acquired lines in the accelerated acquisition. Ideally, the scan time is reduced by approximately the same factor:

$$T_{\mathrm{scan,acc}} \approx \frac{T_{\mathrm{scan,full}}}{R}. \tag{11}$$

Undersampling below the Nyquist criterion inevitably produces aliasing artifacts in the image domain. In Cartesian imaging, undersampling in the phase-encoding direction reduces the effective field of view (FOV) by the acceleration factor:

$$\mathrm{FOV}_{\mathrm{acc}} = \frac{\mathrm{FOV}_{\mathrm{full}}}{R}. \tag{12}$$

As a result, structures separated by multiples of the reduced FOV become superimposed in the reconstructed image. The relevant concept demonstrates the formation of fold-over artifacts produced by k-space undersampling.

The essential idea of parallel imaging is that the aliased voxels are observed differently by the individual receiver coils because each coil possesses a distinct spatial sensitivity profile. Although two voxels may overlap in the undersampled image, their relative signal contributions vary from coil to coil. This additional information allows the original unaliased image to be reconstructed.

The reconstruction problem in parallel imaging may therefore be viewed as an inverse problem. The measured aliased signals are known, and the unknown quantities are the true underlying voxel intensities. The coil sensitivity maps provide the encoding information required to solve this system.

The achievable acceleration factor depends strongly on the geometry of the receiver array. If aliased voxels exhibit very similar combinations of coil sensitivities, the reconstruction becomes poorly conditioned and noise amplification increases substantially. Consequently, practical acceleration factors are limited by coil design, anatomical geometry, and signal-to-noise ratio considerations [2, 5, 8].

Figure 5 shows Parallel imaging reconstruction pipeline.

1. acquisition with undersampled k-space,
2. formation of aliased coil images,
3. utilization of coil sensitivity information,
4. reconstruction of the unfolded image.

Modern parallel imaging methods can broadly be divided into two principal categories. In image-domain techniques such as SENSE, aliased images are unfolded directly using explicit coil sensitivity

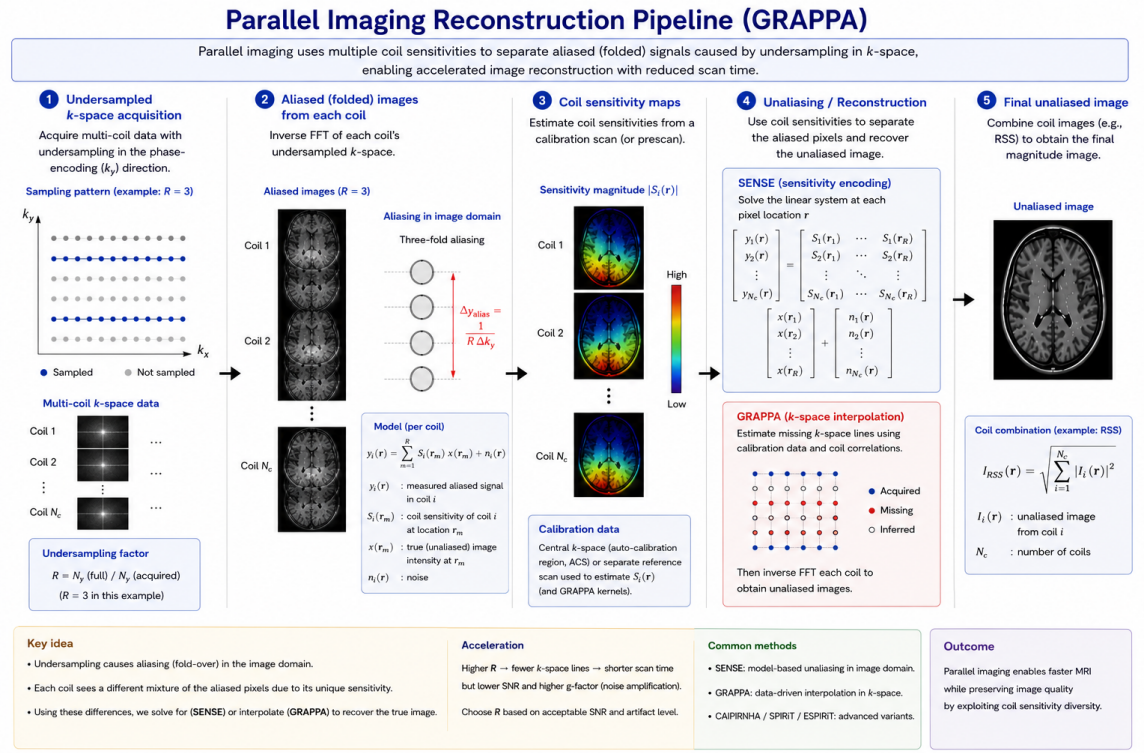

Figure 5: Parallel imaging reconstruction pipeline.

maps [8]. In k-space methods such as GRAPPA, missing k-space lines are synthesized from neighboring acquired data using calibration information derived from fully sampled reference regions [9]. Although mathematically different, both approaches exploit the same fundamental principle: additional spatial encoding provided by phased-array receiver coils [20].

Parallel imaging rapidly became indispensable in many MRI applications because it not only shortens acquisition time but can also reduce artifacts associated with long readout durations. In echo-planar imaging, for example, reduced echo-train length and shorter effective echo spacing decrease susceptibility-related geometric distortion, blurring, and related signal degradation. In cardiac imaging, parallel imaging enables shorter breath-hold acquisitions, improved temporal resolution, and more efficient dynamic assessment of cardiac function. In multiecho sequences such as turbo spin-echo, particularly at 3 T and above, parallel imaging can also help reduce specific absorption rate (SAR) or total RF energy deposition by reducing the number of refocusing pulses required per unit time or by permitting longer repetition times at fixed scan duration [2, 10].

3 Image-Space Parallel Imaging

3.1 SENSE Reconstruction

Sensitivity Encoding (SENSE) represents one of the most important image-domain approaches to parallel MRI. Introduced by Pruessmann et al. in 1999, SENSE reconstructs the unaliased image from undersampled data by explicitly incorporating the spatial sensitivity profiles of the receiver coils into the reconstruction [5, 8].

In SENSE imaging, Cartesian k-space is undersampled by an acceleration factor R, typically along

the phase-encoding direction. After Fourier transformation, each individual coil image exhibits aliasing because the reduced sampling density decreases the effective field of view. The aliased pixels in the reconstructed image correspond to the superposition of several spatial locations separated by multiples of the reduced field of view [2, 5, 8].

The central idea of SENSE is that the aliased voxels contribute differently to each coil image because of the spatial variation of the coil sensitivities. The measured signal in a particular aliased pixel may therefore be written as a weighted sum of the true voxel intensities:

$$v_c = \sum_{m=1}^{R} S_c(r_m)\, a_m, \tag{13}$$

where v_c is the measured signal in coil c, $S_c(r_m)$ is the sensitivity of coil c at spatial position r_m, and a_m denotes the unknown true voxel intensity at position r_m.

For a receiver array with N_c coils, the system may be written compactly in matrix form:

$$\mathbf{v} = \mathbf{S}\mathbf{a}, \tag{14}$$

where

$$\mathbf{v} = \begin{bmatrix} v_1 \\ v_2 \\ \vdots \\ v_{N_c} \end{bmatrix}, \tag{15}$$

and

$$\mathbf{a} = \begin{bmatrix} a_1 \\ a_2 \\ \vdots \\ a_R \end{bmatrix}. \tag{16}$$

The sensitivity matrix $\mathbf{S}$ contains the coil sensitivities corresponding to the aliased voxel locations:

$$\mathbf{S} = \begin{bmatrix} S_1(r_1) & S_1(r_2) & \cdots & S_1(r_R) \\ S_2(r_1) & S_2(r_2) & \cdots & S_2(r_R) \\ \vdots & \vdots & \ddots & \vdots \\ S_{N_c}(r_1) & S_{N_c}(r_2) & \cdots & S_{N_c}(r_R) \end{bmatrix}. \tag{17}$$

The reconstruction problem therefore reduces to solving a linear system for the unknown voxel intensities $\mathbf{a}$. In the presence of correlated coil noise, the noise-weighted least-squares solution becomes

$$\mathbf{a} = (\mathbf{S}^H \mathbf{C}^{-1} \mathbf{S})^{-1} \mathbf{S}^H \mathbf{C}^{-1} \mathbf{v}, \tag{18}$$

where $\mathbf{C}$ denotes the noise covariance matrix between the receiver coils and $\mathbf{S}^H$ is the Hermitian transpose of the sensitivity matrix [8].

Figure 6 shows the SENSE unfolding process.

The key elements are:

1. the undersampled k-space,

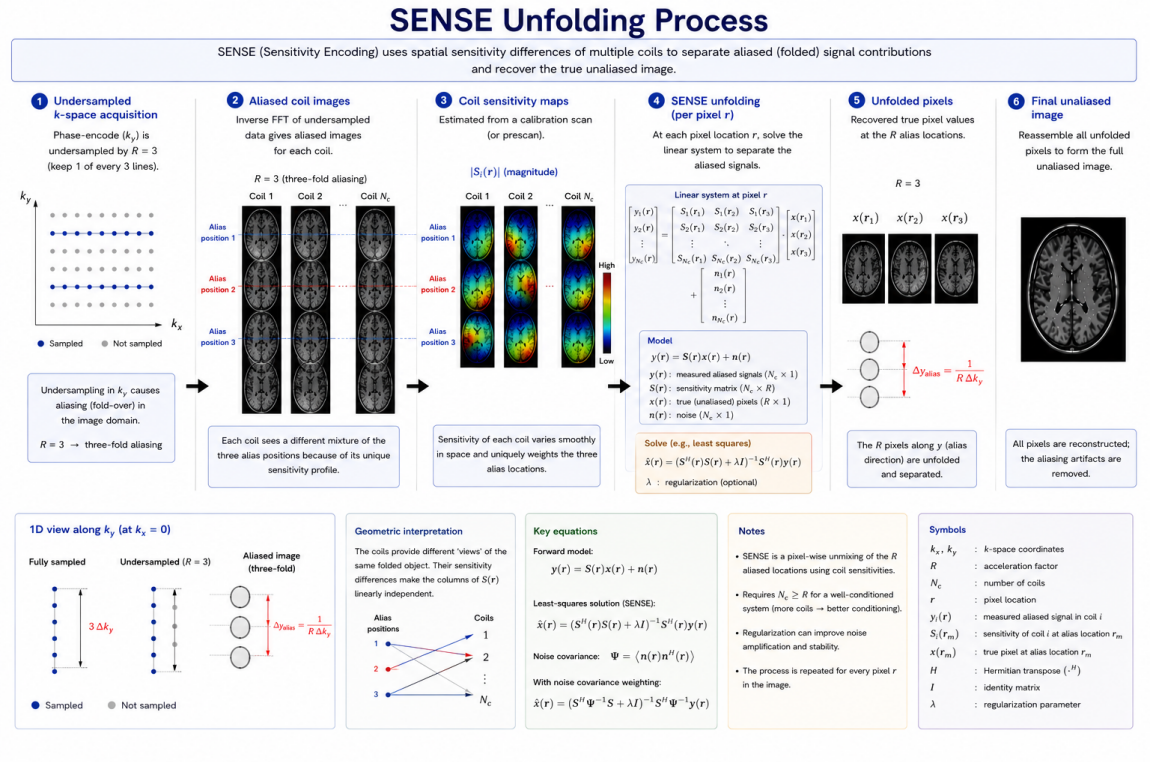

Figure 6: SENSE unfolding process.

2. the aliased coil images,

3. the coil sensitivity maps,

4. the reconstructed unfolded image.

An important characteristic of SENSE is that reconstruction is performed independently for each aliased pixel position. The quality of the reconstruction therefore depends critically on the conditioning of the sensitivity matrix $\mathbf{S}$. If the coil sensitivities are too similar at the aliased voxel locations, the matrix inversion becomes unstable and noise amplification increases substantially [2, 5, 8].

The signal-to-noise ratio (SNR) in SENSE imaging is reduced compared with fully sampled imaging. In addition to the intrinsic reduction associated with undersampling, further degradation arises from the conditioning of the unfolding problem. The resulting SNR may be written as

$$\mathrm{SNR}_{\mathrm{SENSE}} = \frac{\mathrm{SNR}_{\mathrm{full}}}{g\sqrt{R}}, \tag{19}$$

where g denotes the geometry factor (g-factor) [8]. The g-factor quantifies noise amplification caused by the geometry and overlap of the coil sensitivities.

Figure 7 shows g-factor maps.

One important practical requirement of SENSE is accurate estimation of the coil sensitivity maps. In clinical and research implementations, these maps are commonly obtained either from separate calibration scans or from low-resolution reference information acquired in conjunction with the accelerated scan. Errors in sensitivity estimation may produce residual aliasing artifacts, intensity modulation, or reconstruction instability [2, 6, 8].

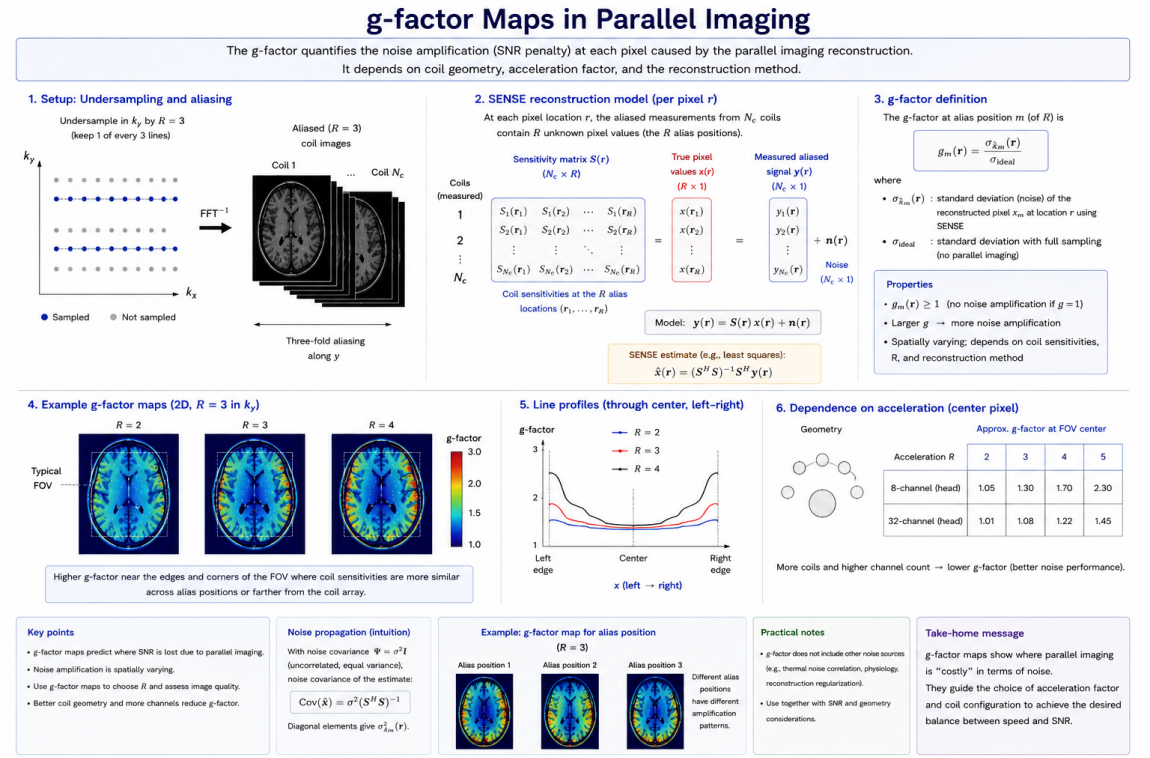

Figure 7: g-factor maps.

Despite these limitations, SENSE became one of the foundational methods of modern parallel imaging because of its elegant mathematical formulation and its direct exploitation of coil sensitivity encoding. It remains a central conceptual framework for later developments in accelerated MRI reconstruction.

3.2 Geometry Factor and Noise Amplification

One of the fundamental limitations of parallel imaging is the reduction in signal-to-noise ratio (SNR) associated with accelerated acquisition. In conventional MRI, the SNR is approximately proportional to the square root of the acquisition time:

$$\text{SNR} \propto \sqrt{T_{\text{scan}}}. \tag{20}$$

Since parallel imaging reduces the acquisition time by approximately a factor of R, a corresponding reduction in SNR is unavoidable:

$$\text{SNR}_{\text{acc}} \approx \frac{\text{SNR}_{\text{full}}}{\sqrt{R}}. \tag{21}$$

However, in parallel MRI the SNR degradation is generally more severe because the reconstruction process itself amplifies noise. In SENSE reconstruction, the unfolding operation requires inversion of the sensitivity matrix, and poorly conditioned inversions lead to substantial noise amplification. This additional penalty is quantified by the geometry factor, or g-factor, introduced by Pruessmann et al. [8].

The resulting SNR in parallel imaging may therefore be expressed as

$$\text{SNR}_{\text{PI}} = \frac{\text{SNR}_{\text{full}}}{g\sqrt{R}}, \tag{22}$$

where g denotes the geometry factor. The g-factor is always greater than or equal to unity:

$$g \geq 1. \tag{23}$$

Ideal reconstructions correspond to $g = 1$, whereas poorly conditioned reconstructions produce significantly larger values [8].

The geometry factor depends primarily on:

1. the spatial arrangement of the receiver coils,
2. the overlap of the coil sensitivity profiles,
3. the acceleration factor R,
4. the imaging geometry and anatomy.

Figure 8 shows the g-factor conditioning principle.

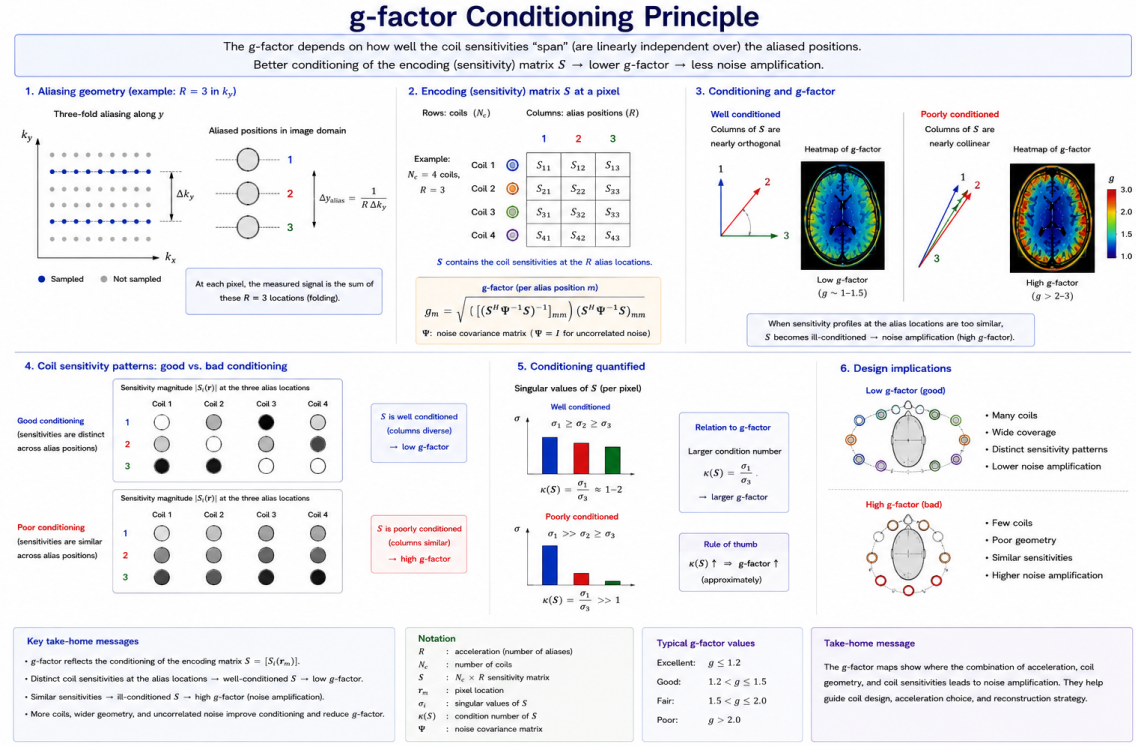

Figure 8: g-factor conditioning principle.

The key comparison is between well-conditioned and poorly conditioned coil configurations.

If the coil sensitivities are highly distinct at the aliased voxel locations, the unfolding problem is well conditioned and the g-factor remains close to unity. Conversely, if the sensitivities become too similar, the matrix inversion required for reconstruction becomes unstable and noise amplification increases substantially [2, 5, 8].

The spatial distribution of the g-factor is generally nonuniform across the image. Regions near the center of the field of view often exhibit larger g-factors because the coil sensitivities become less distinct in these regions, whereas peripheral regions closer to the receiver coils frequently show lower noise amplification [2].

The achievable acceleration factor is therefore fundamentally limited by coil geometry. Increasing the number of receiver channels can improve the spatial encoding capability of the array and reduce geometry-related noise amplification, particularly at higher acceleration factors, although the benefit depends on coil layout, anatomy, and imaging direction. Clinical and research MRI systems consequently employ increasingly dense receiver arrays, commonly with 16 or 32 elements, while 64-channel and still higher-channel configurations have been explored in specialized research settings [2, 10, 19, 21].

The dependence of the g-factor on the acceleration factor is particularly important. At low accelerations, such as $R = 2$, many clinical coil arrays provide acceptable SNR performance. As the acceleration factor increases, however, aliased voxels become more difficult to separate, the reconstruction becomes progressively more ill conditioned, and geometry-dependent noise amplification rises substantially. For conventional clinical parallel imaging at low-to-moderate field strengths, practical acceleration is therefore often limited to the low single-digit range [5, 6].

Figure 9 shows SNR degradation versus acceleration factor.

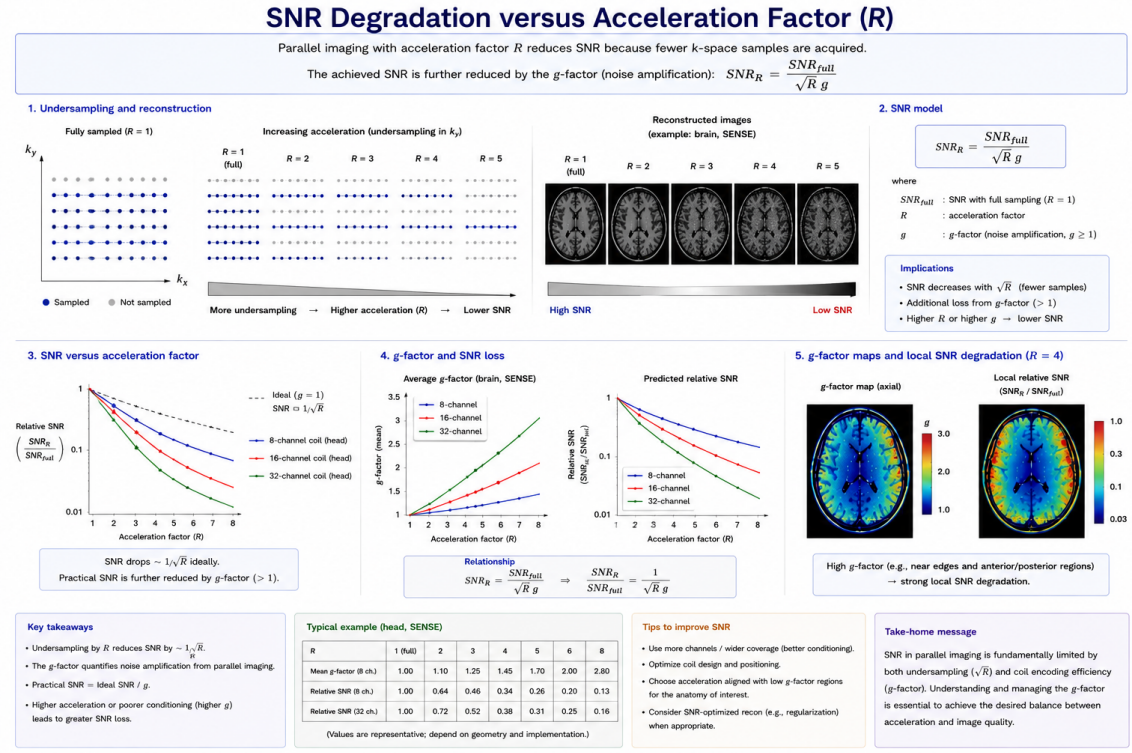

Figure 9: SNR degradation versus acceleration factor.

Noise correlations between receiver coils also influence reconstruction performance. In practical phased-array systems, receiver noise is not completely independent across channels because of overlapping coil sensitivity regions, mutual coil coupling, and receiver-dependent electronic noise contributions. These correlations are described by the noise covariance matrix $\mathbf{C}$ appearing in Eq. (18). Proper incorporation of noise statistics, together with adequate coil decoupling and receiver-channel isolation, is therefore important for preserving SNR efficiency in parallel MRI reconstruction [18, 21].

An additional practical limitation arises from imperfect sensitivity estimation. Errors in the sensitivity maps may amplify noise and produce residual aliasing artifacts. This problem becomes increasingly severe at high acceleration factors because the reconstruction depends more strongly on accurate spatial encoding

information and because aliased voxel locations become more difficult to separate [2, 12].

Although SENSE reconstruction most directly illustrates the concept of geometry-dependent noise amplification through the g-factor formalism, analogous image-quality penalties also occur in k-space methods such as GRAPPA. In GRAPPA, residual aliasing and noise enhancement may arise when the acceleration factor is too high for the available coil geometry or when the autocalibration data are insufficient to determine stable reconstruction weights. Thus, despite the different reconstruction formulation, the fundamental limitations imposed by undersampling, coil geometry, and calibration quality remain present [2, 9, 12].

The tradeoff between acceleration and SNR constitutes one of the central design considerations in parallel MRI. In practice, acceleration factors are selected to balance acquisition speed against image quality and diagnostic reliability. This compromise depends strongly on the clinical application, anatomical region, receiver-array geometry, acceleration direction, and magnetic field strength [2, 5, 6].

3.3 Practical Limitations of SENSE

Although SENSE reconstruction provides an elegant and mathematically rigorous framework for parallel MRI, its practical implementation is associated with several important limitations. These limitations arise primarily from imperfect coil sensitivity estimation, geometry-dependent noise amplification, motion-related mismatch between calibration and imaging data, and reconstruction instability at high acceleration factors [2, 5, 8].

A fundamental requirement of SENSE is accurate knowledge of the spatial coil sensitivity profiles. In the original SENSE formulation, these maps are obtained from reference measurements acquired with the definitive imaging setup. In broader practical implementations of parallel imaging, sensitivity or calibration information may also be derived from low-resolution reference data or from autocalibrating information acquired in conjunction with the accelerated scan. Because SENSE reconstruction explicitly depends on these maps through Eq. (18), errors in sensitivity estimation directly propagate into the reconstructed image and may cause residual aliasing or other reconstruction artifacts [2, 6, 8].

Figure 10 shows Sensitivity map estimation errors.

Sensitivity estimation becomes particularly difficult in regions with low signal intensity or spatially inhomogeneous object signal, such as the lung and abdomen, where precise coil sensitivity information may be difficult to determine. Sensitivity estimation can also be complicated by rapidly varying image-dependent phase, which may need to be removed before spatial smoothing of complex coil data. Furthermore, motion occurring between the calibration scan and the accelerated acquisition may lead to misregistration of the sensitivity maps. Respiratory motion or other changes in the relative position of the object and flexible receiver array can therefore produce residual aliasing artifacts or local reconstruction failures [6, 22].

Another important limitation of SENSE is its sensitivity to the conditioning of the unfolding problem. As discussed previously, the reconstruction requires inversion of the sensitivity matrix. If the coil sensitivities are insufficiently distinct at the aliased voxel locations, the matrix inversion becomes poorly conditioned and noise amplification increases substantially. This effect is quantified by the geometry factor (g-factor) [5, 8].

At high acceleration factors, the unfolding problem may become nearly singular in some image regions:

$$\det(\mathbf{S}^H \mathbf{C}^{-1} \mathbf{S}) \to 0. \tag{24}$$

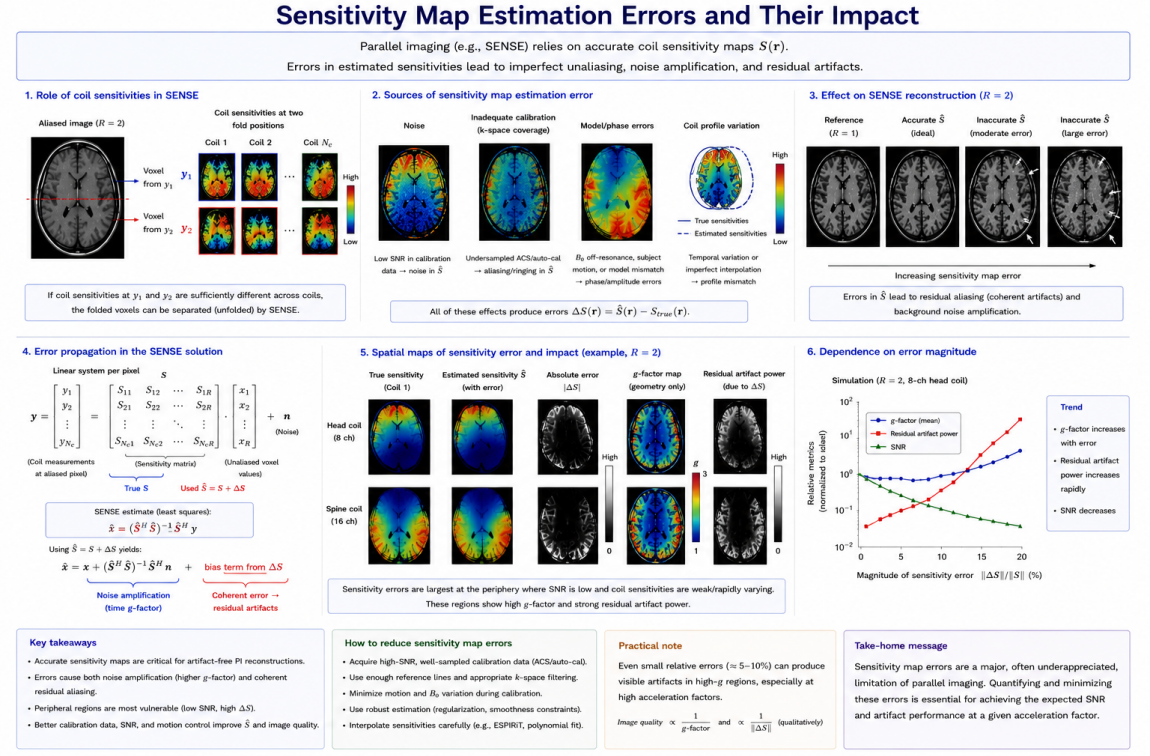

Figure 10: Sensitivity map estimation errors.

In such cases, the reconstructed image exhibits severe noise amplification and residual artifacts.

The practical acceleration limit therefore depends strongly on:

1. receiver-array geometry,
2. anatomical region,
3. field strength,
4. signal-to-noise ratio,
5. quality of sensitivity estimation.

In many routine clinical applications, acceleration factors between $R = 2$ and $R = 4$ represent a practical compromise between acquisition speed and image quality. Higher accelerations are possible with optimized high-density receiver arrays but generally require favorable coil geometry and more sophisticated reconstruction strategies [2, 5, 6].

Magnetic field inhomogeneity and susceptibility effects may also degrade SENSE performance in specific acquisition settings. In single-shot echo-planar imaging (EPI), for example, susceptibility-related image distortions can cause the apparent spatial distribution of the accelerated image data to differ from that represented by the sensitivity maps. This mismatch may impair unfolding accuracy and increase residual artifacts [6].

Additional challenges arise in dynamic or motion-sensitive applications when the effective sensitivity information changes over time. Breathing, scan-plane manipulation, or other relative motion of the receive coils may make previously estimated sensitivity maps less accurate. Adaptive approaches such as TSENSE

were developed in part to track such changes and reduce residual aliasing caused by imperfect sensitivity estimates [22].

Computational complexity also represented an important challenge for generalized SENSE formulations, particularly for arbitrary k-space trajectories. In such settings, direct solution of the reconstruction problem can require inversion of very large systems, motivating the use of iterative methods such as conjugate-gradient reconstruction. Modern hardware and optimized numerical algorithms have greatly reduced these computational barriers [18].

Despite these challenges, SENSE remains one of the foundational parallel imaging frameworks because of several important advantages:

1. mathematically direct reconstruction,
2. explicit use of coil sensitivity information,
3. compatibility with arbitrary k-space trajectories, including non-Cartesian imaging,
4. efficient reduction of echo-train length and associated distortions in applications such as EPI.

These properties made SENSE highly influential in the development of subsequent parallel imaging methods and model-based reconstruction strategies [2, 8, 18].

The conceptual framework introduced by SENSE also informed later hybrid approaches that combine explicit sensitivity modeling with autocalibrated reconstruction principles. ESPIRiT, for example, explicitly links SENSE-like sensitivity-map reconstruction with GRAPPA-like calibration concepts and extends the framework through relaxed multi-map reconstruction [20].

An alternative strategy for parallel MRI reconstruction avoids explicit image-space unfolding altogether. Instead of solving the reconstruction problem directly in image space, missing k-space lines may be synthesized from neighboring acquired data using calibration information. This approach forms the basis of k-space parallel imaging methods such as SMASH and GRAPPA, which are discussed in the following section [6, 7, 9].

4 k-Space Parallel Imaging

4.1 SMASH and AUTO-SMASH

While SENSE reconstructs accelerated MRI data directly in image space, an alternative class of methods performs the reconstruction in k-space. These approaches synthesize missing phase-encoding lines before Fourier transformation and therefore avoid explicit image-space unfolding. The first successful in vivo implementation of this concept was SMASH (Simultaneous Acquisition of Spatial Harmonics), introduced by Sodickson and Manning in 1997 [1, 7].

The central idea of SMASH is to use appropriately weighted combinations of receiver-coil sensitivities to synthesize spatial harmonic functions that mimic conventional phase encoding. Instead of explicitly measuring all phase-encoding steps with magnetic field gradients, part of the missing encoding information is generated mathematically from the spatial sensitivity variations of the receiver array, thereby producing shifted k-space lines from weighted combinations of simultaneously acquired coil signals [6, 7, 23].

In Cartesian MRI, a conventional phase-encoding gradient produces a spatial phase modulation of the form

$$e^{im\Delta k_y y}, \tag{25}$$

where m denotes the phase-encoding order and Δk_y is the fundamental k-space increment in the phase-encoding direction. SMASH attempts to reproduce these spatial harmonic functions through linear combinations of the coil sensitivities:

$$\sum_{c=1}^{N_c} w_c^{(m)} S_c(y) \approx e^{im\Delta k_y y}, \tag{26}$$

where $w_c^{(m)}$ are weighting coefficients for harmonic order m, and $S_c(y)$ denotes the sensitivity profile of coil c [6, 7].

Figure 11 shows SMASH spatial harmonic synthesis.

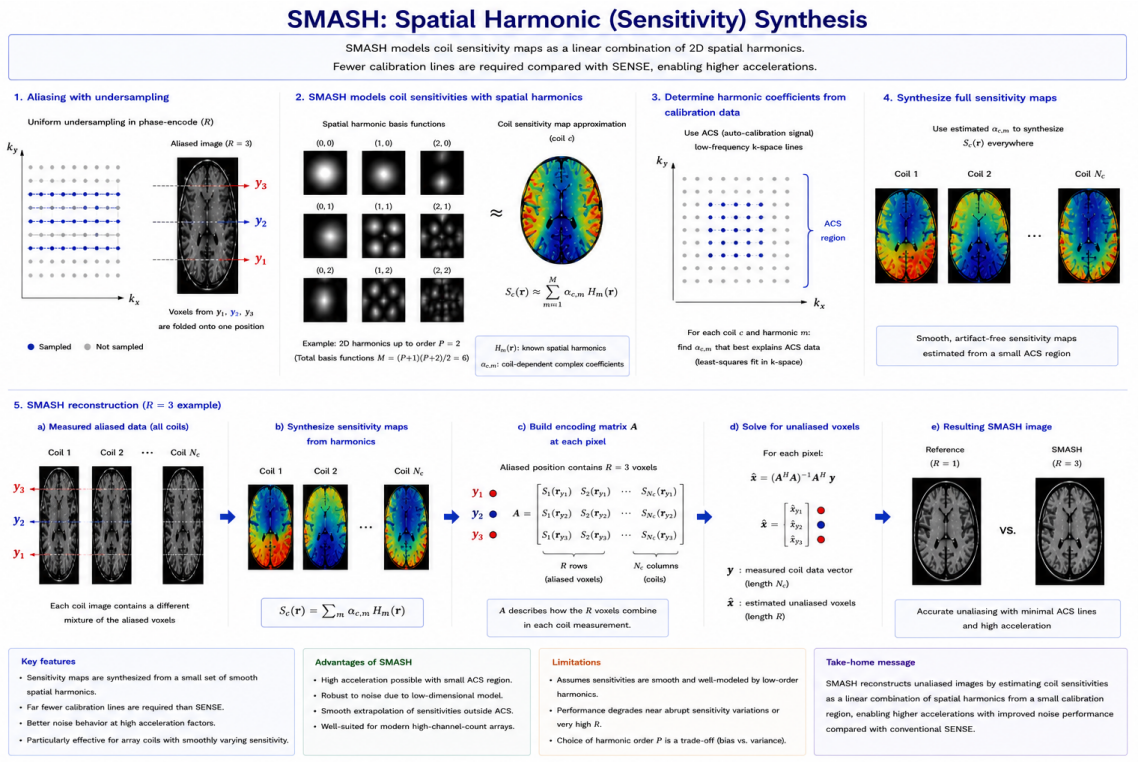

Figure 11: SMASH spatial harmonic synthesis.

Once these harmonic functions are generated, the missing phase-encoding lines in k-space may be synthesized directly from weighted combinations of the acquired coil data. The reconstructed k-space can then be Fourier transformed to produce the final image [6, 7, 23].

An important advantage of SMASH is that reconstruction occurs in k-space before image formation. Consequently, explicit image-space unfolding and pixel-wise matrix inversion are avoided [6, 7].

However, the original SMASH formulation also exhibited several important limitations. Accurate synthesis of the required spatial harmonics proved difficult in practice because real coil sensitivities rarely match ideal harmonic functions over the entire field of view. Imperfect harmonic fitting therefore produced residual artifacts and reduced reconstruction robustness [6, 23].

Another challenge was the strong dependence on coil geometry. The receiver-array sensitivities had to provide sufficient spatial variation to approximate the desired harmonic functions accurately. In practice, this requirement limited robustness and constrained the achievable acceleration when the array could not generate the required spatial harmonics with adequate fidelity [6, 23].

To improve reconstruction stability, several extensions of SMASH were subsequently developed. AUTO-SMASH introduced autocalibration techniques in which additional reference data were acquired during the scan itself to estimate reconstruction coefficients without a separate explicit sensitivity-map measurement. Variable-density AUTO-SMASH further improved reconstruction robustness by acquiring multiple autocalibration signal (ACS) lines in central k-space, which increased the number of available fits for coefficient estimation and reduced residual artifact power in imperfect reconstructions [6, 9, 23].

Although later methods such as GRAPPA addressed many of the limitations of SMASH and became more prominent in clinical k-space parallel imaging, the conceptual importance of SMASH was enormous. The method demonstrated for the first time that phased-array coil sensitivities could successfully replace part of conventional gradient encoding in vivo. Many central concepts of modern parallel imaging, including calibration-based reconstruction and k-space synthesis of missing data, emerged directly from the SMASH framework [1, 6, 7, 9].

SMASH also helped establish the fundamental distinction between image-domain and k-space-domain parallel imaging approaches. Whereas SENSE performs explicit unfolding in image space using sensitivity maps, SMASH-type methods attempt to reconstruct a complete k-space representation before Fourier transformation. This distinction strongly influenced the subsequent evolution of accelerated MRI reconstruction techniques [1, 6].

The limitations of SMASH ultimately motivated the development of more robust calibration-based k-space methods, most importantly GRAPPA (Generalized Autocalibrating Partially Parallel Acquisitions), which became one of the principal clinically used parallel imaging methods [6, 9].

4.2 GRAPPA Reconstruction

GRAPPA (Generalized Autocalibrating Partially Parallel Acquisitions), introduced by Griswold et al. in 2002, represents one of the most influential and widely used k-space parallel imaging methods [9]. In contrast to SENSE, GRAPPA reconstructs missing k-space data directly from neighboring acquired samples without requiring explicit image-space unfolding or direct inversion of coil sensitivity matrices.

The fundamental concept of GRAPPA is illustrated schematically in Fig. 12.

During acquisition, k-space is undersampled along the phase-encoding direction, while a fully sampled central calibration region is additionally acquired. These fully sampled reference lines are commonly referred to as autocalibration signal (ACS) lines [9].

The ACS data are used to estimate interpolation coefficients, or reconstruction weights, that relate neighboring acquired k-space samples to missing samples. The missing k-space lines are then synthesized by applying these weights throughout the undersampled acquisition [9, 12].

In GRAPPA, each missing k-space point is reconstructed from a local neighborhood of acquired samples across multiple receiver coils. The reconstruction may be expressed as

$$S_j(k_y + m\Delta k_y) = \sum_{l=1}^{N_c} \sum_{b} n(j, b, l, m)\, S_l(k_y + bA\Delta k_y), \tag{27}$$

where:

- S_j denotes the reconstructed signal in coil j,
- S_l denotes acquired signals from neighboring coils,

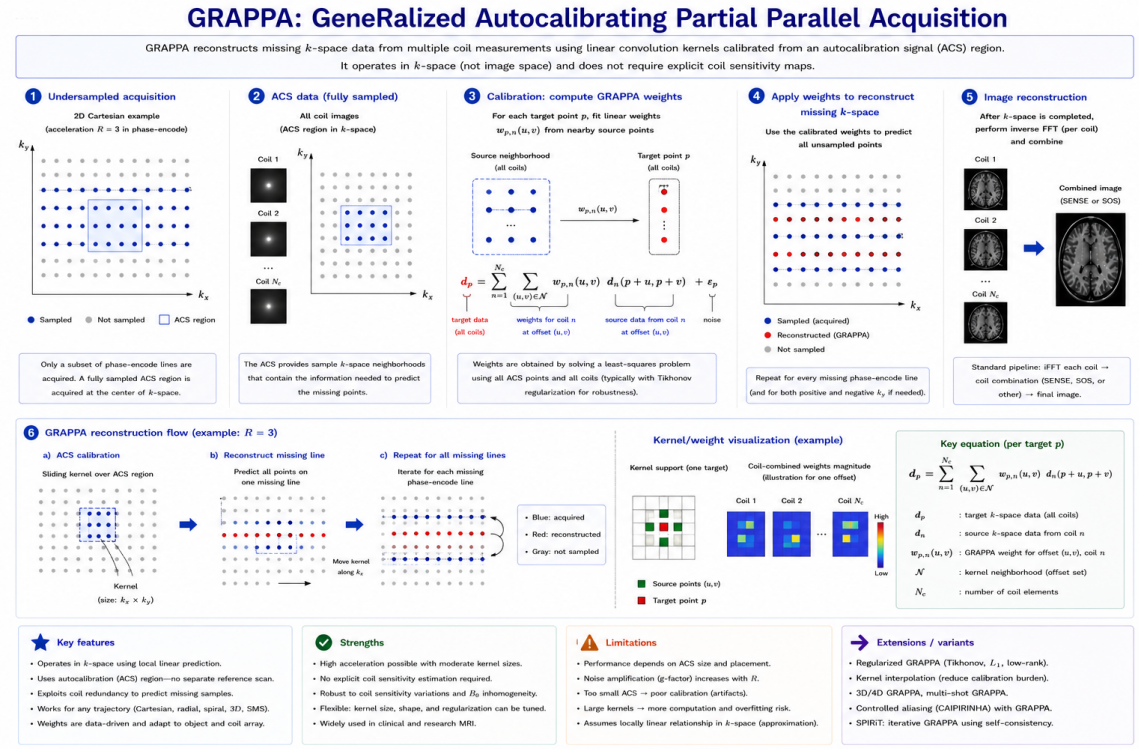

Figure 12: GRAPPA overview.

- $n(j, b, l, m)$ are the GRAPPA reconstruction weights,
- A is the acceleration factor,
- b indexes neighboring acquired samples.

The reconstruction weights are determined from the ACS region by solving an overdetermined linear fitting problem. Because the ACS data are fully sampled, both the target samples and the neighboring source samples are known within the calibration region. The calibration process therefore estimates the interpolation kernels directly from the measured data [9].

Figure 13 shows GRAPPA kernel geometry.

1. acquired source points,
2. missing target points,
3. neighboring coil contributions.

Once the reconstruction kernels have been calibrated, the missing k-space lines are synthesized throughout the undersampled acquisition. After reconstruction of the missing data, each coil possesses a complete k-space dataset. Standard Fourier transformation is then applied independently to each coil, followed by coil combination using methods such as root-sum-of-squares reconstruction or other array-combination strategies [9, 12].

An important practical advantage of GRAPPA is that the reconstruction occurs directly in k-space and does not require explicit precomputed coil sensitivity maps. Because its calibration information is commonly acquired together with the accelerated scan, GRAPPA can be less vulnerable than conventional

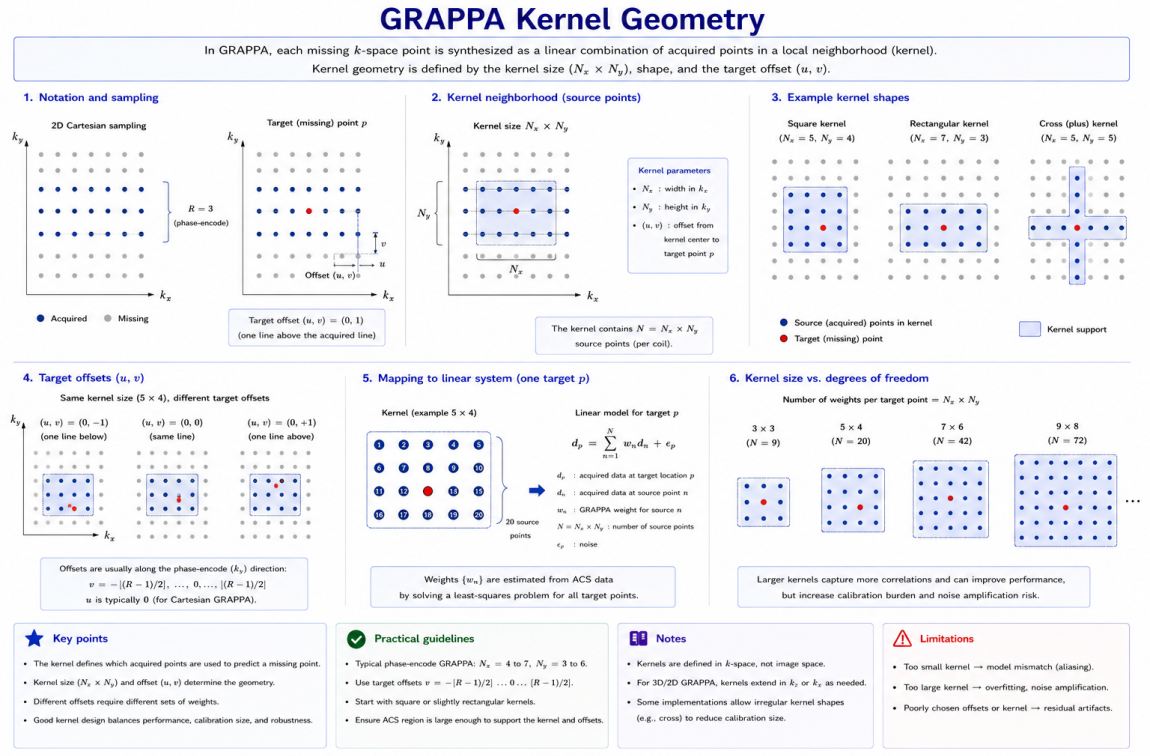

Figure 13: GRAPPA kernel geometry.

prescan-based SENSE to errors caused by patient motion, coil-position changes, or mismatches between calibration and imaging data. This robustness contributed substantially to its broad clinical adoption [6, 9, 20].

Figure 14 shows the SENSE versus GRAPPA reconstruction pipeline.

The GRAPPA reconstruction process may be summarized as follows:

1. acquisition of undersampled k-space,
2. acquisition of fully sampled ACS lines,
3. calibration of reconstruction kernels,
4. synthesis of missing k-space lines,
5. Fourier transformation of reconstructed coil data,
6. combination of coil images.

Because the reconstruction kernels are estimated directly from the measured calibration data, GRAPPA adapts naturally to the actual coil sensitivities and imaging geometry without requiring explicit sensitivity-map estimation. This self-calibrating property makes the method particularly attractive in clinical practice, where separate sensitivity calibration scans may be undesirable or vulnerable to mismatch between calibration and imaging data [2, 9].

The size and geometry of the reconstruction kernel strongly influence image quality and reconstruction stability. Small kernels may insufficiently capture the spatial correlations required for accurate interpolation, whereas excessively large kernels reduce the number of independent calibration examples available within

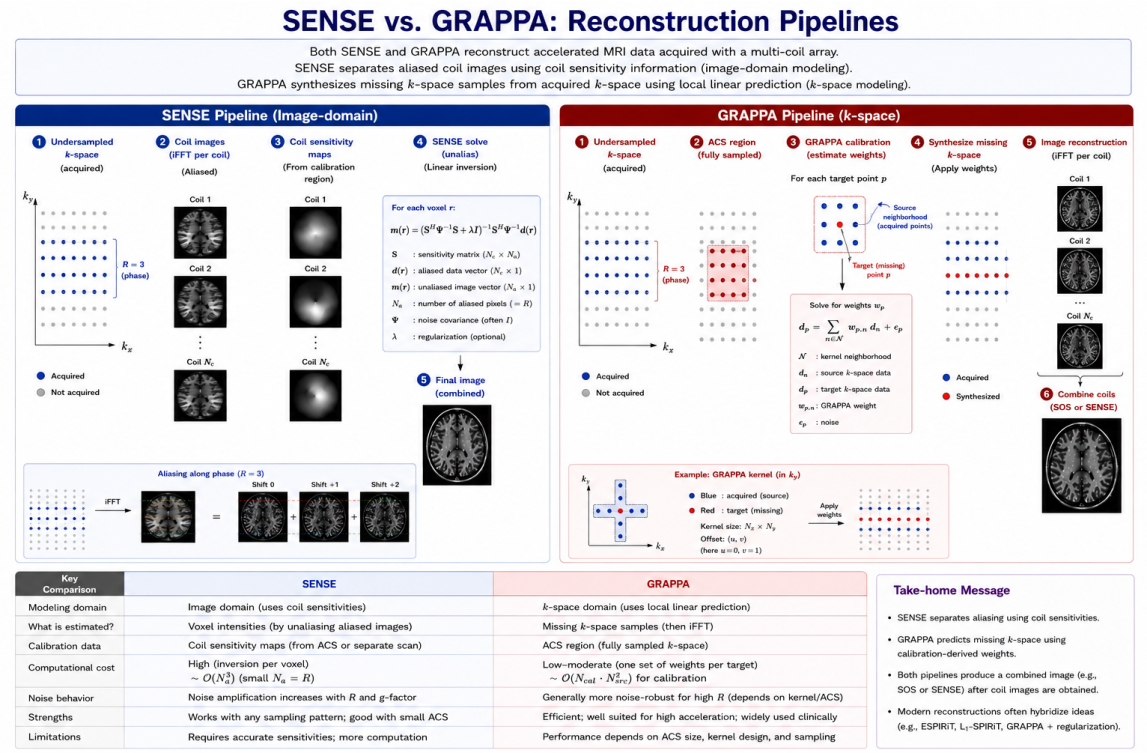

Figure 14: SENSE versus GRAPPA pipeline.

the ACS region and may compromise kernel estimation. Practical implementations therefore employ carefully optimized kernel configurations together with a sufficient number of ACS lines [2, 9, 12].

As in all parallel imaging methods, GRAPPA reconstruction is associated with noise amplification and SNR reduction. The corresponding spatially varying noise penalty may be characterized by a GRAPPA g-factor. Unlike the SENSE g-factor, which is derived directly from the coil-sensitivity matrix, the GRAPPA g-factor is computed from the reconstruction weights or kernels. Thus, the noise behavior is described within a different mathematical framework, even though it reflects the same underlying dependence on coil geometry and undersampling [2, 19].

Another important characteristic of GRAPPA is the broad flexibility of calibration-based k-space reconstruction. GRAPPA and closely related variants have been developed for:

- Cartesian imaging,
- echo-planar imaging (EPI),
- radial imaging,
- spiral imaging,
- dynamic imaging with temporal recalibration.

In parallel, GRAPPA-related calibration concepts have also contributed to more advanced accelerated imaging strategies, including simultaneous multislice and CAIPIRINHA-type methods [9, 14, 24–26].

This flexibility contributed greatly to the broad clinical and methodological success of GRAPPA and related calibration-based methods.

The key elements are:

1. fully sampled acquisition,
2. undersampled acquisition,
3. GRAPPA reconstruction,
4. residual artifact patterns.

GRAPPA rapidly became integrated into many MRI applications, including diffusion-weighted imaging, functional MRI, cardiovascular imaging, and angiographic imaging. In echo-planar imaging, parallel imaging shortens the effective readout and can thereby reduce geometric distortion; specialized GRAPPA-based methods have also been developed to address EPI ghosting and phase-error correction directly [2, 4, 19].

4.3 GRAPPA Variants and Extensions

Following the introduction of GRAPPA, numerous extensions and modifications were developed to improve reconstruction robustness, extend applicability to dynamic imaging, and support non-Cartesian acquisition trajectories. Several of these variants remain important components of modern accelerated MRI methodology.

One important extension is TGRAPPA (Temporal GRAPPA), which was developed for dynamic and cardiac MRI applications [26]. In dynamic imaging, coil sensitivities and object position may vary over time, making static calibration insufficient. TGRAPPA addresses this problem by using a time-interleaved acquisition scheme in which neighboring temporal frames are combined to generate full-resolution autocalibration data and update the GRAPPA reconstruction weights dynamically.

TGRAPPA proved particularly useful in real-time cardiac MRI, where respiratory motion and changing coil positions can complicate conventional calibration procedures. The method was demonstrated for accelerated, nongated, free-breathing cardiac imaging and provided dynamically updated reconstruction parameters with improved artifact suppression [10, 26].

Another important extension is radial GRAPPA, developed for non-Cartesian radial k-space trajectories [24]. In radial imaging, k-space is sampled along rotating spokes rather than Cartesian lines. Although radial trajectories inherently oversample central k-space and may offer some robustness to motion, reconstruction of undersampled radial acquisitions remains challenging.

Radial GRAPPA extends the GRAPPA concept by synthesizing missing radial projections from neighboring acquired projections across multiple receiver coils. Because the geometry of radial trajectories differs fundamentally from Cartesian sampling, specialized reconstruction weights and trajectory-aware calibration procedures are required [24].

Parallel imaging methods were also developed for accelerated spiral trajectories. Auto-calibrated parallel spiral imaging demonstrated the feasibility of calibration-based acceleration for spiral readouts, while later spiral GRAPPA approaches extended these ideas to direct non-Cartesian k-space reconstruction [25, 27]. Spiral trajectories provide highly efficient k-space coverage but are particularly sensitive to off-resonance effects and gradient imperfections. Parallel imaging can improve their practical utility by reducing readout duration and thereby limiting associated distortions.

Echo-planar imaging (EPI) also became one of the most important applications of GRAPPA-type acceleration. In EPI, long readout trains produce geometric distortion, susceptibility-related artifacts,

and image blurring. Parallel imaging reduces the required number of phase-encoding steps and therefore shortens the EPI echo train substantially [2, 19].

The reduction of EPI distortion proved especially valuable in:

- diffusion-weighted imaging (DWI),
- functional MRI (fMRI),
- perfusion imaging,
- high-resolution brain imaging.

Another major development was the use of GRAPPA-type reconstruction for simultaneous multi-slice (SMS) imaging. In SMS acquisitions, several slices are excited simultaneously, producing intentional slice aliasing. Slice-GRAPPA separates the simultaneously acquired slices by applying slice-specific GRAPPA kernels that are calibrated from individually acquired reference data [14].

Controlled aliasing methods such as CAIPIRINHA (Controlled Aliasing in Parallel Imaging Results in Higher Acceleration) further improved SMS imaging by deliberately shifting the aliased slices relative to each other. This shift increases the effective variation of coil sensitivities among simultaneously excited slices, improves conditioning of the slice-separation problem, and reduces geometry-dependent noise amplification [14].

Figure 15 shows SMS and CAIPIRINHA slice shifting.

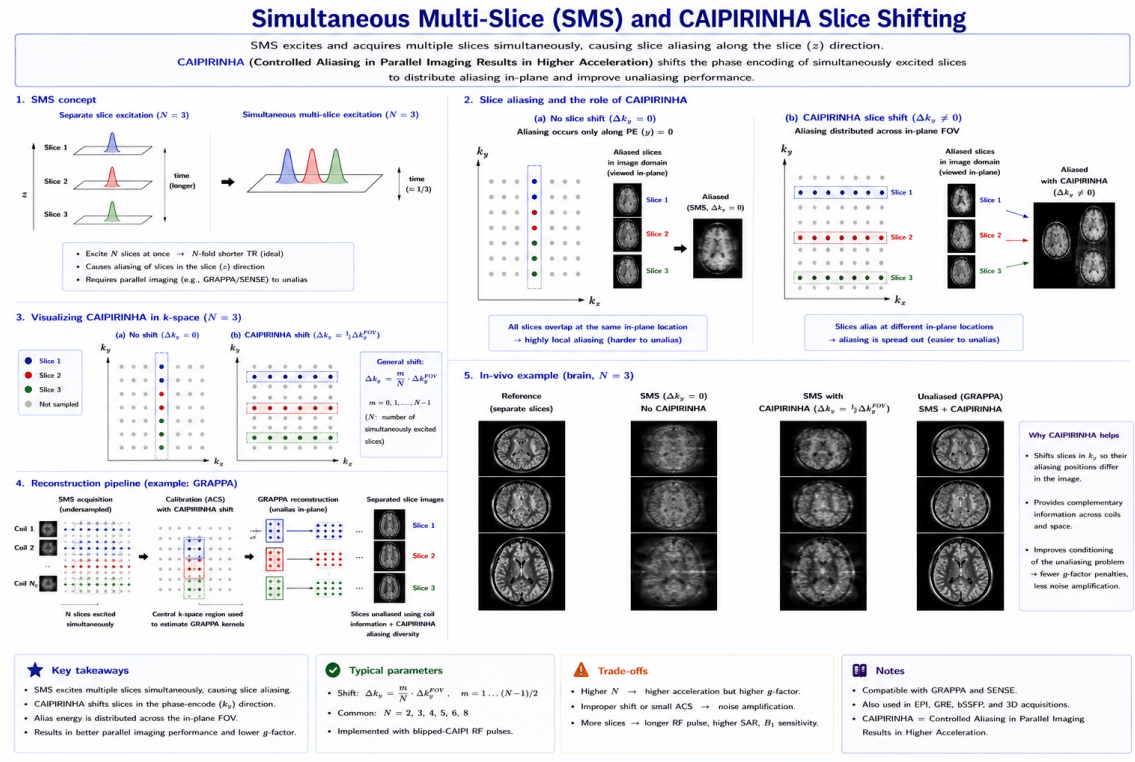

Figure 15: SMS and CAIPIRINHA slice shifting.

1. simultaneous multi-slice excitation,
2. slice aliasing,

3. CAIPIRINHA slice shifting,

4. reconstructed separated slices.

Modern variants such as Wave-CAIPI combine controlled aliasing with additional sinusoidal gradient modulations during readout to distribute aliasing more favorably across all three spatial dimensions [15]. These approaches permit very high acceleration factors while maintaining relatively low geometry-factor penalties in suitable 3D imaging applications.

Iterative reconstruction methods also emerged as important extensions of calibration-based parallel imaging. SPIRiT (Iterative Self-Consistent Parallel Imaging Reconstruction) generalized the GRAPPA calibration concept by enforcing self-consistency among all receiver channels through iterative optimization [12]. In SPIRiT, the reconstructed multi-coil k-space must remain consistent both with the acquired data and with calibration relationships learned from autocalibration data.

The SPIRiT framework also facilitated integration with compressed sensing methods. Hybrid approaches combining:

- parallel imaging,
- sparsity constraints,
- iterative regularization,
- calibration consistency

became increasingly important in modern MRI acceleration [28]. Related dynamic MRI methods further incorporated low-rank structure together with sparsity constraints to exploit spatiotemporal redundancy [13].

Figure 16 shows parallel imaging plus compressed sensing.

1. conventional parallel imaging,

2. compressed sensing,

3. hybrid PI+CS reconstruction.

A major conceptual advance was ESPIRiT (Eigenvalue-based Parallel Imaging Reconstruction), which unified aspects of SENSE and GRAPPA within a common mathematical framework [20]. ESPIRiT derives sensitivity maps directly from calibration data through eigenvalue decomposition and thereby combines the explicit encoding interpretation of SENSE with the robustness of autocalibrated k-space methods.

The continuing evolution of GRAPPA-type and calibration-based methods reflects a broader trend in MRI reconstruction: the transition from direct analytical reconstruction toward increasingly sophisticated iterative and model-based reconstruction frameworks. Modern accelerated MRI frequently combines multiple complementary strategies, including:

- parallel imaging,
- compressed sensing,
- low-rank modeling,

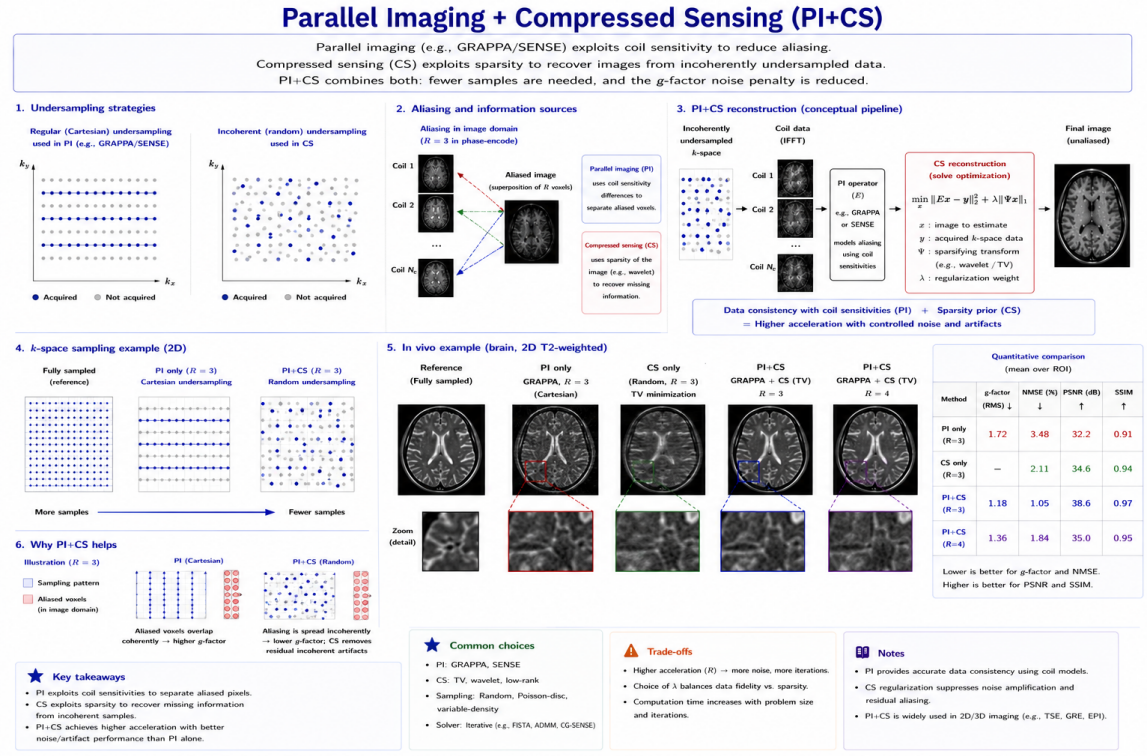

Figure 16: Parallel imaging plus compressed sensing.

- motion-aware reconstruction,
- deep-learning-based reconstruction.

These developments have substantially expanded the practical acceleration range of MRI and have transformed accelerated reconstruction into a central component of contemporary MRI methodology [13, 16, 20, 28].

4.4 Noise Amplification and Artifacts in GRAPPA

As in all parallel imaging techniques, GRAPPA reconstruction is associated with signal-to-noise ratio (SNR) degradation and reconstruction artifacts. Accelerated acquisition inevitably reduces the amount of acquired data and thereby lowers SNR. Additional noise amplification is introduced during reconstruction of the missing k-space lines. Compared with conventional prescan-based SENSE, GRAPPA can be more robust to inconsistencies between calibration and accelerated acquisition data because it does not require explicit precomputed sensitivity maps, although it remains vulnerable to inaccurate or insufficient calibration [2, 9, 19].

The intrinsic SNR reduction caused by undersampling follows approximately the same relationship as in other parallel imaging methods:

$$\mathrm{SNR}_{\mathrm{acc}} \approx \frac{\mathrm{SNR}_{\mathrm{full}}}{\sqrt{R}}, \tag{28}$$

where R denotes the acceleration factor.

In GRAPPA, however, the reconstruction process itself further modifies the noise distribution because the missing k-space samples are synthesized from weighted combinations of neighboring acquired

data. Since the interpolation kernels combine noisy measurements from multiple receiver coils, the reconstruction introduces spatially varying noise propagation throughout the final image [2, 9].

Unlike SENSE, where the geometry factor (g-factor) is derived directly from the conditioning of the coil-sensitivity matrix, the GRAPPA g-factor is computed from the reconstruction weights or kernels. GRAPPA reconstructions therefore also exhibit geometry-dependent noise amplification, although the mathematical description is formulated in terms of calibrated interpolation operators rather than explicit image-space matrix inversion [2, 19]. Noise amplification generally increases with:

1. higher acceleration factors,
2. insufficient coil sensitivity variation,
3. inadequate ACS calibration data,
4. suboptimal kernel geometry.

Figure 17 shows GRAPPA noise amplification.

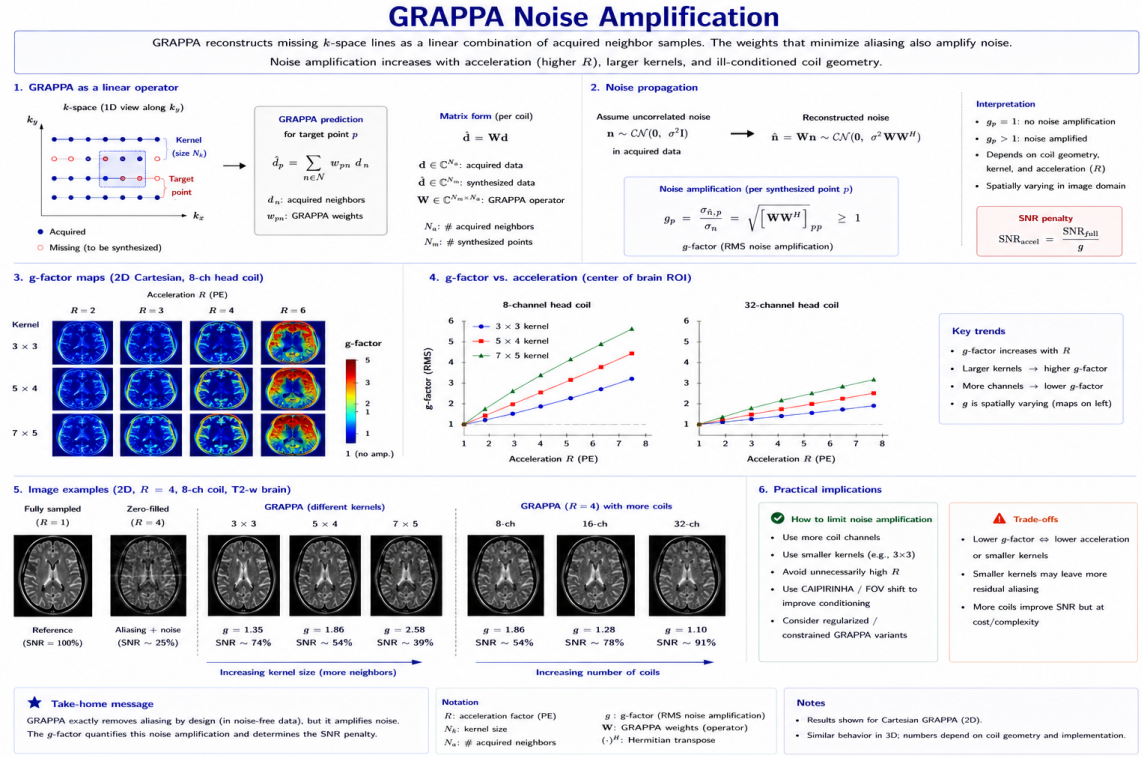

Figure 17: GRAPPA noise amplification.

One of the most important practical factors in GRAPPA reconstruction is the size and quality of the ACS region. The ACS lines provide the calibration data required to estimate the reconstruction kernels. If too few ACS lines are acquired, the calibration problem becomes insufficiently constrained or unstable, leading to inaccurate kernel estimation and elevated reconstruction artifacts. Increasing the ACS size generally improves the robustness of the estimated weights, although at the cost of additional acquisition time [2, 9].

Figure 18 shows the effect of ACS size on GRAPPA.

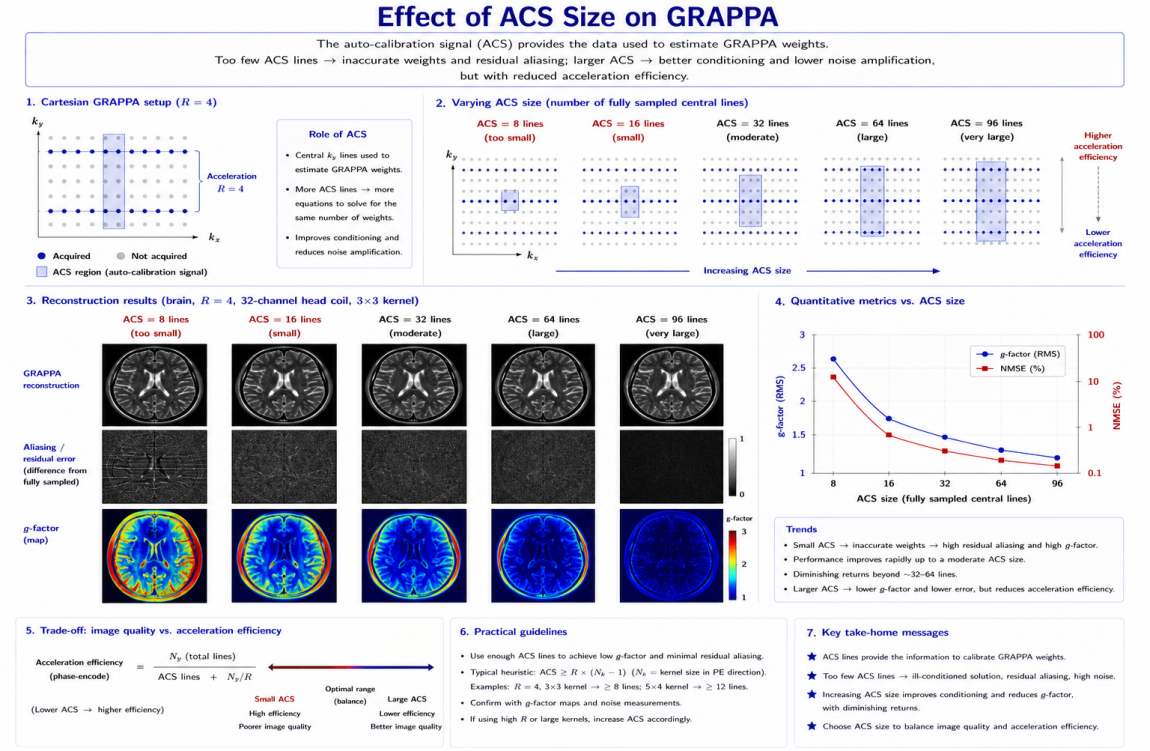

Figure 18: Effect of ACS size on GRAPPA.

Several characteristic artifact types may occur in GRAPPA imaging. Residual aliasing artifacts arise when the interpolation kernels fail to reconstruct the missing k-space lines accurately. These artifacts often appear as ghost structures or residual fold-over patterns. Noise enhancement may also produce spatially nonuniform image texture and local SNR degradation. In many cases, residual aliasing and noise enhancement arise from the same underlying limitation: the chosen acceleration factor is too high for the available coil geometry and calibration quality [2].

Another important source of artifacts is inconsistency between the ACS calibration data and the undersampled acquisition data. Motion occurring between calibration and acquisition may alter the effective coil sensitivities or object geometry, thereby degrading kernel accuracy. GRAPPA is often less sensitive to this problem than conventional SENSE, but sufficiently large calibration mismatch can still impair reconstruction quality. This issue is especially relevant in motion-prone settings such as cardiac, abdominal, and free-breathing acquisitions [19, 25].

Echo-planar imaging (EPI) introduces additional reconstruction challenges. In EPI, phase inconsistencies between data acquired with alternating readout-gradient polarities may produce Nyquist ghost artifacts. Parallel imaging reconstruction may interact with these phase errors and degrade image quality unless appropriate correction procedures are applied. Dual-Polarity GRAPPA was developed specifically to combine accelerated EPI reconstruction with correction of higher-order phase errors and Nyquist ghosting [4].

The geometry of the reconstruction kernel also strongly influences artifact behavior. Small kernels may insufficiently capture local spatial correlations, whereas excessively large kernels reduce the number of independent calibration examples available within the ACS region and may compromise the stability of weight estimation. Practical GRAPPA implementations therefore employ carefully optimized kernel

dimensions and, where needed, regularization strategies [2, 12].

Non-Cartesian GRAPPA methods such as radial or spiral GRAPPA introduce additional challenges because the local sampling geometry varies across k-space. Each target point may require a distinct local reconstruction geometry, making calibration more complex than in Cartesian imaging. Specialized calibration procedures, segmentation strategies, or through-time calibration approaches are therefore required for robust reconstruction [19, 24, 25].

Despite these limitations, GRAPPA possesses several important practical advantages compared with image-domain methods such as SENSE:

1. no explicit sensitivity maps are required,
2. reduced sensitivity to calibration mismatch in many practical settings,
3. compatibility with conventional Fourier-based reconstruction workflows,
4. strong robustness in many clinical applications,
5. flexibility for Cartesian and non-Cartesian trajectories.

These advantages contributed substantially to the widespread adoption of GRAPPA in clinical MRI systems. In practice, GRAPPA often provides superior robustness in challenging imaging situations involving sensitivity-map mismatch, whereas SENSE may offer greater theoretical reconstruction efficiency when highly accurate coil sensitivity maps are available [2, 19, 20].

The complementary strengths and weaknesses of image-domain and k-space-domain reconstruction methods motivated extensive comparisons between SENSE and GRAPPA and stimulated the development of hybrid reconstruction frameworks that combine aspects of both approaches [12, 20].

5 Comparison of SENSE and GRAPPA

SENSE and GRAPPA represent the two major classical approaches to parallel MRI reconstruction. Although both methods exploit the spatial encoding information provided by phased-array receiver coils, they differ fundamentally in reconstruction strategy, calibration requirements, noise behavior, and practical implementation [8, 9, 20].

The most important conceptual distinction lies in the reconstruction domain. SENSE performs reconstruction directly in image space by explicitly unfolding aliased images using coil sensitivity maps. GRAPPA, in contrast, reconstructs missing k-space samples prior to image formation through local interpolation kernels derived from calibration data [8, 9].

In SENSE, the reconstruction problem is formulated explicitly as a linear inverse problem:

$$\mathbf{v} = \mathbf{S}\mathbf{a}, \tag{29}$$

where $\mathbf{S}$ contains the coil sensitivity information and $\mathbf{a}$ denotes the unknown unfolded image voxels. Reconstruction therefore requires explicit estimation of the coil sensitivity maps.

GRAPPA avoids explicit image-space inversion by synthesizing missing k-space lines from neighboring acquired data:

$$S_{\text{missing}} = \sum_i w_i S_i, \tag{30}$$

where the weights w_i are estimated from fully sampled autocalibration signal (ACS) lines [9].

One important practical consequence of this distinction is the differing sensitivity to calibration errors and motion. Because SENSE depends directly on accurate coil sensitivity maps, it is particularly vulnerable to:

- patient motion between calibration and imaging,
- mismatch between reference data and accelerated acquisition,
- inaccuracies in estimated coil sensitivity maps,
- incomplete or poorly conditioned spatial encoding.

GRAPPA is often more robust to these specific sensitivity-map mismatches because the reconstruction kernels are calibrated directly from measured reference data acquired in conjunction with the scan. This autocalibrating property contributed substantially to the broad clinical adoption of GRAPPA-type methods [6, 20].

The noise behavior of the two methods also differs substantially. In SENSE, noise amplification is directly related to the conditioning of the sensitivity matrix and is quantified explicitly by the geometry factor (g-factor):

$$\mathrm{SNR}_{\mathrm{SENSE}} = \frac{\mathrm{SNR}_{\mathrm{full}}}{g\sqrt{R}}. \tag{31}$$

In GRAPPA, noise propagation occurs through interpolation of missing k-space data using calibrated reconstruction weights. The resulting noise amplification is less directly linked to an explicit sensitivity-matrix inversion, but it remains geometry dependent and can be characterized through the reconstruction kernels. Both methods therefore exhibit increased noise amplification at high acceleration factors and for poorly conditioned coil geometries [2, 6].

Another important distinction concerns computational structure. Classical Cartesian SENSE reconstruction involves local matrix inversion for each set of aliased voxel locations, whereas GRAPPA requires calibration and convolution-like interpolation operations in k-space. These algorithmic differences historically influenced implementation strategies, although modern reconstruction hardware has reduced their practical importance.

The two methods also differ in their compatibility with non-Cartesian imaging trajectories. SENSE extends naturally to arbitrary trajectories because the reconstruction can be formulated directly in terms of the acquisition encoding operator [18]. Non-Cartesian GRAPPA methods are also possible, but they generally require more specialized reconstruction strategies and calibration procedures tailored to the local sampling geometry [24, 25].

In clinical and methodological practice, GRAPPA-type approaches have been widely used in:

- echo-planar imaging (EPI),
- diffusion-weighted imaging,
- functional MRI,
- cardiac cine imaging,
- angiographic and other dynamic applications.

SENSE-type approaches have remained especially important in:

- applications requiring explicit sensitivity-based reconstruction,
- cardiovascular imaging,
- non-Cartesian imaging,
- flexible model-based reconstruction frameworks.

A concise comparison between both methods is summarized in Table 1.

Table 1: Comparison between SENSE and GRAPPA reconstruction methods.

Property	SENSE	GRAPPA
Reconstruction domain	Image space	k-space
Calibration	Coil sensitivity maps	ACS-based kernel calibration
Reconstruction type	Local linear inversion	Local k-space interpolation
Sensitivity to calibration mismatch	Higher	Often lower
Noise description	Explicit g-factor formulation	Kernel-based noise propagation
Non-Cartesian imaging	Natural extension	More specialized variants
Clinical implementation	Widely used	Widely used
Representative strengths	Sensitivity-based modeling	Autocalibrated robustness

Despite their differences, SENSE and GRAPPA are fundamentally closely related. Both methods exploit the same underlying principle: replacement of part of conventional gradient encoding by spatial encoding provided through phased-array coil sensitivities. ESPIRiT later demonstrated this connection explicitly by showing that SENSE-like sensitivity maps can be derived from GRAPPA-like calibration operators [20].

Modern iterative reconstruction methods increasingly blur the distinction between image-domain and k-space-domain approaches. Frameworks such as SPIRiT and ESPIRiT combine aspects of SENSE and GRAPPA within unified mathematical formulations [12, 20]. Furthermore, contemporary accelerated MRI frequently integrates parallel imaging with compressed sensing, low-rank modeling, and deep-learning-based reconstruction.

Figure 19 shows a unified iterative reconstruction framework.

The comparison between SENSE and GRAPPA ultimately demonstrates that parallel imaging is not a single reconstruction method but rather a broad family of approaches exploiting phased-array coil encoding to accelerate MRI acquisition. The choice of reconstruction strategy depends strongly on the imaging application, acquisition trajectory, receiver-array geometry, and desired balance between acquisition speed, robustness, and image quality.

6 Advanced Parallel Imaging Methods

6.1 Dynamic and Time-Resolved Parallel Imaging

Many MRI applications require rapid acquisition of temporally varying data. Examples include cardiac cine imaging, perfusion MRI, functional MRI (fMRI), dynamic contrast-enhanced imaging, and real-time MRI. In these applications, both spatial and temporal resolution are important, creating particularly demanding acquisition requirements.

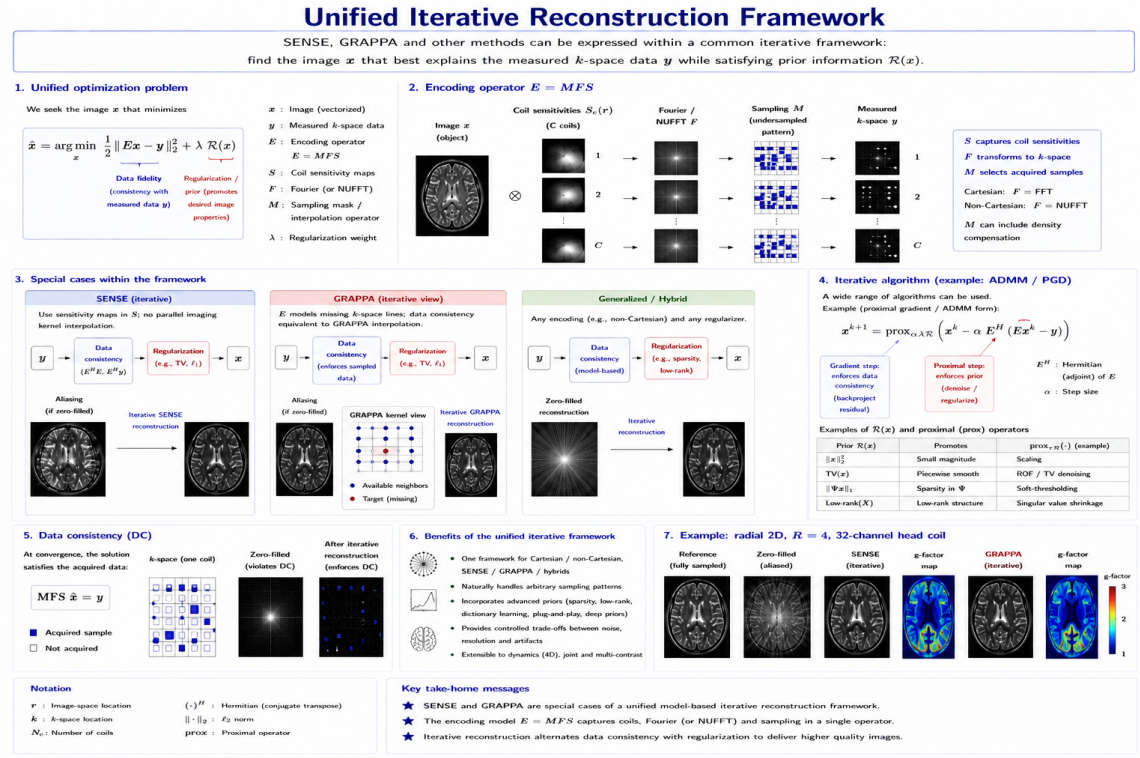

Figure 19: Unified iterative reconstruction framework.

Parallel imaging proved highly valuable for dynamic MRI because accelerated acquisition directly improves temporal resolution. However, dynamic imaging also introduces additional reconstruction challenges, including motion, changing contrast, and time-varying signal distributions [10, 26, 29].

One important development was TSENSE (Temporal SENSE), which extends the original SENSE framework to dynamic imaging [22]. In TSENSE, sensitivity information is estimated adaptively from temporally interleaved data rather than from separate static calibration scans. Temporal low-pass filtering is used to suppress aliased components in the reference estimate, allowing coil sensitivity estimates to track relatively slow changes caused by breathing, scan-plane manipulation, or other motion while maintaining compatibility with dynamic acquisitions.

A closely related approach is TGRAPPA (Temporal GRAPPA), in which GRAPPA reconstruction kernels are updated dynamically using temporally neighboring k-space frames [26]. In this approach, adjacent time frames are merged to generate fully encoded autocalibration information, enabling frame-by-frame updating of the reconstruction weights and improved tracking of time-varying relative coil sensitivities.

These dynamic parallel imaging methods enabled major advances in cardiovascular MRI. TSENSE was demonstrated for nonbreath-held real-time cardiac imaging during exercise stress, while TGRAPPA was applied to accelerated, nongated, free-breathing cardiac studies with reduction factors of approximately $R = 2$–4 [22, 26]. More broadly, parallel imaging improved cine imaging, myocardial perfusion imaging, and coronary MR angiography by increasing temporal resolution and reducing acquisition burden [2, 10].

Parallel imaging furthermore became highly important in functional MRI (fMRI) and diffusion-weighted imaging (DWI). In these applications, echo-planar imaging (EPI) is commonly employed because of its extremely rapid acquisition speed. However, long EPI echo trains produce susceptibility-related

geometric distortion, signal dropout, and image blurring. Parallel imaging reduces the required number of phase-encoding steps and thereby shortens the EPI readout duration substantially [2, 19].

The reduction of EPI distortion becomes particularly important at higher magnetic field strengths, where susceptibility effects are more pronounced. Modern high-field accelerated imaging therefore frequently combines parallel imaging with advanced controlled-aliasing strategies, including blipped-CAIPI and Wave-CAIPI, to preserve image quality at 3 T and 7 T [14, 15].

Another major development was simultaneous multi-slice (SMS) imaging, also referred to as multiband imaging. In SMS acquisitions, several slices are excited and acquired simultaneously using multiband RF pulses. The resulting slice superposition is then resolved using coil sensitivity encoding and dedicated slice-separation reconstruction [14].

The SMS signal for receiver coil c may be written schematically as

$$s_c^{\mathrm{SMS}} = \sum_{m=1}^{N_s} S_c(z_m)\, \rho(z_m), \tag{32}$$

where N_s denotes the number of simultaneously excited slices, $S_c(z_m)$ represents the coil sensitivity of receiver c at slice position z_m, and $\rho(z_m)$ denotes the corresponding slice signal.

Controlled aliasing methods such as CAIPIRINHA further improved SMS imaging by introducing deliberate phase modulations that shift the aliased slices relative to one another [14]. These shifts increase the effective variation in coil sensitivities across the simultaneously excited slices, improve the conditioning of the slice-separation problem, and reduce geometry-factor penalties.

Wave-CAIPI extended this concept further by introducing additional sinusoidal gradient modulations during readout [15]. The resulting corkscrew-like k-space trajectory spreads aliasing more favorably across all three spatial dimensions, enabling highly accelerated volumetric imaging with relatively low geometry-factor penalties in suitable applications.

Parallel imaging also became increasingly integrated with compressed sensing methods. Compressed sensing exploits image sparsity to reconstruct images from highly undersampled k-space data [30]. In many modern reconstruction frameworks, parallel imaging provides spatial encoding while compressed sensing contributes sparsity-based regularization and additional constraints on the solution [11, 28].

The combined reconstruction problem may be written schematically as

$$\min_x \; \|Ax - y\|_2^2 + \lambda \|Wx\|_1, \tag{33}$$

where:

- A represents the parallel imaging forward operator,
- y denotes the measured k-space data,
- W is a sparsifying transform,
- λ is a regularization parameter.

The integration of parallel imaging with compressed sensing enabled highly accelerated reconstructions in applications such as cardiac perfusion MRI, real-time cardiac cine MRI, dynamic contrast-enhanced imaging, and free-breathing body MRI [28, 31, 32].

More recently, deep-learning-based reconstruction methods have emerged as another major extension of accelerated MRI. Learned reconstruction models may be incorporated into iterative reconstruction frameworks as trainable regularizers or unrolled optimization networks, and related approaches have also been developed for direct multicoil MRI reconstruction [16, 17].

Modern accelerated MRI therefore increasingly combines:

- parallel imaging,
- compressed sensing,
- low-rank modeling,
- motion-aware reconstruction,
- deep-learning-based regularization.

These developments transformed MRI reconstruction from a largely analytical inverse problem into a sophisticated computational imaging framework capable of achieving acquisition speeds far beyond those possible with conventional Fourier imaging alone [13, 16, 32].

6.2 Iterative Reconstruction and Unified Parallel Imaging Frameworks

As parallel imaging methods evolved, the distinction between classical image-domain approaches such as SENSE and k-space approaches such as GRAPPA became increasingly blurred. Modern reconstruction methods are frequently formulated as generalized inverse problems solved iteratively rather than through direct analytical reconstruction [12, 20].

In conventional SENSE, reconstruction is performed through explicit matrix inversion in image space. GRAPPA, in contrast, synthesizes missing k-space samples through local interpolation kernels. Both approaches, however, may be interpreted within a more general encoding framework:

$$y = Ax + n, \tag{34}$$

where:

- y denotes the measured k-space data,
- x is the unknown image,
- A represents the MRI encoding operator,
- n denotes measurement noise.

The encoding operator A may include:

- Fourier encoding,
- sampling trajectory,
- coil sensitivity encoding,
- undersampling pattern.

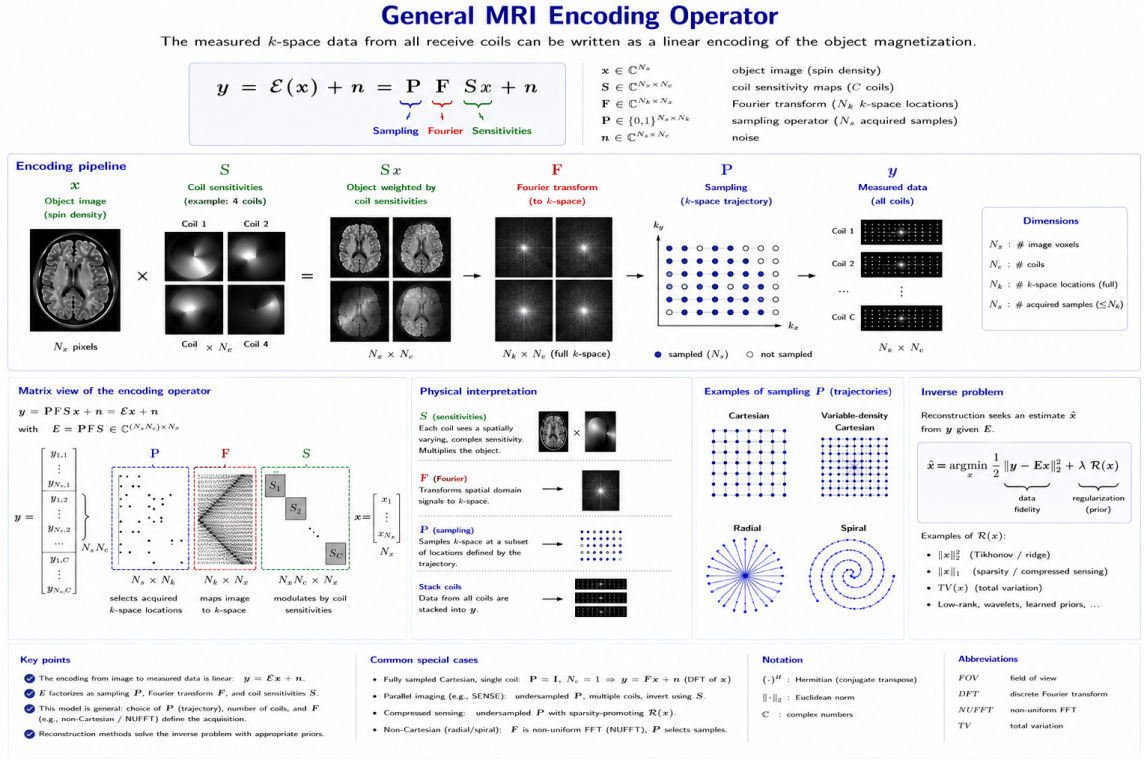

Figure 20: General MRI encoding operator.

Figure 20 shows the general MRI encoding operator.

Within this framework, image reconstruction becomes an inverse problem in which the unknown image x must be estimated from incomplete and noisy measurements. Because the reconstruction problem is often ill posed, additional regularization constraints are introduced to stabilize the solution.

A general regularized reconstruction problem may be written as

$$\hat{x} = \arg\min_{x} \left(\|Ax - y\|_2^2 + \lambda R(x) \right), \tag{35}$$

where $R(x)$ denotes a regularization functional and λ controls the regularization strength.

The regularization term may enforce:

- image smoothness,
- sparsity,
- temporal consistency,
- low-rank structure,
- learned image priors.

Iterative reconstruction methods solve Eq. (35) through repeated optimization steps rather than direct analytical inversion. Common optimization strategies in accelerated MRI and compressed-sensing MRI include:

- conjugate-gradient methods,

- iterative least-squares optimization,
- proximal gradient methods,
- alternating direction method of multipliers (ADMM),
- primal-dual algorithms.

These algorithmic families are widely used for regularized MRI reconstruction problems involving sparsity or related nonsmooth penalties [33].

Figure 21 shows the iterative reconstruction loop.

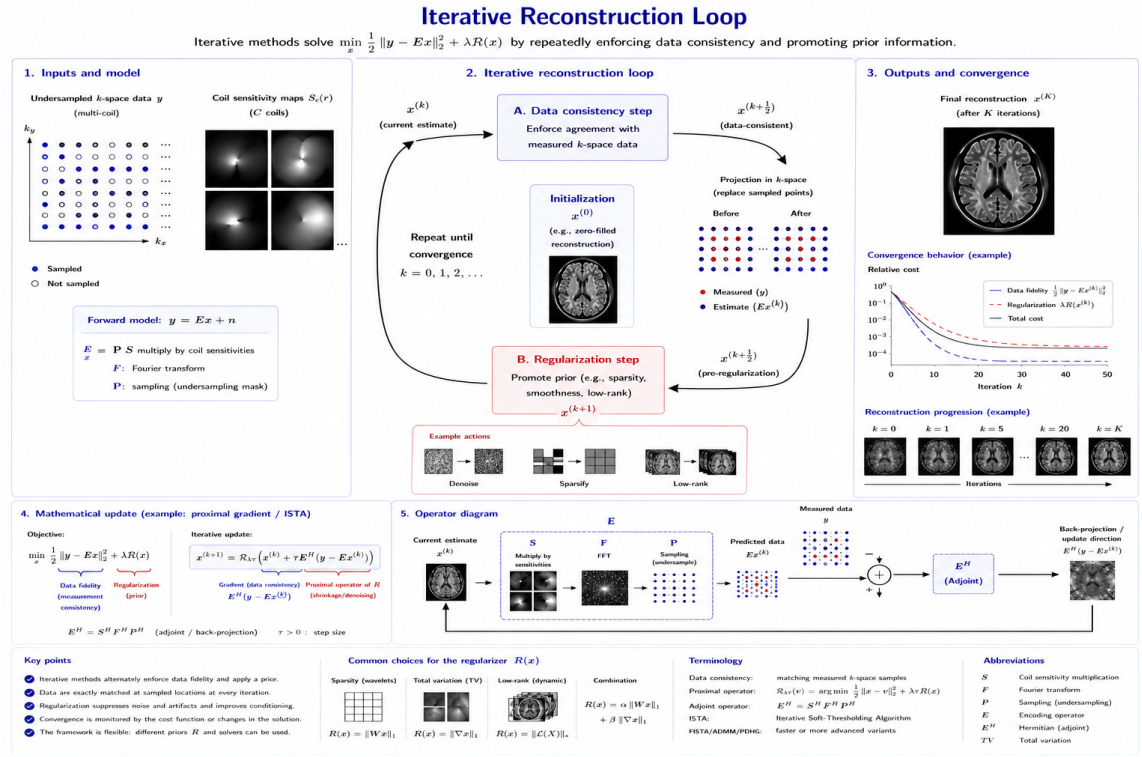

Figure 21: Iterative reconstruction loop.

One of the most influential unified frameworks is SPIRiT (Iterative Self-Consistent Parallel Imaging Reconstruction) [12]. Instead of explicitly reconstructing missing k-space lines or sensitivity maps in a purely direct manner, SPIRiT enforces self-consistency relationships among all receiver channels through iterative optimization.

In SPIRiT, the reconstructed multicoil k-space data must satisfy a self-consistency relation of the form

$$x = Gx, \tag{36}$$

where G is a calibration operator derived from autocalibration data. The reconstruction therefore enforces agreement both with the acquired measurements and with the learned multichannel calibration relationships.

Figure 22 shows SPIRiT self-consistency.

An important conceptual advance was ESPIRiT (Eigenvalue-based Parallel Imaging Reconstruction), which unified aspects of SENSE and GRAPPA within a common mathematical framework [20]. ESPIRiT

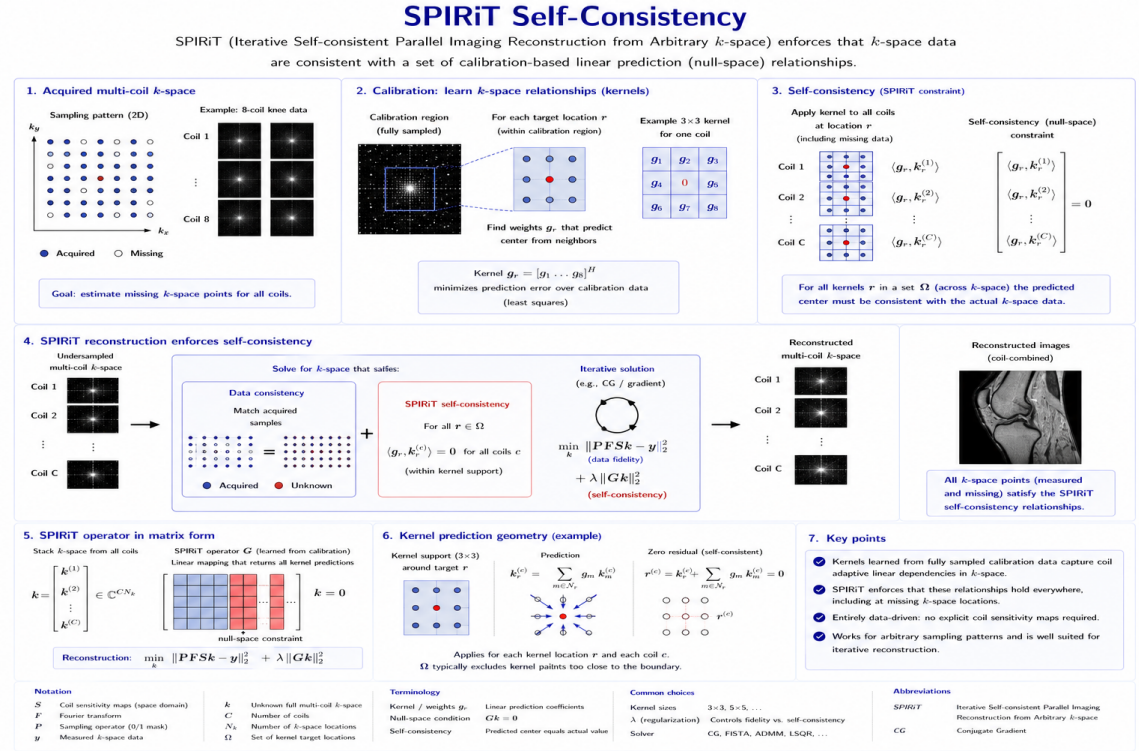

Figure 22: SPIRiT self-consistency.

derives effective sensitivity maps directly from calibration data using eigenvalue decomposition and thereby combines:

- the explicit encoding interpretation of SENSE,
- the autocalibration robustness of GRAPPA-like methods.

Figure 23 shows ESPIRiT eigenvalue sensitivity maps.

Iterative reconstruction frameworks proved especially valuable for arbitrary and non-Cartesian sampling trajectories, including:

- radial imaging,
- spiral imaging,
- other generalized k-space trajectories.

In such acquisitions, direct Fourier reconstruction becomes more complicated because the sampled k-space locations do not lie on a regular Cartesian grid. Iterative methods naturally accommodate arbitrary sampling trajectories through generalized forward models [12, 18, 27].

Parallel imaging also became increasingly integrated with compressed sensing reconstruction. In compressed sensing MRI, sparsity constraints are introduced to stabilize highly undersampled reconstructions [30]. The resulting optimization problem combines:

- data consistency,
- coil encoding,

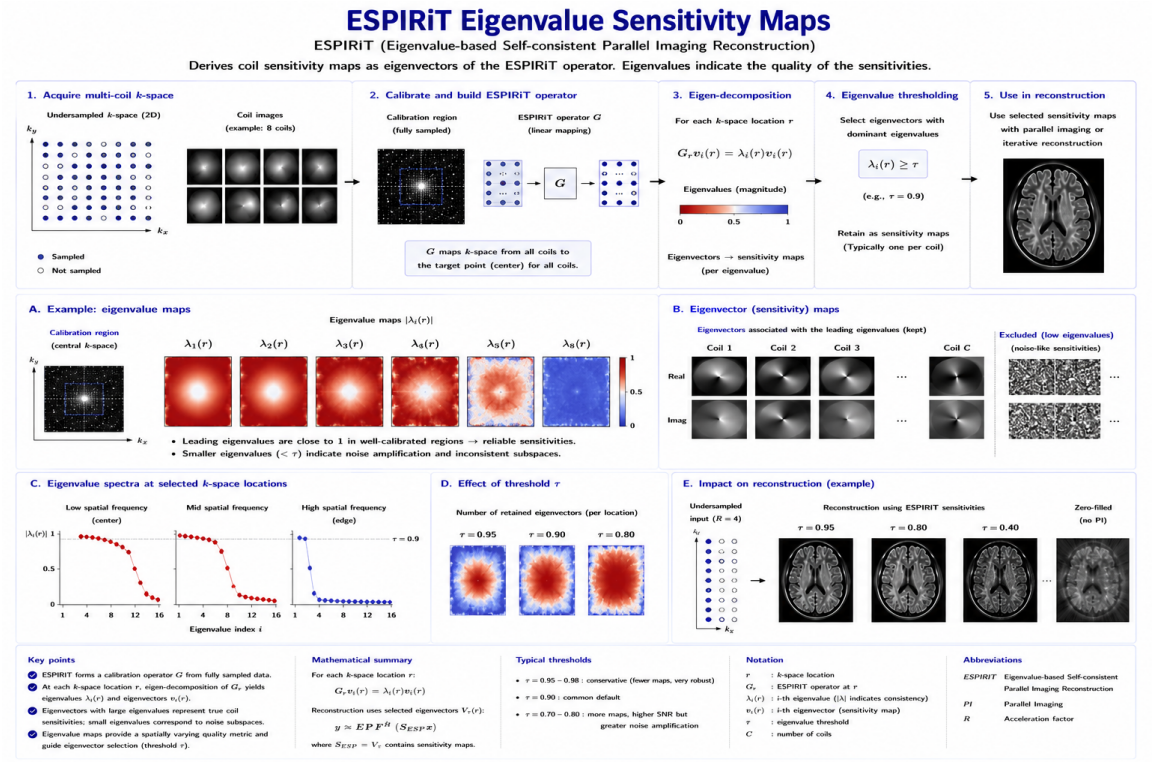

Figure 23: ESPIRiT eigenvalue sensitivity maps.

- sparsity regularization.

The key elements are:

1. classical parallel imaging,
2. compressed sensing,
3. unified iterative reconstruction.

Low-rank reconstruction methods further extended this framework by exploiting temporal and spatial redundancies in dynamic MRI datasets [13]. Dynamic image series often exhibit strong correlations between neighboring frames, allowing reconstruction from highly undersampled acquisitions.

Deep-learning-based methods now represent another major extension of iterative reconstruction. Neural networks may be incorporated:

- as learned regularizers,
- as unrolled iterative optimization networks,
- as direct multicoil reconstruction models.

These developments build on the same broad inverse-problem framework while replacing hand-designed regularization terms with learned reconstruction components [16, 17].

Figure 24 shows deep-learning-assisted reconstruction.

The evolution toward unified iterative frameworks reflects a major conceptual shift in MRI reconstruction. Modern accelerated MRI no longer relies solely on Fourier inversion but instead treats image reconstruction as a computational imaging problem integrating:

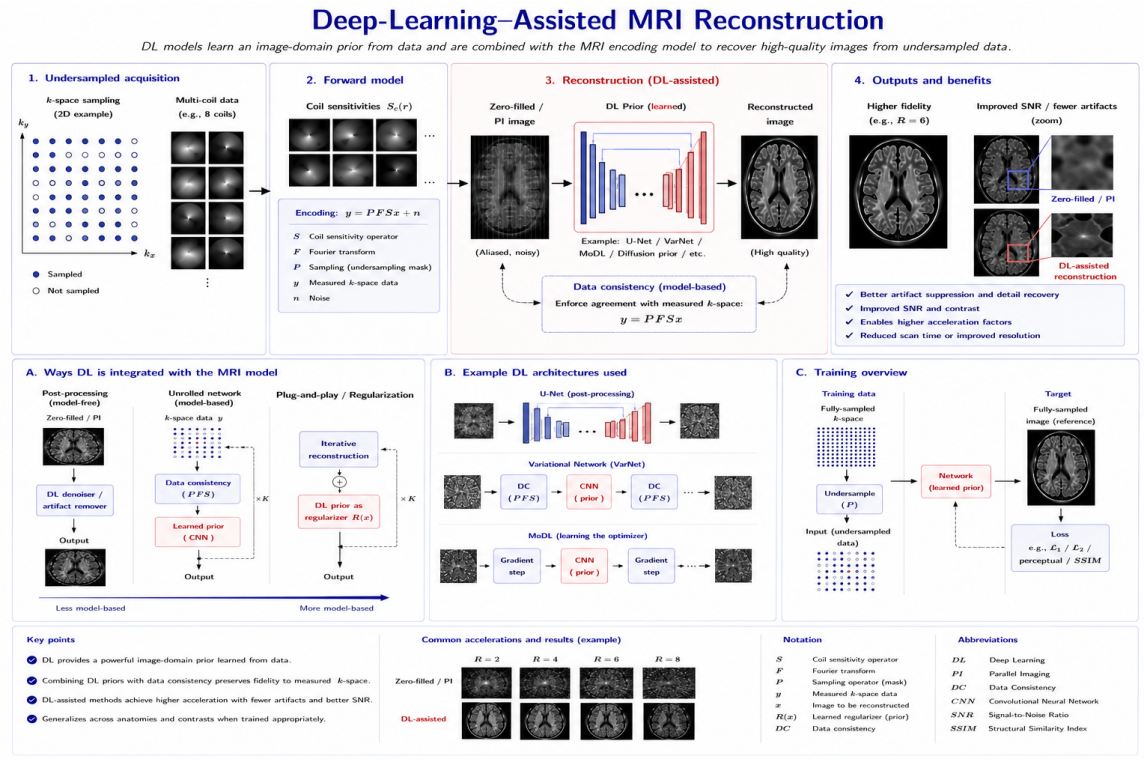

Figure 24: Deep-learning-assisted reconstruction.

- acquisition physics,
- coil encoding,
- signal models,
- optimization theory,
- statistical inference,
- machine learning.

This development enabled acceleration factors and reconstruction capabilities far beyond those achievable with the original classical SENSE and GRAPPA formulations and continues to drive ongoing advances in ultrafast MRI [12, 16, 20].

7 Applications of Parallel Imaging

7.1 Echo-Planar Imaging and Diffusion MRI

One of the most important applications of parallel imaging is echo-planar imaging (EPI). EPI is an ultrafast MRI technique in which an entire image, or a substantial portion of k-space, is acquired following a single RF excitation by rapidly oscillating readout gradients combined with phase-encoding blips. Because of its exceptional acquisition speed, EPI became a central acquisition strategy for:

- diffusion-weighted imaging (DWI),

- functional MRI (fMRI),
- perfusion-sensitive imaging,
- other rapid single-shot and time-resolved applications.

However, conventional EPI also suffers from several important limitations. The long echo trains required for full k-space acquisition produce:

- geometric distortion,
- susceptibility-related artifacts,
- image blurring,
- chemical-shift-related displacement,
- signal loss in regions with strong magnetic field inhomogeneity.

These problems become increasingly severe at higher magnetic field strengths because off-resonance effects and susceptibility-related distortions become more pronounced [2, 34].

Parallel imaging substantially improves EPI by reducing the number of required phase-encoding steps. If the acquisition is accelerated by a factor R, the EPI echo train is shortened approximately in proportion to the reduction in acquired phase-encoding lines:

$$T_{\text{echo train,acc}} \approx \frac{T_{\text{echo train,full}}}{R}. \tag{37}$$

The shorter readout duration reduces the time during which off-resonance phase accumulation occurs, thereby decreasing geometric distortion, blurring, and related signal degradation [2, 3].

Figure 25 shows a shortened EPI echo train with parallel imaging.

1. conventional EPI echo trains,
2. accelerated EPI trajectories,
3. resulting distortion reduction.

This improvement proved especially important in diffusion-weighted imaging (DWI). Diffusion MRI commonly relies on single-shot spin-echo EPI because diffusion sensitization already produces substantial signal attenuation and because rapid acquisition reduces sensitivity to bulk motion. However, DWI is highly susceptible to EPI-related geometric distortion, particularly near air–tissue interfaces in the head and neck region and in anatomically complex areas with strong local field inhomogeneity.

Parallel imaging therefore became highly valuable in diffusion MRI by reducing EPI echo-train length, limiting off-resonance-induced distortion, and helping to improve the feasibility of higher-resolution diffusion acquisitions [2, 35].

Figure 26 shows diffusion MRI with and without parallel imaging.

Parallel imaging also enabled improvements in spatial resolution for diffusion MRI. Because the EPI echo train is shortened, smaller voxel sizes may be used with less severe image distortion or T_2^*-related blurring. This capability proved particularly valuable in:

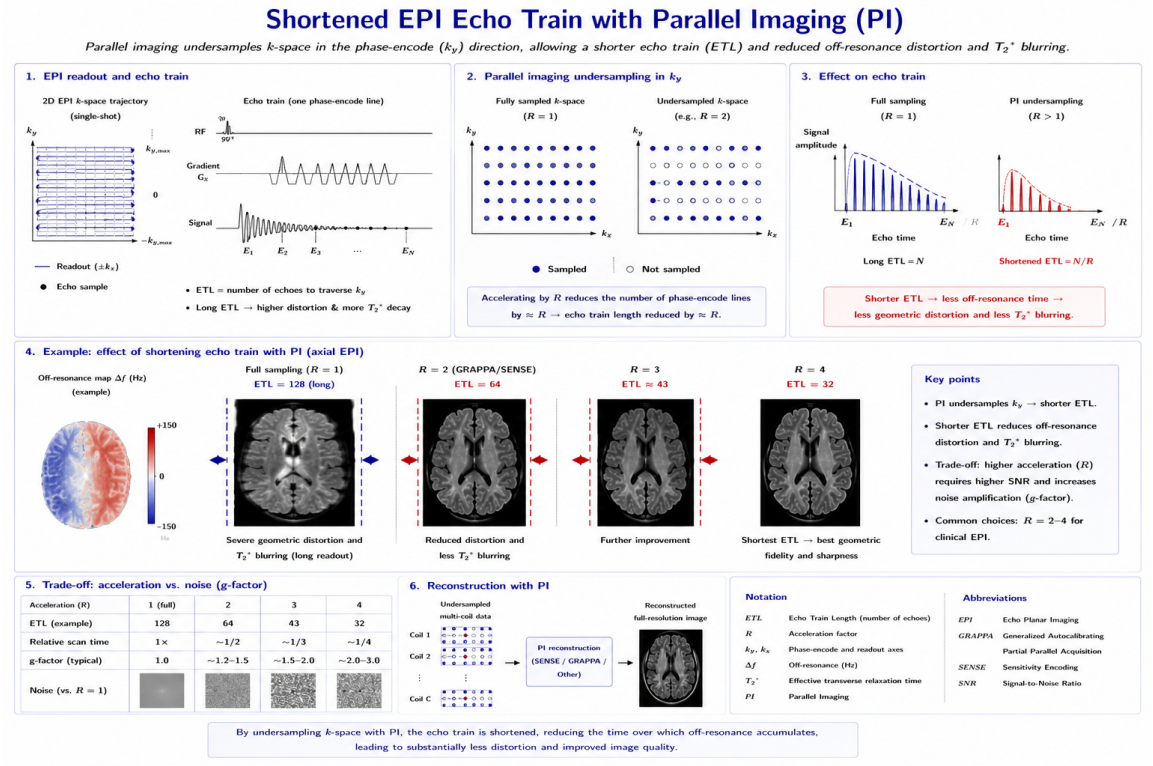

Figure 25: Shortened EPI echo train with parallel imaging.

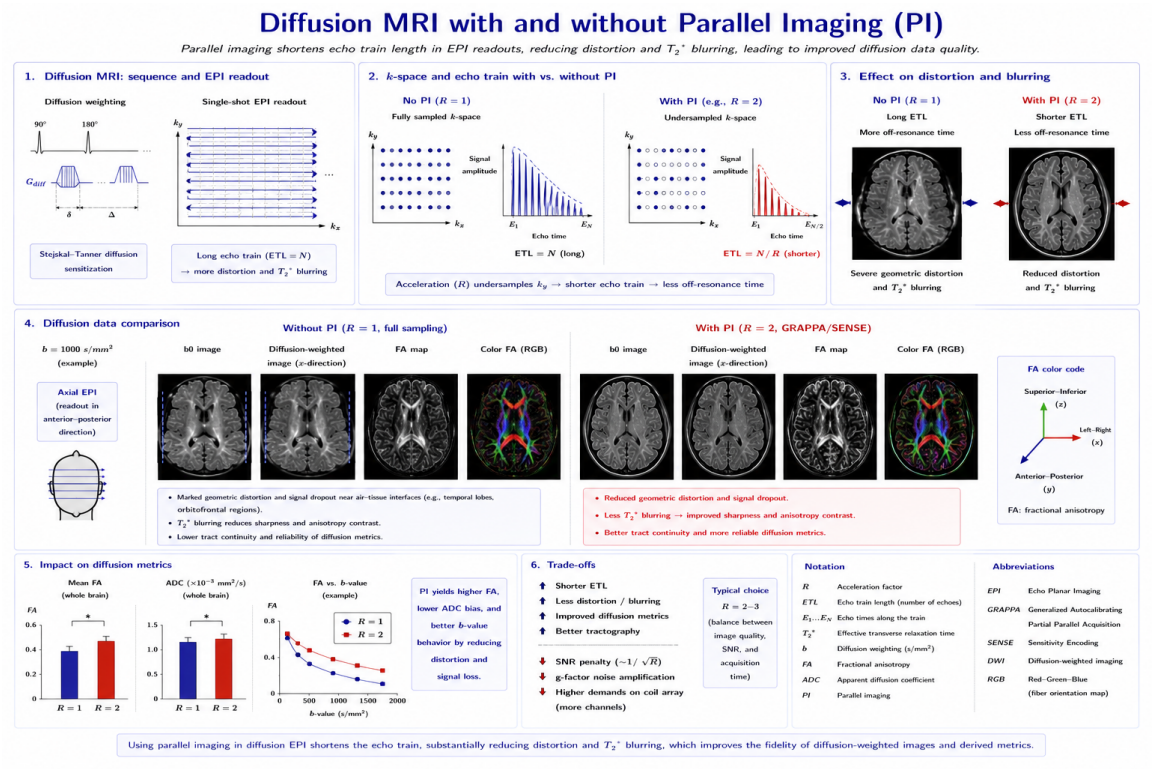

Figure 26: Diffusion MRI with and without parallel imaging.

- diffusion tensor imaging (DTI),
- tractography-oriented acquisitions,
- high-resolution brain diffusion imaging,
- other applications requiring improved geometric fidelity.

[2, 35]

Functional MRI (fMRI) similarly benefited greatly from parallel imaging. Blood oxygen level dependent (BOLD) fMRI commonly relies on gradient-echo EPI acquisitions, which are highly sensitive to susceptibility-induced artifacts and geometric distortion. Parallel imaging reduces these distortions and can improve temporal resolution and spatial accuracy of functional localization [2, 3, 36].

The importance of parallel imaging became even greater with the emergence of ultra-high-field MRI systems operating at 7 T and above. At such field strengths, susceptibility-related distortions and signal nonuniformities become particularly challenging. Parallel imaging, and later simultaneous multi-slice controlled-aliasing strategies, became especially valuable for maintaining practical EPI-based neuroimaging performance at high field strengths [14, 15, 34].

Simultaneous multi-slice (SMS) imaging further transformed diffusion MRI and fMRI by enabling acquisition of multiple slices simultaneously. Combined with parallel imaging reconstruction, SMS techniques substantially increase temporal efficiency while preserving whole-brain coverage [14].

Figure 27 shows SMS-accelerated fMRI.

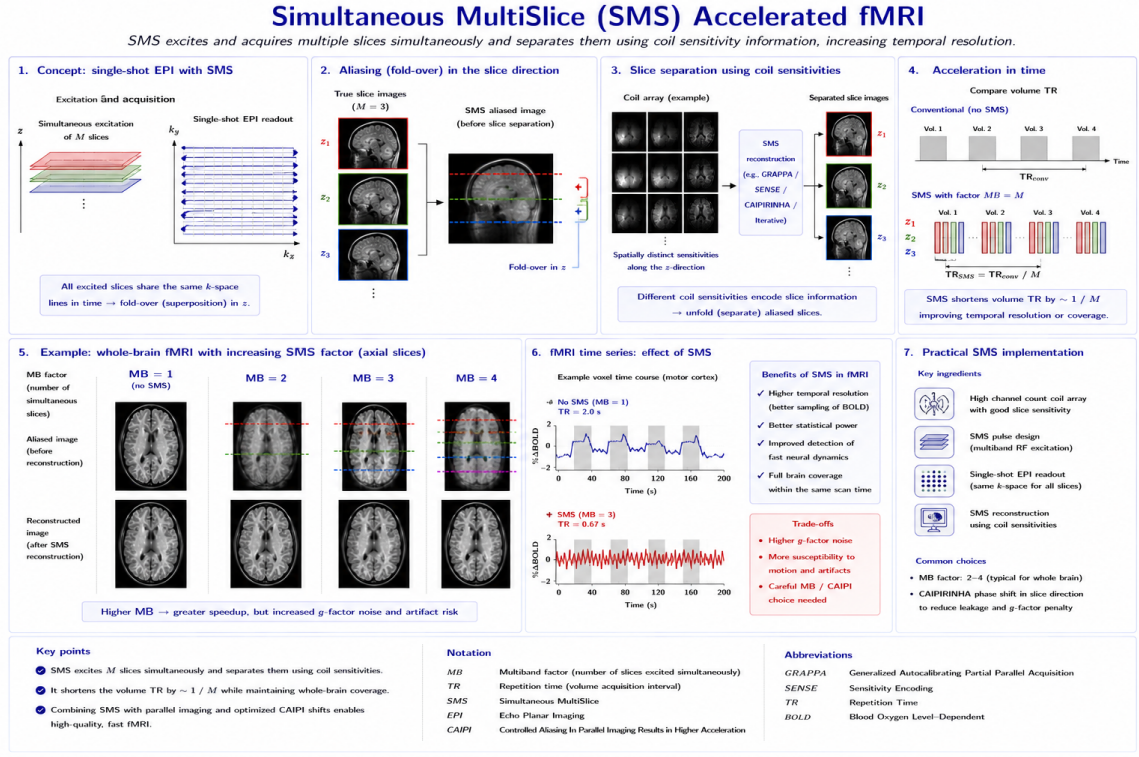

Figure 27: SMS-accelerated fMRI.

Modern neuroimaging protocols therefore often combine:

- EPI,

- parallel imaging,
- simultaneous multi-slice acquisition,
- advanced controlled-aliasing strategies,
- iterative or regularized reconstruction methods.

These developments substantially expanded the temporal and spatial performance of modern neuroimaging and established parallel imaging as a central component of accelerated EPI-based MRI [14, 15, 19].

7.2 Cardiovascular MRI

Cardiovascular MRI represents one of the most demanding applications of medical imaging because both cardiac motion and respiratory motion occur continuously during data acquisition. High spatial resolution, high temporal resolution, and large volumetric coverage are often required simultaneously. Parallel imaging therefore became a key enabling technology for modern cardiovascular MRI [10].

One of the earliest major applications was cine MRI for assessment of cardiac function. Conventional cine imaging often requires segmented k-space acquisitions synchronized to the electrocardiogram (ECG). Because data acquisition extends over multiple cardiac cycles, respiratory motion may introduce substantial artifacts unless patients repeatedly hold their breath.

Parallel imaging substantially reduces acquisition time and enables:

- shorter breath-hold durations,
- improved temporal resolution,
- larger anatomical coverage,
- higher spatial resolution within a practical scan time.

[10]

Figure 28 shows accelerated cardiac cine MRI.

The temporal resolution of cine MRI is particularly important for accurate visualization of cardiac wall motion and valve dynamics. By reducing the number of acquired phase-encoding lines, parallel imaging allows temporal resolution to be improved or scan duration to be reduced:

$$T_{\text{frame}} \propto \frac{N_{\text{PE}}}{R}. \tag{38}$$

Accelerated cine imaging therefore supports more efficient assessment of:

- ventricular contraction,
- diastolic filling,
- valve motion,
- myocardial synchrony.

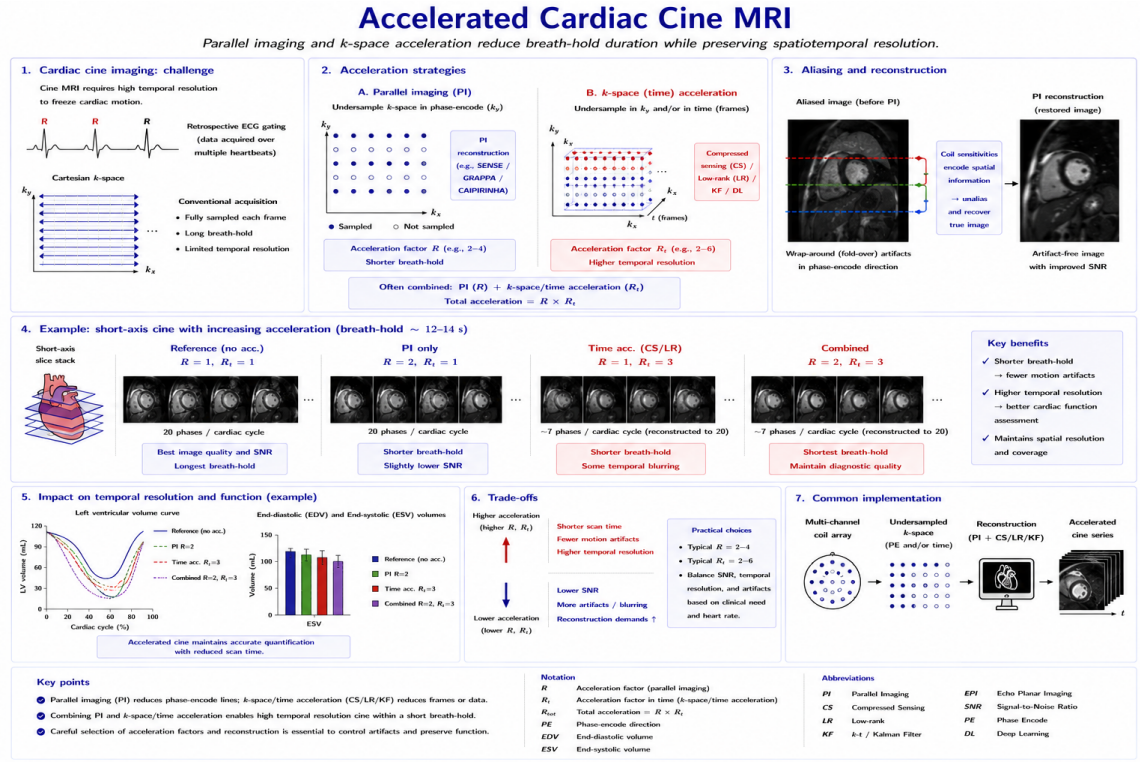

Figure 28: Accelerated cardiac cine MRI.

[10]

Myocardial perfusion imaging also benefited substantially from parallel imaging. First-pass perfusion MRI requires rapid repeated acquisition during passage of contrast agent through the myocardium. Because signal enhancement evolves rapidly over time, both high temporal and spatial resolution are essential.

Parallel imaging enabled:

- increased slice coverage,
- improved in-plane spatial resolution,
- more efficient temporal sampling,
- better balance among coverage, resolution, and acquisition speed.

More advanced hybrid approaches combining parallel imaging and compressed sensing later enabled still higher acceleration factors for first-pass cardiac perfusion MRI [10, 31].

Coronary MR angiography (MRA) presents another particularly demanding application because the coronary arteries are small, tortuous, and continuously moving. Conventional high-resolution coronary imaging requires long acquisition times and is highly sensitive to respiratory motion.

Parallel imaging reduced acquisition duration sufficiently to support:

- shorter breath-hold coronary acquisitions,
- navigator-gated free-breathing coronary imaging,
- thicker-volume or broader-coverage acquisitions,

- improved visualization of long and tortuous coronary segments.

[10]

Real-time cardiac MRI became increasingly feasible through the combination of:

- parallel imaging,
- radial or spiral trajectories,
- dynamic calibration methods,
- iterative reconstruction.

These developments are particularly relevant in motion-sensitive settings such as free-breathing cardiac imaging and real-time evaluation of ventricular function [25, 26].

Parallel imaging can also help reduce specific absorption rate (SAR) burdens in selected pulse-sequence settings, particularly for RF-intensive multiecho sequences at 3 T and above. By reducing the number of required phase-encoding steps, parallel imaging can either shorten acquisition time or permit longer repetition periods at fixed scan duration, thereby reducing RF energy deposition per unit time in appropriate protocols. This consideration is relevant for some cardiovascular MRI applications at higher field strengths [2, 10].

Respiratory motion remains one of the principal challenges in cardiovascular MRI. Dynamic parallel imaging methods such as TSENSE and TGRAPPA proved especially valuable because they adapt sensitivity or calibration information over time in the presence of changing object position and coil sensitivity relationships [22, 26].

Parallel imaging furthermore became increasingly integrated with non-Cartesian trajectories in cardiovascular MRI. Radial and spiral acquisitions provide useful motion properties and efficient k-space coverage, while parallel imaging compensates for the associated undersampling burden [18, 25].

Modern cardiovascular MRI therefore frequently combines:

- parallel imaging,
- radial or spiral trajectories,
- compressed sensing,
- motion-aware reconstruction,
- iterative reconstruction.

These developments transformed cardiovascular MRI from a comparatively slow and motion-sensitive technique into a highly flexible dynamic imaging modality capable of visualizing cardiac anatomy, function, perfusion, and vascular structures with markedly improved spatial and temporal efficiency [10, 25, 31].

7.3 Magnetic Resonance Angiography and Dynamic Contrast Imaging

Magnetic resonance angiography (MRA) was among the earliest MRI applications to benefit substantially from parallel imaging. Vascular imaging requires high spatial resolution over large anatomical regions while simultaneously maintaining short acquisition times to minimize motion artifacts and optimize contrast

timing. Parallel imaging therefore became a key enabling technology for modern contrast-enhanced MRA [2, 5, 10].

In conventional contrast-enhanced MRA, a gadolinium-based contrast agent is injected intravenously, and image acquisition must be synchronized with the arterial passage of the contrast bolus. Because vascular enhancement changes rapidly over time, acquisition speed is critically important.

Parallel imaging reduces scan duration by decreasing the number of required phase-encoding steps:

$$T_{\mathrm{MRA}} \approx \frac{T_{\mathrm{full}}}{R}. \tag{39}$$

The shorter acquisition time improves temporal synchronization between contrast enhancement and image acquisition, thereby facilitating arterial-phase imaging and reducing overlap with later venous enhancement [5, 10].

Figure 29 shows contrast-enhanced MRA with parallel imaging.

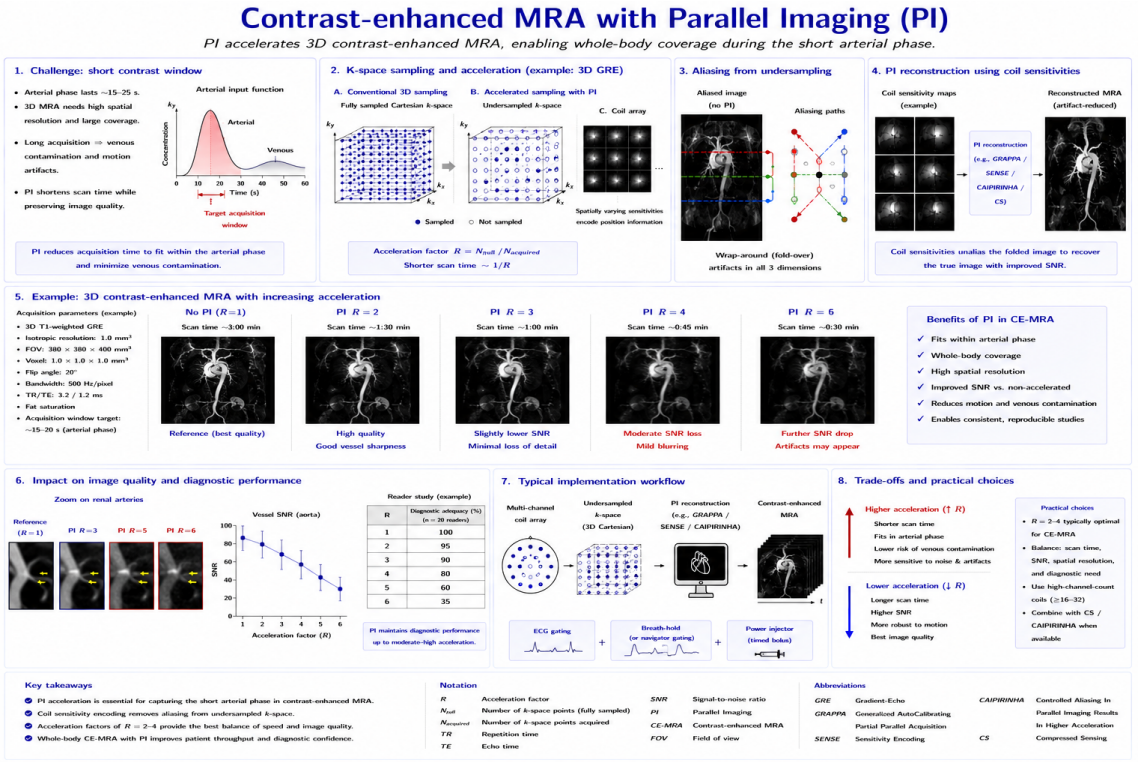

Figure 29: Contrast-enhanced MRA with parallel imaging.

Parallel imaging also enabled substantial increases in spatial resolution for MRA. Because acquisition time is reduced, smaller voxel sizes or larger volumetric coverage can be pursued while maintaining clinically practical scan durations. This improvement proved valuable in:

- carotid and intracranial angiography,
- peripheral vascular imaging,
- renal artery imaging,
- coronary MR angiography.

[2, 10]

Time-resolved contrast-enhanced MRA represented another important application of acceleration. In dynamic MRA, multiple image volumes are acquired sequentially during passage of the contrast bolus. This permits visualization of vascular filling dynamics and helps distinguish arterial from venous phases.

Dynamic MRA requires rapid volumetric acquisition. Parallel imaging therefore became highly valuable for achieving sufficient temporal resolution while preserving acceptable spatial resolution. In contemporary practice, dynamic angiographic and contrast-enhanced protocols are often combined with additional acceleration strategies such as view sharing, radial sampling, compressed sensing, and iterative reconstruction [10, 32].

Figure 30 shows a representative time-resolved sampling strategy and view-sharing concept.

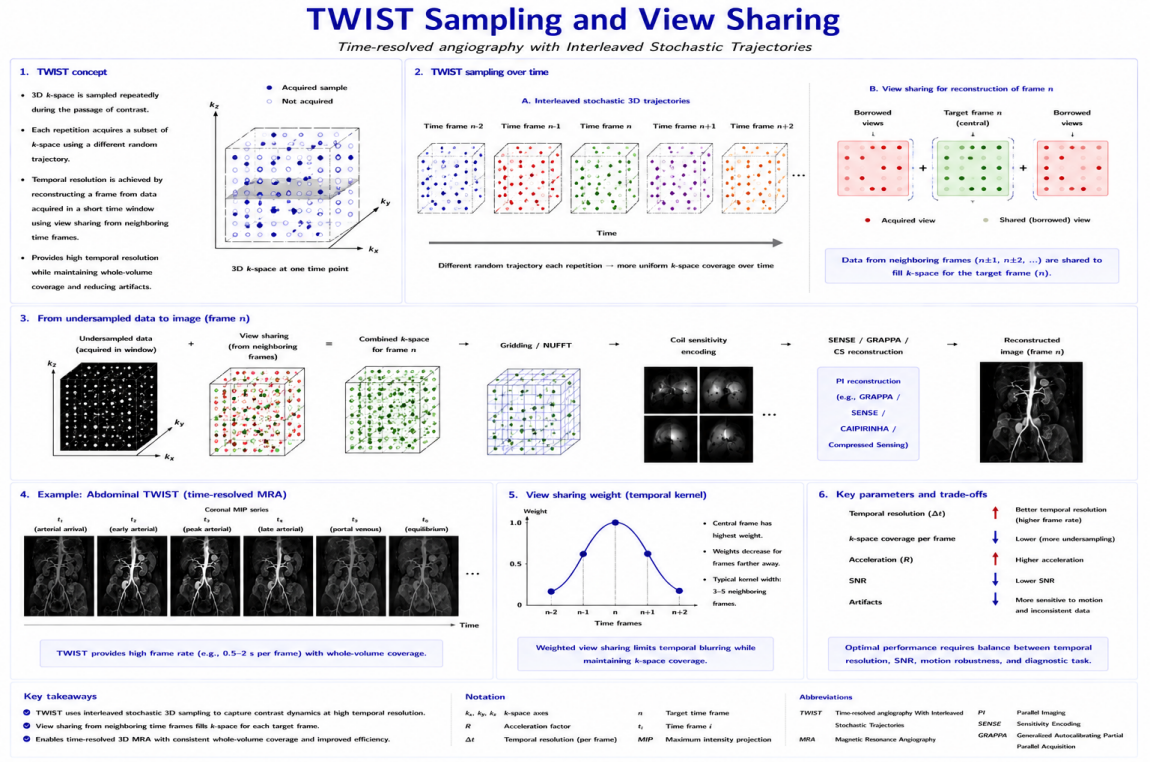

Figure 30: Representative time-resolved sampling and view-sharing strategy.

Parallel imaging also proved valuable in non-contrast angiographic and vascular applications. Techniques such as:

- time-of-flight (TOF) MRA,
- phase-contrast angiography,
- free-breathing non-contrast vascular imaging,
- other flow-sensitive vascular acquisitions

benefit from reduced acquisition duration and improved efficiency, particularly when high spatial resolution or broad anatomical coverage is required [2, 10].

At higher magnetic field strengths, acceleration methods may further help manage some sequence-design constraints and shorten demanding acquisitions, although image quality remains affected by the broader challenges of high-field MRI such as susceptibility effects and field inhomogeneity [2, 34].

Dynamic contrast-enhanced MRI (DCE-MRI) also benefited substantially from accelerated imaging. In DCE-MRI, repeated volumetric acquisitions are performed during and after administration of contrast agent in order to characterize tissue enhancement dynamics and perfusion-related behavior.

Applications include:

- abdominal dynamic MRI,
- liver imaging,
- prostate imaging,
- renal and other body imaging applications,
- other multiphase contrast-enhanced examinations.

Because contrast enhancement evolves rapidly, both temporal resolution and spatial resolution are important. Parallel imaging, increasingly combined with compressed sensing and non-Cartesian sampling, supports this tradeoff in dynamic body MRI [32].

Modern angiographic and dynamic imaging protocols frequently combine:

- parallel imaging,
- compressed sensing,
- radial or spiral trajectories,
- view-sharing or time-resolved sampling strategies,
- iterative reconstruction.

These combinations enabled substantial improvements in both spatial and temporal resolution while maintaining clinically practical acquisition times [10, 32].

The integration of parallel imaging into angiographic and dynamic MRI applications illustrates one of the central strengths of accelerated MRI: the ability to trade redundant spatial encoding for improved temporal performance. This capability substantially expanded the utility of MRI for visualizing dynamic physiologic and vascular processes.

7.4 Pediatric MRI and PET/MR Imaging

Pediatric MRI presents unique technical and clinical challenges because long acquisition times increase the likelihood of patient motion and may increase the need for sedation or general anesthesia. Reduction of scan duration is therefore particularly important in pediatric imaging, both to improve image quality and to reduce the logistical burden associated with prolonged examinations [37].

Parallel imaging became highly valuable in pediatric body MRI because accelerated acquisition directly shortens scan time while preserving diagnostically useful image quality. Combined parallel imaging and compressed sensing strategies were specifically explored to improve the feasibility of fast pediatric body MRI and to reduce motion sensitivity in challenging examinations [37].

In pediatric body imaging, acceleration strategies are especially attractive for:

- abdominal imaging,

- free-breathing acquisitions,
- volumetric imaging,
- protocols in patients who have difficulty remaining still.

[32, 37]

The importance of efficient MRI acquisition becomes even clearer in integrated PET/MR systems. PET/MR combines the metabolic information of positron emission tomography (PET) with the high soft-tissue contrast of MRI while substantially reducing radiation exposure compared with PET/CT. In the initial pediatric oncology experience reported by Hirsch et al., PET/MR enabled simultaneous metabolic and morphologic assessment and included whole-body diffusion-weighted MRI, but examination duration remained longer than PET/CT and therefore continued to pose practical workflow challenges [38].

One of the principal technical limitations of PET/MR is therefore the duration of the MRI component. While PET and MR data can be acquired simultaneously in integrated systems, the MR protocol remains a major determinant of examination time. Long examinations may increase:

- motion artifacts,
- patient discomfort,
- workflow complexity,
- the practical burden of pediatric oncologic imaging.

[38]

In pediatric oncology PET/MR, the need for efficient acquisition is particularly evident because examinations may combine:

- whole-body imaging,
- diffusion-weighted imaging,
- high-resolution regional imaging,
- multiparametric MR protocols.

The available PET/MR experience demonstrates the clinical relevance of comprehensive but time-efficient pediatric imaging, while the broader pediatric MRI literature shows why acceleration strategies are attractive in this setting [37, 38].

Diffusion-weighted imaging is particularly important in oncologic PET/MR because it provides complementary information to FDG uptake and contributes to multiparametric assessment of disease burden. Whole-body DWI formed part of the pediatric PET/MR protocol reported by Hirsch et al. [38].

Parallel imaging also became increasingly important for ultrafast pediatric MRI protocols designed to shorten examination times and reduce motion vulnerability. Modern accelerated protocols may combine:

- parallel imaging,
- compressed sensing,
- non-Cartesian trajectories,

- motion-aware reconstruction.

These strategies are particularly attractive in children because they can improve robustness in settings where long breath-holds or prolonged immobility are difficult to achieve [32, 37].

Free-breathing imaging approaches are especially valuable in pediatric MRI because many young patients cannot reliably perform breath-holds. Acceleration strategies facilitate free-breathing and motion-robust acquisition by reducing the effective sampling burden and enabling more flexible reconstruction frameworks [32, 37].

Modern pediatric MRI increasingly relies on accelerated acquisition frameworks integrating:

- phased-array receiver systems,
- parallel imaging,
- iterative reconstruction,
- compressed sensing,
- motion-aware acquisition and reconstruction.

These developments have made MRI more practical in demanding pediatric applications and have supported the broader expansion of multiparametric, radiation-sparing imaging workflows. Parallel imaging plays an important role in this progress, especially when combined with more advanced accelerated reconstruction strategies [32, 37, 38].

8 Parallel Imaging in MRI Simulation

8.1 General Signal Model

Simulation provides a valuable framework for investigating parallel imaging under controlled conditions. Because accelerated MRI involves interactions between:

- spatial encoding,
- coil sensitivity encoding,
- undersampling,
- noise propagation,
- reconstruction algorithms,

numerical experiments are especially useful for evaluating how acquisition and reconstruction choices influence image quality and artifact behavior [18, 23].

A general signal model for the data acquired by receiver coil c may be written as

$$s_c(t) = \int S_c(\mathbf{r})\, \rho(\mathbf{r})\, e^{-i2\pi \mathbf{k}(t)\cdot \mathbf{r}}\, d\mathbf{r}, \tag{40}$$

where:

- $\rho(\mathbf{r})$ denotes the spatial spin density distribution,

- $S_c(\mathbf{r})$ is the sensitivity profile of receiver coil c,
- $\mathbf{k}(t)$ describes the k-space trajectory generated by the gradient system.

The k-space trajectory itself is determined by the applied magnetic field gradients:

$$\mathbf{k}(t) = \frac{\gamma}{2\pi} \int_0^t \mathbf{G}(\tau)\, d\tau, \tag{41}$$

where $\mathbf{G}(t)$ represents the vector gradient waveform.

Figure 31 shows a parallel MRI simulation pipeline.

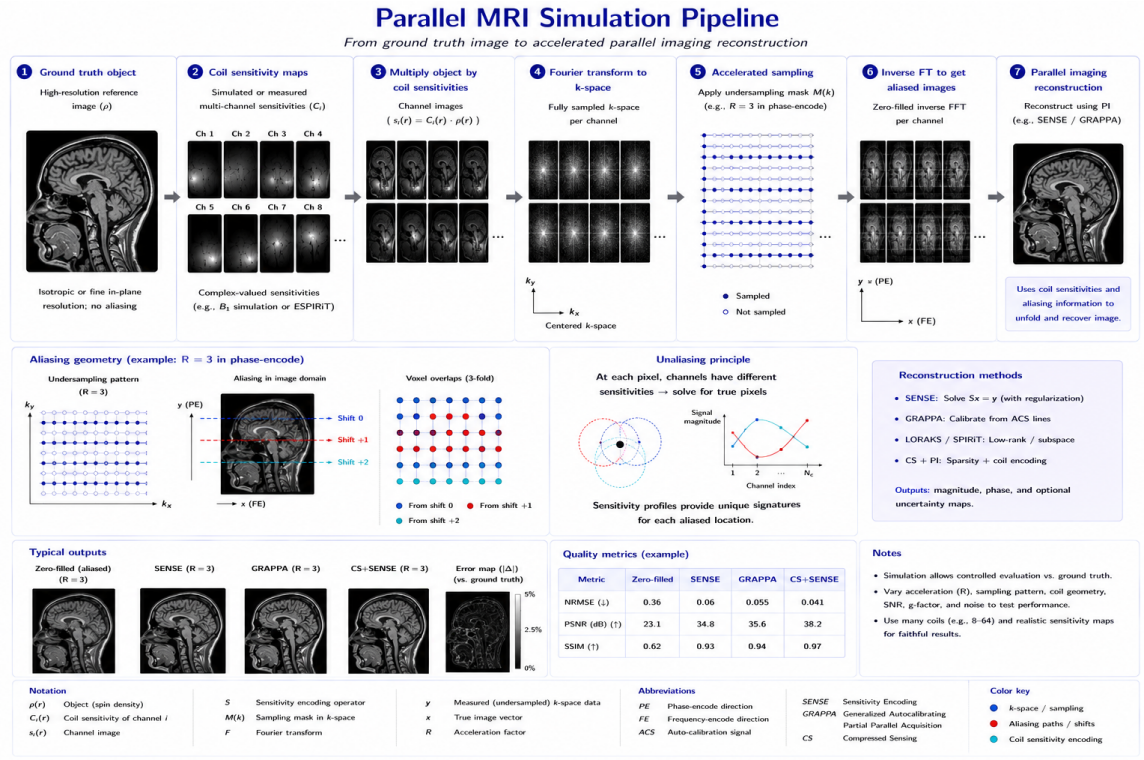

Figure 31: Parallel MRI simulation pipeline.

In computational parallel-imaging studies, the object is commonly represented on a discrete spatial grid:

$$\rho(\mathbf{r}) \to \rho_{m,n}, \tag{42}$$

so that simulated coil images and k-space data can be generated numerically. Depending on the purpose of the simulation, one may further incorporate simplified models of:

- relaxation-related signal weighting,
- off-resonance effects,
- diffusion weighting,
- motion or time-varying object structure.

In parallel MRI simulations, each receiver coil possesses an individual spatial sensitivity profile:

$$S_c(x, y) = |S_c(x, y)| e^{i\phi_c(x,y)}, \tag{43}$$

where both amplitude and phase may vary spatially. The measured signal is therefore generated independently for each receiver channel, and the collection of all coil signals forms the basis for subsequent parallel imaging reconstruction [2, 8].

An important component of realistic parallel-imaging simulation is noise modeling. Receiver noise may be approximated as additive complex Gaussian noise:

$$s_{\text{measured}} = s_{\text{ideal}} + n, \tag{44}$$

where n denotes complex-valued noise. In phased-array systems, noise correlations between receiver channels may additionally be represented through a covariance matrix:

$$\mathbf{C} = E[\mathbf{n}\mathbf{n}^H]. \tag{45}$$

This covariance structure is relevant because correlated receiver noise directly influences parallel imaging reconstruction and g-factor behavior [8, 18].

Figure 32 shows noise modeling in MRI simulation.

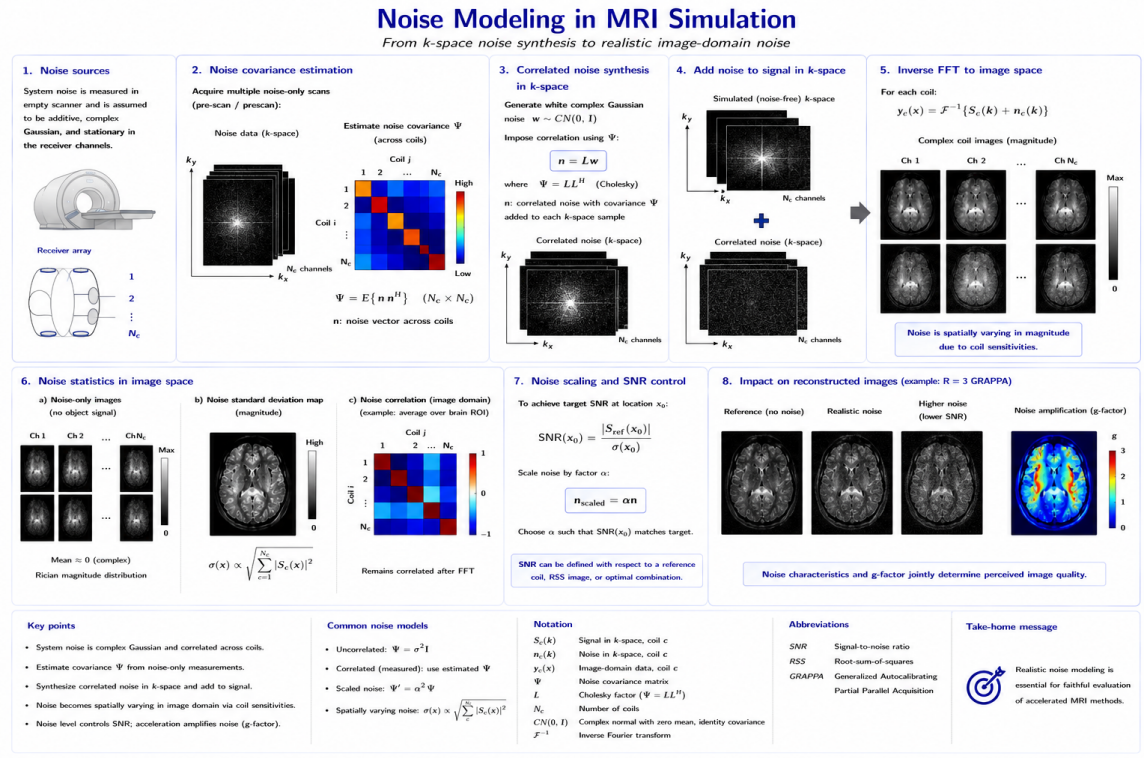

Figure 32: Noise modeling in MRI simulation.

Parallel imaging simulations typically involve deliberate k-space undersampling. In Cartesian imaging, undersampling masks may be applied directly:

$$s_{\text{acc}}(k_x, k_y) = M(k_x, k_y)\, s(k_x, k_y), \tag{46}$$

where $M(k_x, k_y)$ denotes the sampling mask.

The key elements are:

1. fully sampled k-space,
2. regular undersampling,
3. variable-density undersampling,
4. randomly distributed undersampling patterns.

Simulation is particularly valuable for evaluating:

- acceleration limits,
- geometry-factor behavior,
- residual aliasing,
- SNR degradation,
- calibration requirements,
- reconstruction performance for non-Cartesian trajectories.

These aspects were investigated explicitly in simulation studies of accelerated SENSE and VD-AUTO-SMASH reconstruction [18, 23].

Parallel MRI simulations may be performed at several levels of abstraction. Simplified simulations can operate directly on digital phantoms, sensitivity maps, and synthesized k-space data. More detailed studies may additionally account for specific trajectory design, off-resonance effects, or motion-related inconsistencies when these factors are relevant to the acquisition being modeled.

Sequence-specific simulations are particularly useful for studying:

- Cartesian undersampling,
- radial acquisitions,
- spiral imaging,
- simultaneous multi-slice encoding,
- trajectory-dependent reconstruction behavior.

Such studies are useful for examining the interaction between acquisition geometry and parallel imaging reconstruction, particularly when the sampling trajectory departs from a regular Cartesian grid [14, 18].

8.2 Simulation of Coil Sensitivities and Parallel Encoding

A central component of parallel MRI simulation is the modeling of receiver coil sensitivity profiles. Because spatial encoding in parallel imaging relies directly on the variation of coil sensitivities across the imaging volume, realistic sensitivity modeling is essential for accurate simulation of accelerated acquisition and reconstruction.

The sensitivity profile of a receiver coil describes the spatial variation of the detected RF signal amplitude and phase. In general, the sensitivity depends on:

- coil geometry,
- coil size,
- coil position,
- operating frequency,
- the electromagnetic relationship between the coil and the imaged object.

For simulation purposes, simplified analytical sensitivity models are often useful. A general representation is

$$S_c(x,y) = A_c(x,y)\, e^{i\phi_c(x,y)}, \tag{47}$$

where $A_c(x,y)$ denotes the spatial amplitude distribution and $\phi_c(x,y)$ represents the spatial phase variation.

Figure 33 shows coil sensitivity model comparison.

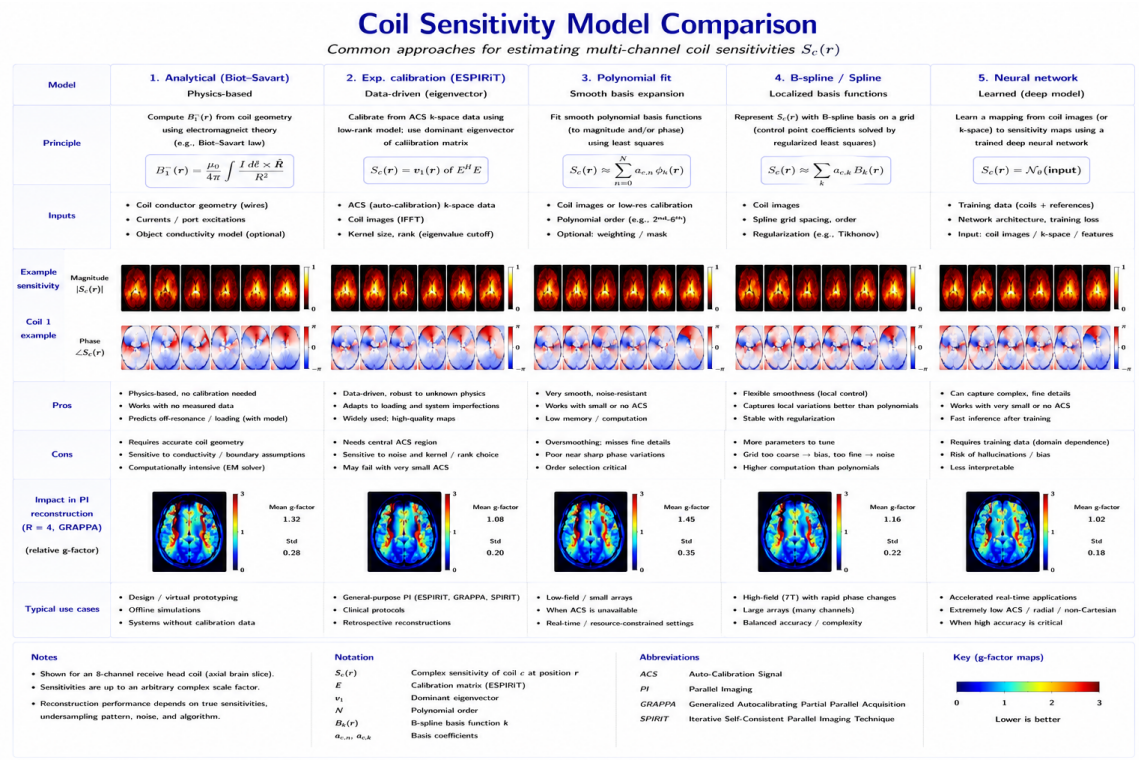

Figure 33: Coil sensitivity model comparison.

1. linear coil arrays,
2. circumferential head coils,
3. body arrays,
4. surface coils.

A particularly relevant example from the parallel-imaging literature is the use of analytically generated coil sensitivity maps based on integration of the Biot–Savart law. Such maps were used in simulation studies of VD-AUTO-SMASH to investigate reconstruction performance as a function of acceleration and ACS sampling [23].

Although simplified analytical models are computationally efficient, sensitivity information may also be derived from measured coil maps or experimentally acquired reference data when the goal is to reproduce realistic system behavior more closely [2, 8].

The number and geometry of the receiver coils strongly influence parallel imaging performance. Increasing the number of receiver channels can improve spatial encoding diversity and may permit higher acceleration factors with reduced geometry-factor penalties, provided that the coil sensitivities remain sufficiently distinct along the accelerated direction [2, 3].

The key elements are:

1. 4-channel arrays,
2. 8-channel arrays,
3. 16-channel arrays,
4. 32-channel arrays.

Simulation frameworks may therefore be used to investigate the relationship between:

- receiver-array geometry,
- acceleration factor,
- SNR behavior,
- geometry-factor distribution,
- reconstruction stability.

In SENSE simulations, the sensitivity maps enter directly into the reconstruction equations:

$$\mathbf{v} = \mathbf{S}\mathbf{a}, \tag{48}$$

where $\mathbf{S}$ contains the spatial sensitivity information [8].

In GRAPPA simulations, coil sensitivities influence reconstruction indirectly through the correlations between neighboring k-space samples across receiver channels. Different coil geometries therefore alter the quality of the calibrated reconstruction kernels and the level of residual noise amplification [2, 9].

An important phenomenon that may be investigated through simulation is geometry-factor (g-factor) behavior. The g-factor depends strongly on the spatial independence of the coil sensitivities:

$$g = g(S_c, R, \mathbf{r}), \tag{49}$$

where the geometry factor depends on:

- coil sensitivity distribution,

- acceleration factor,
- spatial position.

[2, 8]

Simulation also permits systematic evaluation of the influence of correlated receiver noise. Noise covariance may be incorporated explicitly:

$$\mathbf{C} = E[\mathbf{n}\mathbf{n}^H], \tag{50}$$

where $\mathbf{n}$ denotes the vector of complex receiver noise. This allows reconstruction studies to distinguish idealized independent-noise behavior from more realistic phased-array noise conditions [8, 18].

Another important application of coil simulation is the investigation of receiver-array design. By varying:

- coil geometry,
- coil spacing,
- coil orientation,
- channel count,
- anatomical coverage,

one may examine how the array design affects achievable acceleration and noise amplification [2, 3].

Simulation studies are especially attractive for high-channel-count arrays because the relationship between coil geometry, local sensitivity variation, and g-factor behavior becomes increasingly complex as the number of elements rises.

Simulation frameworks may also be used to examine advanced encoding concepts such as:

- simultaneous multi-slice encoding,
- controlled aliasing,
- Wave-CAIPI-type encoding,
- non-Cartesian parallel imaging.

These methods rely fundamentally on the same principle: receiver coil sensitivities provide additional spatial encoding beyond the gradients alone [14, 15, 18].

These studies illustrate that receiver coils are no longer merely signal detectors in modern MRI systems. Instead, the coil array itself has become an integral component of the spatial encoding process and therefore plays a central role in accelerated MRI acquisition.

8.3 Simulation of Undersampled Acquisition and Reconstruction

An essential objective of parallel MRI simulation is the investigation of undersampled acquisition strategies and their associated reconstruction methods. Because accelerated MRI intentionally acquires incomplete

k-space data, the choice of sampling trajectory and reconstruction algorithm strongly influences image quality, artifact behavior, and reconstruction stability.

In Cartesian parallel imaging, undersampling is typically performed along the phase-encoding direction by skipping regularly spaced k-space lines. A schematic representation is

$$k_y^{\text{acc}} = k_y^{\text{full}} \cdot R, \tag{51}$$

where R denotes the acceleration factor.

The corresponding undersampling mask may be represented as

$$M(k_x, k_y) = \begin{cases} 1, & \text{if the sample is acquired,} \\ 0, & \text{otherwise.} \end{cases} \tag{52}$$

Cartesian undersampling produces coherent aliasing in image space. In SENSE simulations, these aliasing patterns are subsequently unfolded using the simulated coil sensitivity maps. In GRAPPA simulations, the missing k-space lines are synthesized from neighboring acquired samples using calibration kernels [8, 9].

Figure 34 shows the SENSE versus GRAPPA simulation pipeline.

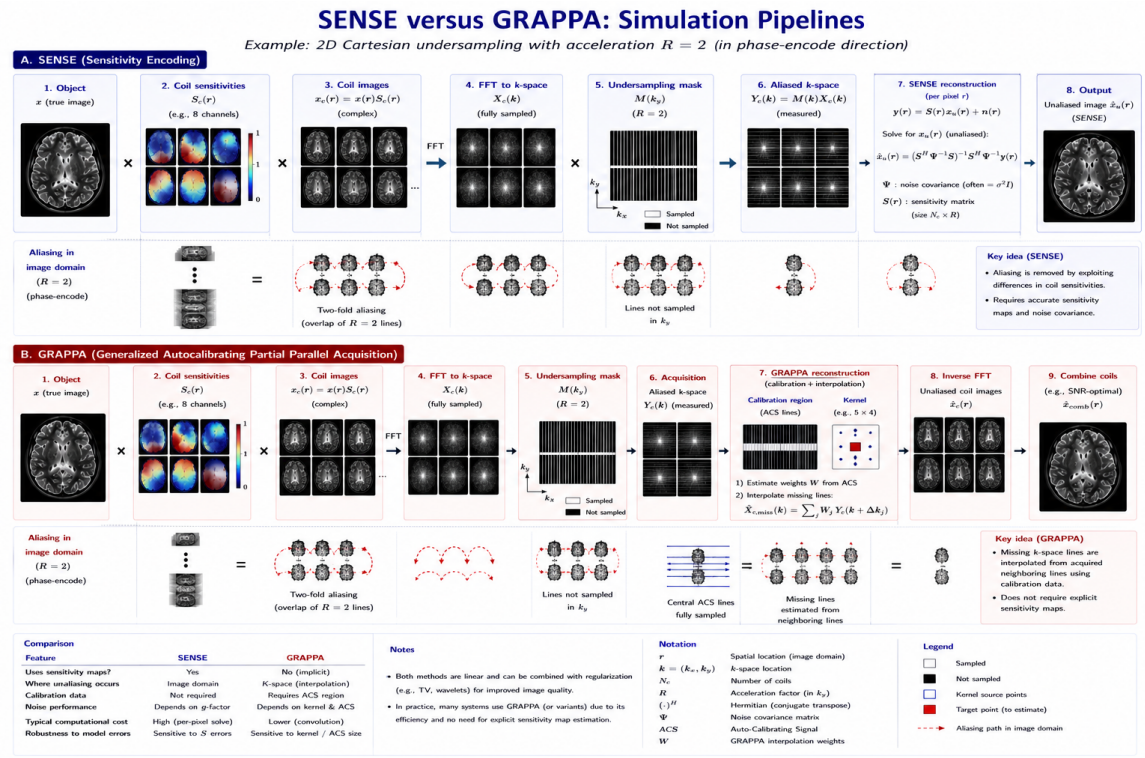

Figure 34: SENSE versus GRAPPA simulation pipeline.

1. Cartesian undersampling,

2. aliased coil images,

3. SENSE reconstruction,

4. GRAPPA reconstruction.

A particularly important application of simulation is the study of echo-planar imaging (EPI). EPI trajectories are sensitive to undersampling because geometric distortion and T_2^*-related blurring depend strongly on the total readout duration.

In EPI simulations, the k-space trajectory follows a zig-zag pattern generated by alternating readout gradients and phase-encoding blips:

$$\mathbf{k}(t) = (k_x(t), k_y(t)). \tag{53}$$

Parallel imaging acceleration reduces the number of phase-encoding steps and thereby shortens the EPI echo train, which can be investigated systematically in numerical models [2, 3].

Simulation is especially useful for investigating:

- susceptibility-related geometric distortion,
- echo-train shortening,
- residual aliasing,
- Nyquist ghosting and phase-error sensitivity,
- off-resonance effects.

[2, 4]

Non-Cartesian trajectories represent another important area of accelerated MRI simulation. Radial imaging acquires k-space along rotating spokes:

$$k_x(t) = k(t)\cos\theta, \qquad k_y(t) = k(t)\sin\theta, \tag{54}$$

where θ denotes the spoke angle.

Figure 35 shows radial sampling trajectories.

Radial and spiral trajectories are especially relevant for simulation because their aliasing patterns differ substantially from Cartesian undersampling and their reconstructions often require iterative or trajectory-specific methods [18, 24, 27].

Parallel imaging reconstruction for radial or spiral imaging may involve:

- non-Cartesian SENSE,
- radial GRAPPA,
- spiral parallel imaging,
- iterative reconstruction.

Spiral imaging similarly benefits from simulation studies because spiral trajectories are sensitive to trajectory design and off-resonance behavior, while accelerated reconstruction depends strongly on the interaction between sampling geometry and coil encoding [18, 27].

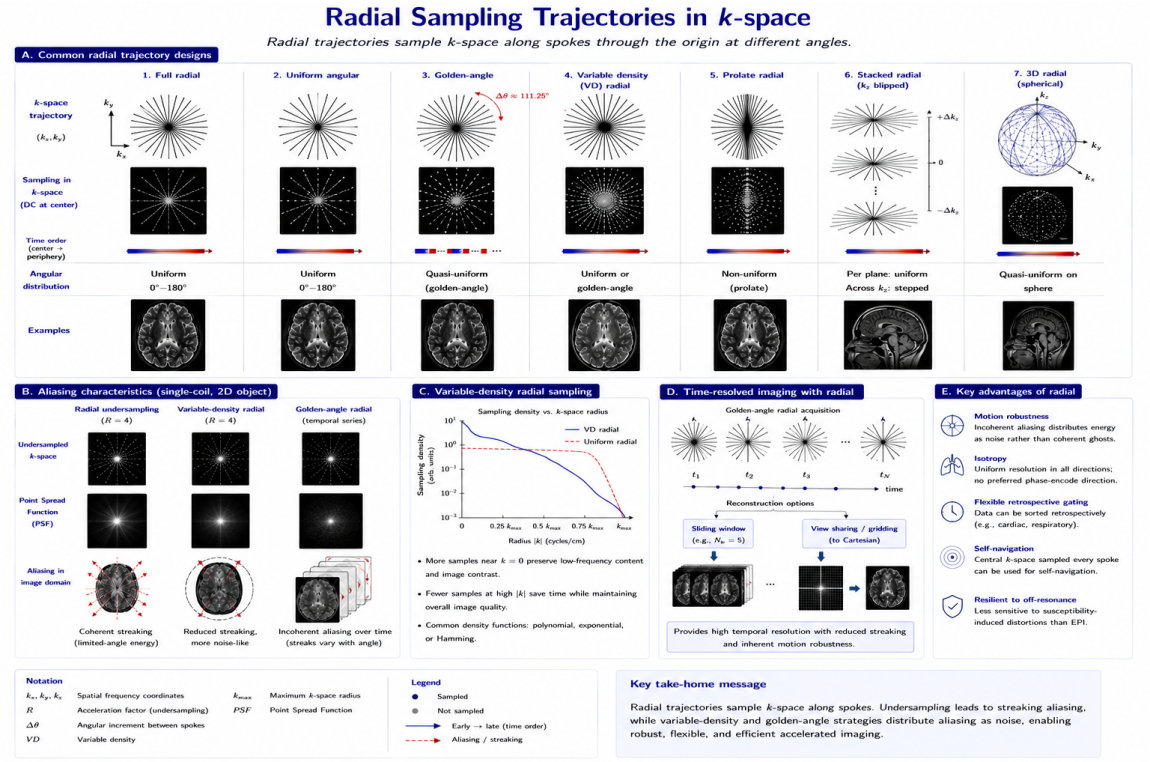

Figure 35: Radial sampling trajectories.

Simulation is also useful for evaluating simultaneous multi-slice (SMS) imaging. In SMS acquisition, several slices are excited simultaneously:

$$s_c^{\mathrm{SMS}} = \sum_{m=1}^{N_s} S_c(z_m)\rho(z_m). \tag{55}$$

The resulting slice aliasing may then be resolved using parallel imaging reconstruction [14].

The key elements are:

1. simultaneous slice excitation,
2. aliased slice superposition,
3. reconstructed slice separation.

Modern accelerated MRI reconstruction may also be represented numerically through regularized inverse problems:

$$\hat{x} = \arg\min_x \left(\|Ax - y\|_2^2 + \lambda R(x) \right). \tag{56}$$

This form provides a flexible framework for exploring:

- compressed sensing,
- sparsity regularization,
- low-rank constraints,
- calibration-based consistency,

- learned reconstruction priors.

[13, 16, 28, 30]

The key elements are:

1. direct reconstruction,
2. iterative reconstruction,
3. compressed sensing reconstruction,
4. learned reconstruction models.

An important advantage of simulation is the ability to evaluate reconstruction performance quantitatively under controlled conditions. Depending on the study design, useful assessment quantities may include:

- residual artifact level,
- image-domain error,
- reconstruction stability,
- geometry-factor maps,
- convergence behavior,
- sensitivity to acceleration and noise.

Simulation studies in the uploaded literature explicitly used such controlled analyses to assess convergence behavior, dependence on acceleration, coil geometry, ACS sampling, and reconstruction fidelity [18, 23].

Figure 36 shows representative quantitative reconstruction metrics.

Simulation therefore provides a powerful means of studying the interaction between:

- acquisition geometry,
- coil encoding,
- undersampling strategy,
- noise propagation,
- reconstruction algorithms.

Within the scope of accelerated and parallel MRI, these numerical investigations are valuable for method development, optimization, and interpretation of reconstruction behavior under controlled conditions.

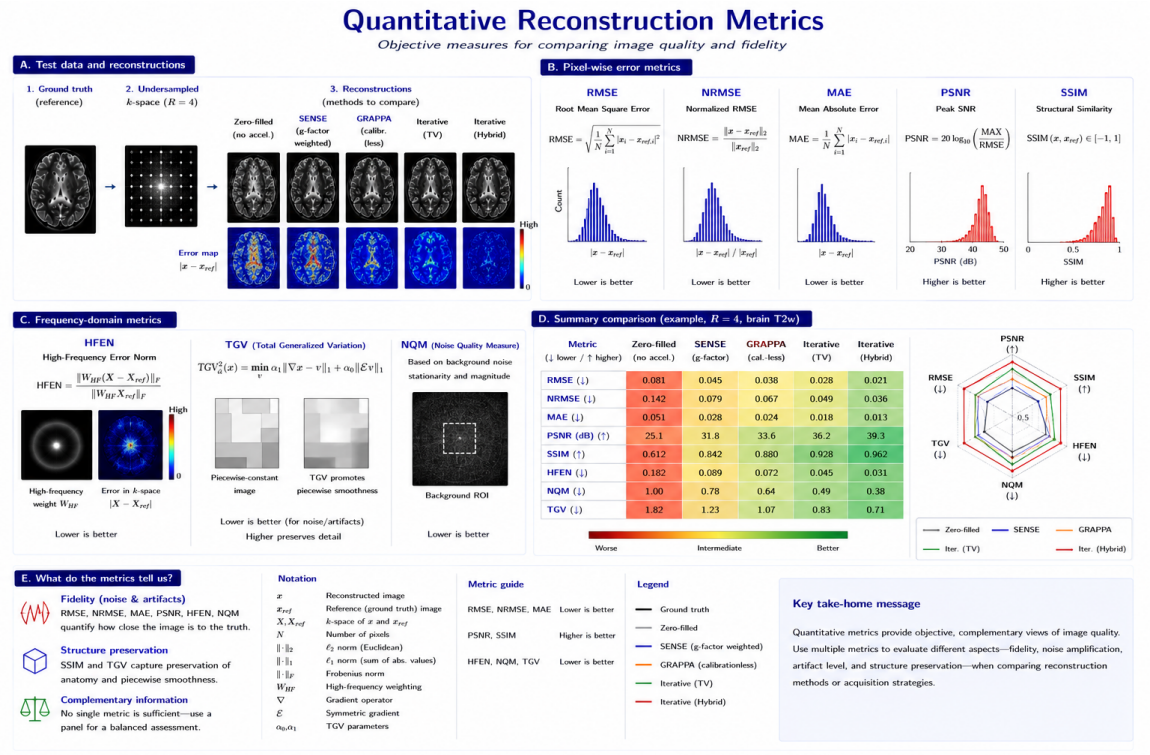

Figure 36: Representative quantitative reconstruction metrics.

9 Future Directions

Parallel imaging fundamentally transformed MRI by introducing phased-array coil sensitivities as an additional source of spatial encoding. Since the introduction of SMASH, SENSE, and GRAPPA, accelerated MRI has evolved from a specialized research concept into a central component of modern MRI methodology and clinical practice. Nevertheless, the development of parallel imaging continues rapidly, driven by increasing demands for higher spatial resolution, faster acquisition speed, improved motion robustness, and more flexible computational reconstruction frameworks [2, 19].

One important trend has been the continuing development of higher-channel-count receiver systems. Early phased-array and clinical parallel imaging systems commonly employed relatively small numbers of receiver elements, whereas later commercial platforms moved toward 32-channel architectures. Specialized research systems demonstrated 64-channel receiver technology and even explored imaging concepts based on very high degrees of parallel reception [21].

Increasing the number of receiver elements can improve:

- spatial encoding diversity,
- achievable acceleration factors,
- geometry-factor performance,
- reconstruction flexibility.

The benefits, however, depend strongly on the geometry of the coil array, the anatomical region being imaged, and the direction of accelerated encoding [19, 21].

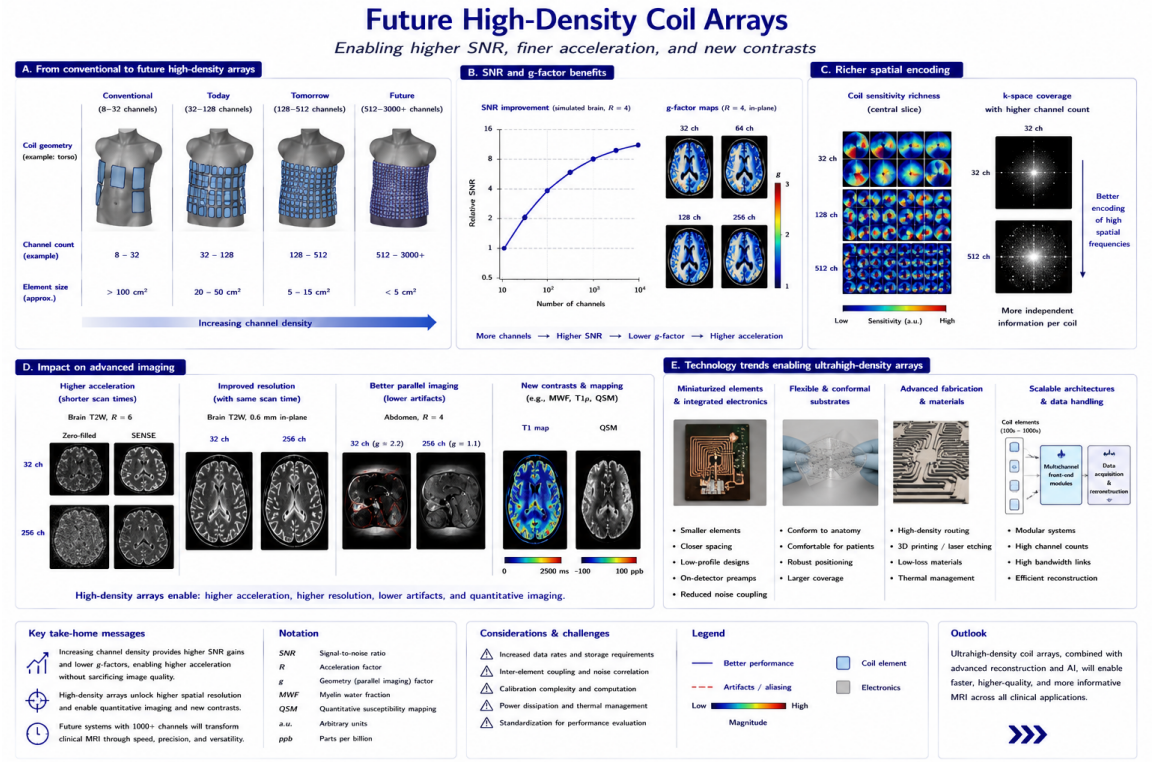

Figure 37: Future high-density coil arrays.

Figure 37 shows future high-density coil arrays.

Another important direction is the reduction of dependence on separate calibration scans and rigid reconstruction assumptions. Classical SENSE requires explicit coil sensitivity maps, while GRAPPA relies on autocalibration signal (ACS) data. Later autocalibrated approaches, such as SPIRiT and ESPIRiT, extended these ideas by using calibration information more flexibly within iterative reconstruction frameworks [12, 20].

A related line of work seeks to reduce or eliminate explicit calibration requirements through structured low-rank and calibrationless parallel imaging approaches, including SAKE-type methods and related matrix-completion formulations. These methods aim to recover missing data by exploiting redundancy and low-rank structure in multichannel k-space rather than relying exclusively on explicit sensitivity maps or conventional ACS calibration [33].

Figure 38 shows calibration-based versus calibration-reduced parallel imaging.

The integration of parallel imaging with compressed sensing represents another major development. Compressed sensing exploits image sparsity to stabilize highly undersampled reconstructions:

$$\hat{x} = \arg\min_{x} \left(\|Ax - y\|_2^2 + \lambda \|Wx\|_1 \right). \tag{57}$$

Combined PI+CS methods enabled acceleration regimes beyond those attainable with conventional linear parallel imaging alone in many applications, particularly when iterative reconstruction and appropriate sparsity constraints are used [11, 28, 30].

The key elements are:

1. conventional parallel imaging,

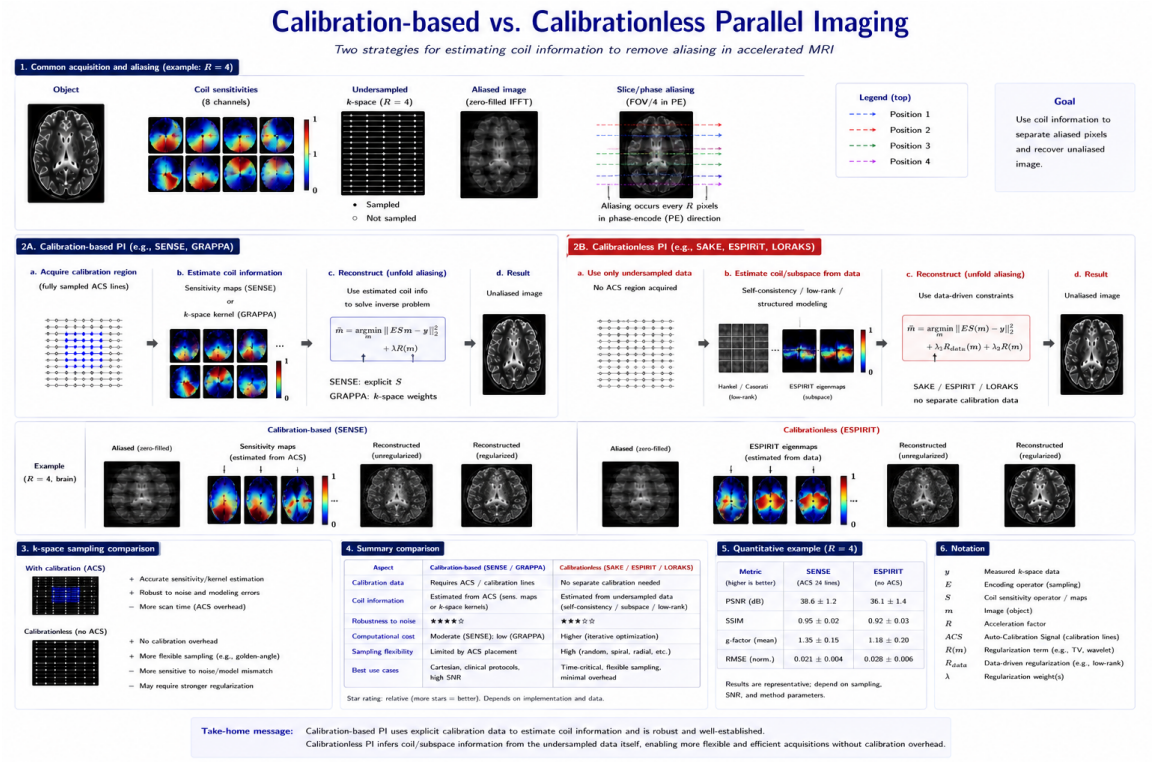

Figure 38: Calibration-based versus calibration-reduced parallel imaging.

2. compressed sensing,

3. combined PI+CS reconstruction.

Deep-learning-based reconstruction methods currently represent one of the most active extensions of accelerated MRI. Neural networks may be incorporated into reconstruction pipelines in several different ways:

- learned regularization,
- unrolled iterative reconstruction,
- direct multicoil reconstruction,
- artifact suppression within hybrid reconstruction frameworks.

Variational-network approaches and GRAPPA-inspired neural architectures have demonstrated improved reconstruction performance in accelerated MRI settings, including multicoil data and high undersampling factors [16, 17].

Deep-learning-based reconstruction offers potential advantages such as:

- improved artifact suppression,
- reduced noise amplification,
- improved reconstruction quality at high acceleration factors,
- tighter integration between physics-based modeling and learned image priors.

At the same time, important challenges remain. The uploaded literature emphasizes that image-quality metrics alone cannot guarantee diagnostic reliability and that proper clinical validation is required before highly accelerated learned reconstructions can be adopted confidently in routine practice [17].

Motion-aware reconstruction is another increasingly important research direction. Many MRI applications remain limited by respiratory, cardiac, or patient motion. Modern accelerated imaging strategies increasingly incorporate:

- motion estimation,
- motion-resolved reconstruction,
- free-breathing acquisition,
- self-navigation or extra motion dimensions.

These strategies are particularly relevant in dynamic body MRI and other applications in which conventional breath-hold or motion-suppression approaches are insufficient [32].

Figure 39 shows motion-resolved reconstruction.

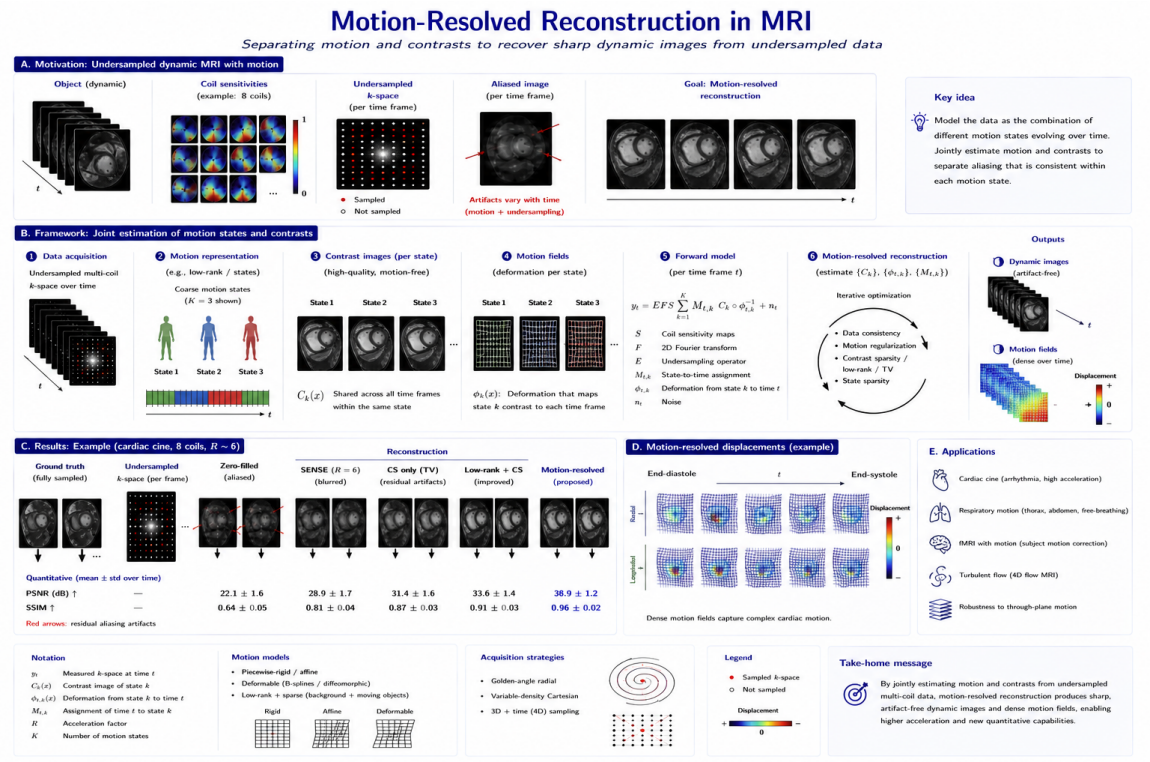

Figure 39: Motion-resolved reconstruction.

Simultaneous multi-slice imaging and controlled aliasing methods such as CAIPIRINHA and Wave-CAIPI are also likely to remain important directions in accelerated MRI. These approaches exploit increasingly sophisticated spatial encoding strategies to distribute aliasing more favorably across the receiver array and thereby reduce geometry-factor penalties [14, 15].

Non-Cartesian imaging trajectories also remain an important complementary direction for accelerated MRI because they offer:

- efficient k-space coverage,

- favorable motion properties,
- compatibility with iterative reconstruction,
- useful combinations with parallel imaging and compressed sensing.

Radial, spiral, and other non-Cartesian strategies continue to motivate specialized reconstruction approaches for highly accelerated and motion-sensitive imaging [18, 25, 32].

Figure 40 shows advanced non-Cartesian trajectories.

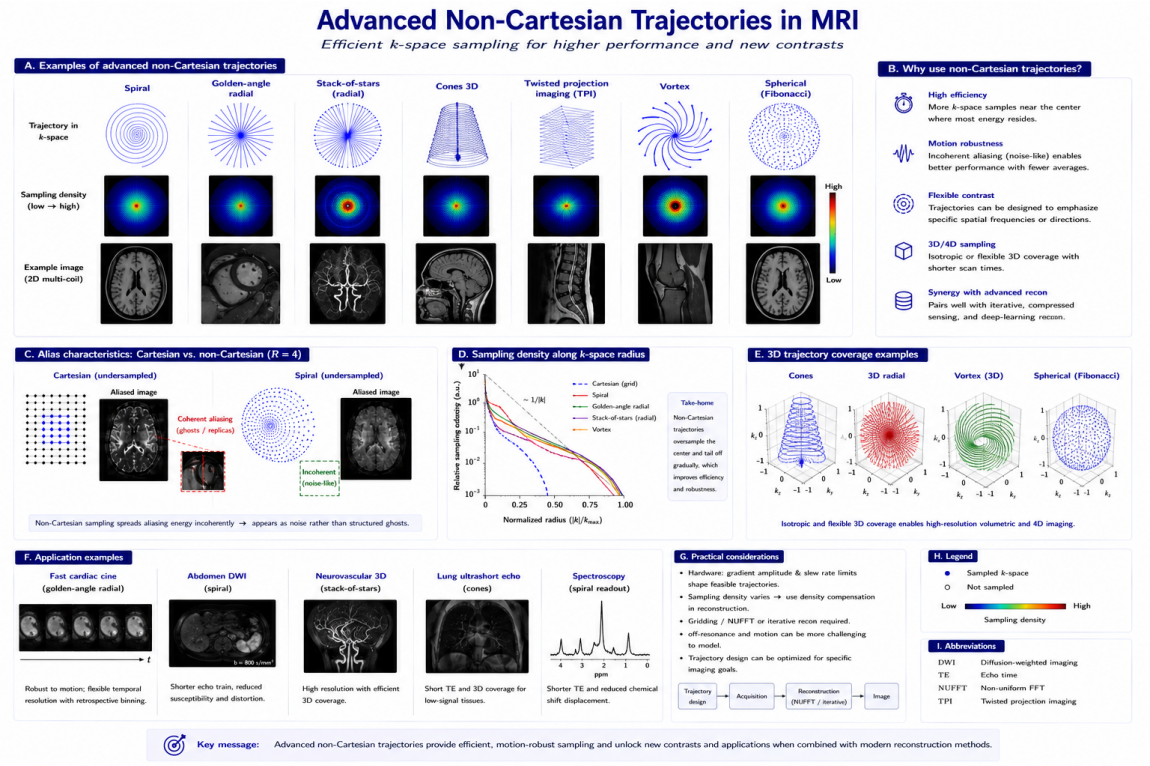

Figure 40: Advanced non-Cartesian trajectories.

Parallel imaging and advanced controlled-aliasing methods are also increasingly relevant for high-resolution phase-sensitive and quantitative applications. Wave-CAIPI, for example, was demonstrated for highly accelerated three-dimensional gradient-echo imaging, high-quality phase imaging, and quantitative susceptibility mapping (QSM), suggesting an important role for advanced parallel encoding in demanding volumetric applications [15].

Integrated PET/MR systems represent another setting in which efficient MRI acquisition is highly valuable. In pediatric PET/MR oncology protocols, the duration and complexity of the MR examination strongly influence overall workflow and patient tolerability. The uploaded PET/MR study emphasizes the need for temporally efficient MR protocols, and its sequence tables already incorporate parallel acquisition techniques such as GRAPPA acceleration [38].

Modern accelerated MRI increasingly combines:

- parallel imaging,
- compressed sensing,
- low-rank modeling,

- model-based reconstruction,
- deep-learning-based reconstruction,
- motion-aware imaging strategies.

The resulting reconstruction frameworks are computationally sophisticated but permit acquisition speeds and imaging capabilities that would have been impossible using conventional Fourier imaging alone [12, 13, 16].

Figure 41 shows selected milestones in the evolution of accelerated MRI reconstruction.

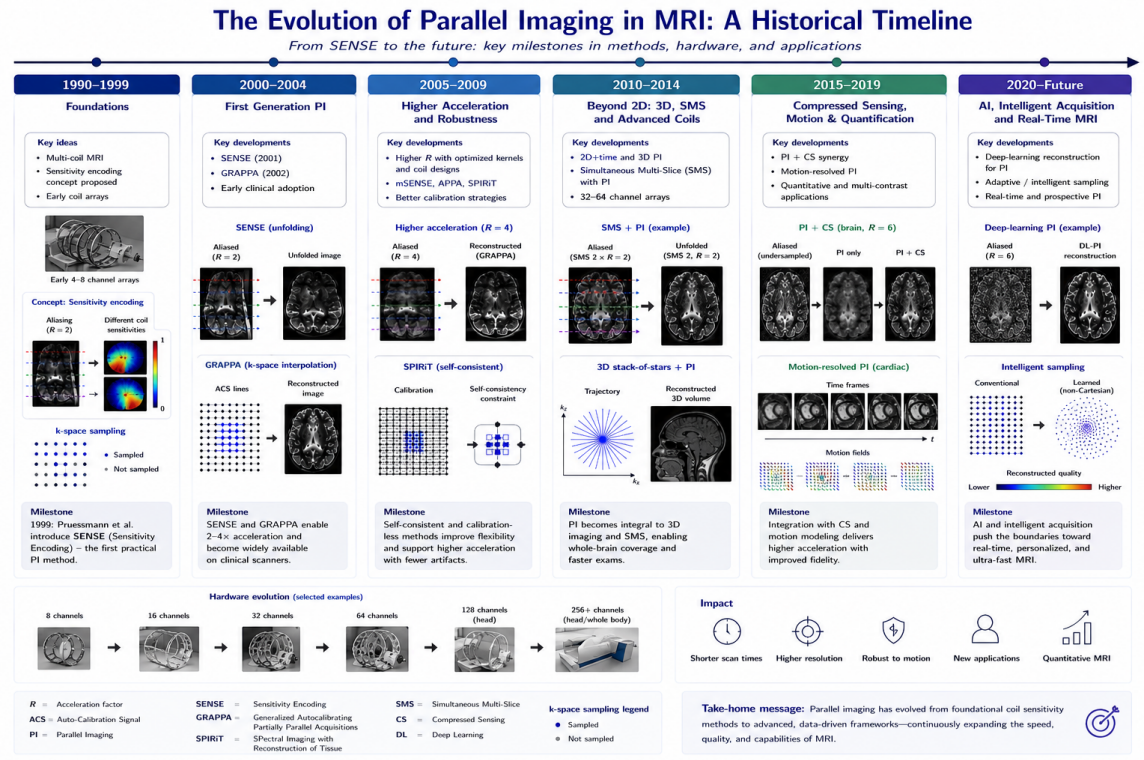

Figure 41: Selected milestones in the evolution of accelerated MRI reconstruction.

SMASH → SENSE → GRAPPA → Compressed Sensing MRI → SPIRiT → ESPIRiT → CAIPI / Wave-CAIPI → De

The future of MRI reconstruction will likely involve increasingly unified computational imaging frameworks integrating acquisition physics, coil encoding, optimization theory, statistical modeling, and machine learning. In this evolving landscape, parallel imaging will remain one of the foundational technologies enabling ultrafast and highly flexible MRI acquisition.

10 Conclusion

Parallel imaging represents one of the most important advances in the history of magnetic resonance imaging. By exploiting the spatial sensitivity variations of phased-array receiver coils, parallel imaging partially replaces conventional gradient encoding and thereby permits substantial acceleration of MRI acquisition [1, 2].

The development of methods such as SMASH, SENSE, and GRAPPA fundamentally transformed accelerated MRI from a specialized research concept into a central component of contemporary MRI methodology and clinical practice [7–9]. Parallel imaging now contributes to a broad range of major MRI applications, including:

- diffusion-weighted imaging,
- functional MRI,
- cardiovascular MRI,
- angiography,
- pediatric body MRI,
- whole-body and dynamic imaging protocols.

[2, 10, 37]

The central principle underlying all parallel imaging methods is the use of coil sensitivity encoding to reconstruct images from undersampled k-space data. Image-domain approaches such as SENSE perform explicit unfolding using sensitivity maps, whereas k-space methods such as GRAPPA synthesize missing k-space samples from neighboring acquired data. Although mathematically different, both strategies rely fundamentally on spatial encoding provided by phased-array receiver coils [8, 9, 20].

Parallel imaging also introduced important new reconstruction challenges, including:

- noise amplification,
- geometry-factor limitations,
- calibration sensitivity,
- motion sensitivity,
- reconstruction instability at high acceleration factors.

These limitations are intrinsic to the tradeoff between acquisition speed, coil encoding efficiency, and reconstruction conditioning [2, 8].

These challenges stimulated the development of increasingly sophisticated reconstruction frameworks integrating:

- iterative reconstruction,
- compressed sensing,
- low-rank modeling,
- motion-aware reconstruction,
- deep-learning-based reconstruction.

[12, 13, 16, 28]

Modern MRI acceleration therefore no longer relies on a single reconstruction paradigm but instead increasingly combines multiple complementary strategies within unified computational imaging frameworks.

Parallel imaging also played a major role in enabling many modern MRI technologies, including:

- simultaneous multi-slice imaging,
- ultrafast EPI,
- high-field accelerated neuroimaging,
- free-breathing dynamic imaging,
- real-time MRI,
- advanced volumetric encoding strategies such as Wave-CAIPI.

[14, 15, 25, 26]

In parallel, numerical simulation became increasingly important for understanding and optimizing accelerated MRI systems. Computational experiments permit systematic investigation of:

- coil encoding,
- undersampling strategies,
- reconstruction artifacts,
- noise behavior,
- motion or phase-error effects,
- advanced reconstruction algorithms.

Simulation studies in the parallel-imaging literature have been used to examine SENSE reconstruction, VD-AUTO-SMASH performance, and EPI phase-error correction in controlled settings [4, 18, 23].

Such simulations are especially valuable because modern accelerated MRI reconstruction methods involve interactions between acquisition physics, coil encoding, sampling design, and regularized reconstruction that are difficult to assess purely analytically.

The continuing evolution of MRI reconstruction suggests that future systems will increasingly integrate:

- parallel imaging,
- compressed sensing,
- model-based reconstruction,
- motion-resolved imaging,
- artificial intelligence.

These developments are progressively transforming MRI into a highly adaptive computational imaging modality capable of achieving acquisition speeds and reconstruction performance that would previously have been unattainable [12, 16, 32].

Although the mathematical formulations and reconstruction algorithms continue to evolve, the core idea introduced by parallel imaging remains unchanged: spatial encoding in MRI can be shared between gradient fields and phased-array receiver coils. This insight fundamentally altered the trajectory of MRI development and continues to shape the future of accelerated imaging.

A Appendix A: Simplified Derivation of SENSE Reconstruction

In SENSE reconstruction, accelerated Cartesian acquisition causes aliasing because the effective field of view (FOV) in the phase-encoding direction is reduced by the acceleration factor R. As a result, several spatial locations become superimposed in the reconstructed image [8].

For simplicity, consider the case of acceleration factor $R = 2$. Two spatial locations, r_1 and r_2, become folded onto the same image position. The signal measured by receiver coil c is then:

$$v_c = S_c(r_1)a_1 + S_c(r_2)a_2, \tag{58}$$

where:

- a_1 and a_2 are the unknown voxel intensities,
- $S_c(r_1)$ and $S_c(r_2)$ are the coil sensitivities.

For multiple receiver coils, the system may be written in matrix form:

$$\mathbf{v} = \mathbf{S}\mathbf{a}, \tag{59}$$

with

$$\mathbf{v} = \begin{bmatrix} v_1 \\ v_2 \\ \vdots \\ v_{N_c} \end{bmatrix}, \qquad \mathbf{a} = \begin{bmatrix} a_1 \\ a_2 \end{bmatrix}. \tag{60}$$

The sensitivity matrix becomes

$$\mathbf{S} = \begin{bmatrix} S_1(r_1) & S_1(r_2) \\ S_2(r_1) & S_2(r_2) \\ \vdots & \vdots \\ S_{N_c}(r_1) & S_{N_c}(r_2) \end{bmatrix}. \tag{61}$$

The unfolded voxel intensities are estimated by least-squares inversion:

$$\mathbf{a} = (\mathbf{S}^H\mathbf{S})^{-1}\mathbf{S}^H\mathbf{v}. \tag{62}$$

In practical MRI systems, correlated receiver noise is included through the covariance matrix $\mathbf{C}$:

$$\mathbf{a} = (\mathbf{S}^H \mathbf{C}^{-1} \mathbf{S})^{-1} \mathbf{S}^H \mathbf{C}^{-1} \mathbf{v}. \tag{63}$$

This noise-weighted reconstruction is the classical SENSE solution [8].

B Appendix B: Simplified Derivation of GRAPPA Reconstruction

GRAPPA reconstructs missing k-space samples from neighboring acquired samples using calibration kernels estimated from autocalibration signal (ACS) data [9].

Assume that every second phase-encoding line is omitted during acquisition ($R = 2$). A missing k-space sample in coil j may be estimated from neighboring acquired samples across all coils:

$$S_j^{\text{missing}} = \sum_{l=1}^{N_c} \sum_{b} w_{jlb} \, S_l^{\text{acquired}}(b), \tag{64}$$

where:

- w_{jlb} are the GRAPPA interpolation weights,
- b indexes neighboring acquired samples,
- l indexes receiver coils.

The reconstruction weights are estimated from fully sampled ACS lines. The calibration problem may be written schematically as:

$$\mathbf{d} = \mathbf{A}\mathbf{w}, \tag{65}$$

where:

- $\mathbf{d}$ contains target ACS samples,
- $\mathbf{A}$ contains neighboring source samples from the ACS region,
- $\mathbf{w}$ contains the unknown interpolation weights.

The reconstruction weights are obtained by solving an overdetermined least-squares fitting problem:

$$\mathbf{w} = (\mathbf{A}^H \mathbf{A})^{-1} \mathbf{A}^H \mathbf{d}. \tag{66}$$

In practice, regularized or numerically stabilized variants may be used when the calibration system is ill conditioned [2, 9].

After calibration, the estimated weights are applied throughout the undersampled k-space dataset to synthesize missing phase-encoding lines.

The key elements are:

1. ACS calibration,
2. kernel fitting,
3. synthesis of missing k-space lines.

C Appendix C: Minimal MATLAB Examples

The following simplified MATLAB fragments illustrate the basic structure of multicoil MRI signal generation and Cartesian undersampling. They are intended only as schematic examples and do not implement a full SENSE or GRAPPA reconstruction.

Generation of Coil Sensitivities

```
for c = 1:Nc
    S(:,:,c) = exp(-((X-xc(c)).^2 + ...
                     (Y-yc(c)).^2)/(2*sigma^2));
end
```

Forward Multicoil MRI Signal Model

```
for c = 1:Nc
    coil_img(:,:,c) = rho .* S(:,:,c);
    kspace(:,:,c) = fftshift(fft2(coil_img(:,:,c)));
end
```

Cartesian Undersampling

```
mask = zeros(size(kspace,1), size(kspace,2));
mask(1:R:end,:) = 1;

for c = 1:Nc
    kspace_acc(:,:,c) = kspace(:,:,c) .* mask;
end
```

Aliased Root-Sum-of-Squares Image

```
for c = 1:Nc
    img_alias(:,:,c) = ifft2(ifftshift(kspace_acc(:,:,c)));
end

rss_alias = sqrt(sum(abs(img_alias).^2,3));
```

The resulting image is the aliased image formed from undersampled multicoil data before any dedicated SENSE or GRAPPA reconstruction is applied.

Bibliography

[1] Robin M. Heidemann, Özkan Özsarlak, Paul M. Parizel, Johan Michiels, Berthold Kiefer, Vladimir Jellus, Mathias Müller, Felix Breuer, Martin Blaimer, Mark A. Griswold, and Peter M. Jakob. A brief review of parallel magnetic resonance imaging. *European Radiology*, 13(10):2323–2337, 2003. doi: 10.1007/s00330-003-1992-7.

[2] Anagha Deshmane, Vikas Gulani, Mark A. Griswold, and Nicole Seiberlich. Parallel MR imaging. *Journal of Magnetic Resonance Imaging*, 36(1):55–72, 2012. doi: 10.1002/jmri.23639.

[3] Xavier Golay, Jacco A. de Zwart, Yi-Ching Lynn Ho, and Yih-Yian Sitoh. Parallel imaging techniques in functional MRI. *Topics in Magnetic Resonance Imaging*, 15(4):255–265, 2004. doi: 10.1097/01.rmr.0000142829.79609.d4.

[4] W. Scott Hoge and Jonathan R. Polimeni. Dual-polarity GRAPPA for simultaneous reconstruction and ghost correction of echo planar imaging data. *Magnetic Resonance in Medicine*, 76(1):32–44, 2016. doi: 10.1002/mrm.25839.

[5] James F. Glockner, Houchun H. Hu, David W. Stanley, Lisa Angelos, and Kevin King. Parallel MR imaging: a user's guide. *RadioGraphics*, 25(5):1279–1297, 2005. doi: 10.1148/rg.255045202.

[6] Martin Blaimer, Felix Breuer, Matthias Mueller, Robin M. Heidemann, Mark A. Griswold, and Peter M. Jakob. SMASH, SENSE, PILS, GRAPPA: How to choose the optimal method. *Topics in Magnetic Resonance Imaging*, 15(4):223–236, 2004. doi: 10.1097/01.rmr.0000136558.09801.dd.

[7] Daniel K. Sodickson and Warren J. Manning. Simultaneous acquisition of spatial harmonics (SMASH): fast imaging with radiofrequency coil arrays. *Magnetic Resonance in Medicine*, 38(4): 591–603, 1997. doi: 10.1002/mrm.1910380414.

[8] Klaas P. Pruessmann, Markus Weiger, Markus B. Scheidegger, and Peter Boesiger. SENSE: Sensitivity encoding for fast MRI. *Magnetic Resonance in Medicine*, 42(5):952–962, 1999. doi: 10.1002/(SICI)1522-2594(199911)42:5<952::AID-MRM16>3.0.CO;2-S.

[9] Mark A. Griswold, Peter M. Jakob, Robin M. Heidemann, Mathias Nittka, Vladimir Jellus, Jianmin Wang, Berthold Kiefer, and Axel Haase. Generalized autocalibrating partially parallel acquisitions (GRAPPA). *Magnetic Resonance in Medicine*, 47(6):1202–1210, 2002. doi: 10.1002/mrm.10171.

[10] Thoralf Niendorf and Daniel K. Sodickson. Parallel imaging in cardiovascular MRI: methods and applications. *NMR in Biomedicine*, 19(3):325–341, 2006. doi: 10.1002/nbm.1051.

[11] Dong Liang, Bo Liu, JiunJie Wang, and Leslie Ying. Accelerating SENSE using compressed sensing. *Magnetic Resonance in Medicine*, 62(6):1574–1584, 2009. doi: 10.1002/mrm.22161.

[12] Michael Lustig and John M. Pauly. SPIRiT: iterative self-consistent parallel imaging reconstruction from arbitrary k-space. *Magnetic Resonance in Medicine*, 64(2):457–471, 2010. doi: 10.1002/mrm.22428.

[13] Sajan Goud Lingala, Yue Hu, Edward V. R. DiBella, and Mathews Jacob. Accelerated dynamic MRI exploiting sparsity and low-rank structure: k-t SLR. *IEEE Transactions on Medical Imaging*, 30(5): 1042–1054, 2011. doi: 10.1109/TMI.2010.2100850.

[14] Kawin Setsompop, Borjan A. Gagoski, Jonathan R. Polimeni, Thomas Witzel, Van J. Wedeen, and Lawrence L. Wald. Blipped-controlled aliasing in parallel imaging for simultaneous multislice echo planar imaging with reduced g-factor penalty. *Magnetic Resonance in Medicine*, 67(5):1210–1224, 2012. doi: 10.1002/mrm.23097.

[15] Berkin Bilgic, Borjan A. Gagoski, Stephen F. Cauley, Audrey P. Fan, Jonathan R. Polimeni, P. Ellen Grant, Lawrence L. Wald, and Kawin Setsompop. Wave-CAIPI for highly accelerated 3d imaging. *Magnetic Resonance in Medicine*, 73(6):2152–2162, 2015. doi: 10.1002/mrm.25347.

[16] Kerstin Hammernik, Teresa Klatzer, Erich Kobler, Michael P. Recht, Daniel K. Sodickson, Thomas Pock, and Florian Knoll. Learning a variational network for reconstruction of accelerated MRI data. *Magnetic Resonance in Medicine*, 79(6):3055–3071, 2018. doi: 10.1002/mrm.26977.

[17] Anuroop Sriram, Jure Zbontar, Tullie Murrell, C. Lawrence Zitnick, Aaron Defazio, and Daniel K. Sodickson. GrappaNet: Combining parallel imaging with deep learning for multi-coil MRI reconstruction. In *Proceedings of the IEEE/CVF Conference on Computer Vision and Pattern Recognition (CVPR)*, pages 14315–14322, 2020. doi: 10.1109/CVPR42600.2020.01432.

[18] Klaas P. Pruessmann, Markus Weiger, Peter Börnert, and Peter Boesiger. Advances in sensitivity encoding with arbitrary k-space trajectories. *Magnetic Resonance in Medicine*, 46(4):638–651, 2001. doi: 10.1002/mrm.1241.

[19] Jesse Hamilton, Dominique Franson, and Nicole Seiberlich. Recent advances in parallel imaging for MRI. *Progress in Nuclear Magnetic Resonance Spectroscopy*, 101:71–95, 2017. doi: 10.1016/j.pnmrs.2017.04.002.

[20] Martin Uecker, Peng Lai, Mark J. Murphy, Patrick Virtue, Michael Elad, John M. Pauly, Shreyas S. Vasanawala, and Michael Lustig. ESPIRiT—an eigenvalue approach to autocalibrating parallel MRI: where SENSE meets GRAPPA. *Magnetic Resonance in Medicine*, 71(3):990–1001, 2014. doi: 10.1002/mrm.24751.

[21] David Gerald Brown. *Instrumentation for parallel magnetic resonance imaging*. PhD thesis, Texas A&M University, 2005.

[22] Peter Kellman, Frederick H. Epstein, and Elliot R. McVeigh. Adaptive sensitivity encoding incorporating temporal filtering (TSENSE). *Magnetic Resonance in Medicine*, 45(5):846–852, 2001. doi: 10.1002/mrm.1113.

[23] Robin M. Heidemann, Mark A. Griswold, Axel Haase, and Peter M. Jakob. VD-AUTO-SMASH imaging. *Magnetic Resonance in Medicine*, 45(6):1066–1074, 2001. doi: 10.1002/mrm.1141.

[24] Mark A. Griswold, Robin M. Heidemann, and Peter M. Jakob. Direct parallel imaging reconstruction of radially sampled data using GRAPPA with relative shifts. In *Proceedings of the 11th Annual Meeting of the International Society for Magnetic Resonance in Medicine*, page 2349, Toronto, Canada, 2003.

[25] Dominique Franson, James Ahad, Yuchi Liu, Alexander Fyrdahl, William Truesdell, Jesse Hamilton, and Nicole Seiberlich. Self-calibrated through-time spiral GRAPPA for real-time, free-breathing evaluation of left ventricular function. *Magnetic Resonance in Medicine*, 89(2):536–549, 2023. doi: 10.1002/mrm.29462.

[26] Felix A. Breuer, Peter Kellman, Mark A. Griswold, and Peter M. Jakob. Dynamic autocalibrated parallel imaging using temporal GRAPPA (TGRAPPA). *Magnetic Resonance in Medicine*, 53(4):981–985, 2005. doi: 10.1002/mrm.20430.

[27] Keith Heberlein and Xiaoping Hu. Auto-calibrated parallel spiral imaging. *Magnetic Resonance in Medicine*, 55(3):619–625, 2006. doi: 10.1002/mrm.20811.

[28] Mark Murphy, Marcus Alley, James Demmel, Kurt Keutzer, Shreyas Vasanawala, and Michael Lustig. Fast ℓ_1-SPIRiT compressed sensing parallel imaging MRI: scalable parallel implementation and clinically feasible runtime. *IEEE Transactions on Medical Imaging*, 31(6):1250–1262, 2012. doi: 10.1109/TMI.2012.2188039.

[29] Jeffrey Tsao, Peter Boesiger, and Klaas P. Pruessmann. k-t BLAST and k-t SENSE: dynamic MRI with high frame rate exploiting spatiotemporal correlations. *Magnetic Resonance in Medicine*, 50(5): 1031–1042, 2003. doi: 10.1002/mrm.10611.

[30] Michael Lustig, David Donoho, and John M. Pauly. Sparse MRI: The application of compressed sensing for rapid MR imaging. *Magnetic Resonance in Medicine*, 58(6):1182–1195, 2007. doi: 10.1002/mrm.21391.

[31] Ricardo Otazo, Daniel Kim, Leon Axel, and Daniel K. Sodickson. Combination of compressed sensing and parallel imaging for highly accelerated first-pass cardiac perfusion MRI. *Magnetic Resonance in Medicine*, 64(3):767–776, 2010. doi: 10.1002/mrm.22463.

[32] Li Feng, Thomas Benkert, Kai Tobias Block, Daniel K. Sodickson, Ricardo Otazo, and Hersh Chandarana. Compressed sensing for body MRI. *Journal of Magnetic Resonance Imaging*, 45(4): 966–987, 2017. doi: 10.1002/jmri.25547.

[33] Jong Chul Ye. Compressed sensing MRI: a review from signal processing perspective. *BMC Biomedical Engineering*, 1(1):8, 2019. doi: 10.1186/s42490-019-0006-z.

[34] Kâmil Uğurbil, Gregor Adriany, Peter Andersen, Wei Chen, Michael Garwood, Rolf Gruetter, Pierre-Gil Henry, Seong-Gi Kim, Haiying Lieu, Ivan Tkac, Tommy Vaughan, Pierre-Francoise Van De Moortele, Essa Yacoub, and Xiao-Hong Zhu. Ultrahigh field magnetic resonance imaging and spectroscopy. *Magnetic Resonance Imaging*, 21(10):1263–1281, 2003. doi: 10.1016/j.mri.2003.08.027.

[35] Xinwei Shi, Xiaodong Ma, Wenchuan Wu, Feng Huang, Chun Yuan, and Hua Guo. Parallel imaging and compressed sensing combined framework for accelerating high-resolution diffusion tensor imaging using inter-image correlation. *Magnetic Resonance in Medicine*, 73(5):1775–1785, 2015. doi: 10.1002/mrm.25290.

[36] Fa-Hsuan Lin, Teng-Yi Huang, Nan-Kuei Chen, Fu-Nien Wang, Steven M. Stufflebeam, John W. Belliveau, Lawrence L. Wald, and Kenneth K. Kwong. Functional MRI using regularized parallel imaging acquisition. *Magnetic Resonance in Medicine*, 54(2):343–353, 2005. doi: 10.1002/mrm.20555.

[37] Shreyas S. Vasanawala, Michael J. Murphy, Marcus T. Alley, Peng Lai, Kurt Keutzer, John M. Pauly, and Michael Lustig. Practical parallel imaging compressed sensing MRI: Summary of two years of experience in accelerating body MRI of pediatric patients. In *Proceedings of the IEEE International Symposium on Biomedical Imaging: From Nano to Macro*, pages 1039–1043, 2011. doi: 10.1109/ISBI.2011.5872579.

[38] Franz Wolfgang Hirsch, Bernhard Sattler, Ina Sorge, Lars Kurch, Adrian Viehweger, Lutz Ritter, Peter Werner, Thies Jochimsen, Henryk Barthel, Uta Bierbach, Holger Till, Osama Sabri, and Regine Kluge. PET/MR in children: initial clinical experience in paediatric oncology using an integrated PET/MR scanner. *Pediatric Radiology*, 43:860–875, 2013. doi: 10.1007/s00247-012-2570-4.